



UNIVERSITAT DE  
BARCELONA

**Development and application of xenograft models  
to predict the prognosis and study the treatment-driven  
evolution of pediatric sarcomas**

Helena Castillo Écija



Aquesta tesi doctoral està subjecta a la llicència **Reconeixement- NoComercial – SenseObraDerivada 4.0. Espanya de Creative Commons.**

Esta tesis doctoral está sujeta a la licencia **Reconocimiento - NoComercial – SinObraDerivada 4.0. España de Creative Commons.**

This doctoral thesis is licensed under the **Creative Commons Attribution-NonCommercial-NoDerivs 4.0. Spain License.**

**SJD**

Sant Joan de Déu  
Fundació de Recerca



UNIVERSITAT DE  
BARCELONA

University of Barcelona

Faculty of Medicine

Doctorate program: Biomedicine

Research line: Molecular and cellular biology of cancer

**Development and application of xenograft models to  
predict the prognosis and study the treatment-driven  
evolution of pediatric sarcomas**

Pediatric Cancer Treatment Group

Pediatric Cancer Program

Institut de Recerca Sant Joan de Déu

&

Department of Pediatric Oncology

Hospital Sant Joan de Déu

PhD candidate: Helena Castillo Ecija

A handwritten signature in blue ink, appearing to read "Helena".

Thesis director: Dr. Ángel M. Carcaboso

A handwritten signature in blue ink, appearing to read "Ángel M. Carcaboso".

Thesis tutor: Dra. Teresa Maria Ribalta Farrés

A handwritten signature in blue ink, appearing to read "T. Ribalta".

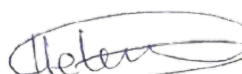


Dr. **Ángel Montero Carcaboso**, director of the thesis entitled ***Development and application of xenograft models to predict the prognosis and study the treatment-driven evolution of pediatric sarcomas*** completed by the PhD candidate **Helena Castillo Ecija**, endorses the originality of the research work included in this thesis.

The results of this work have already been published in well reputed scientific journals:

- One research article entitled *Prognostic value of patient-derived xenograft engraftment in pediatric sarcomas* was published in 2021 in The Journal of Pathology: Clinical Research, IF 2020 = 5.64, ranked in Q1 (12/77) in the area *PATHOLOGY*
- One research article entitled *Treatment-driven selection of chemoresistant Ewing sarcoma tumors with limited drug distribution* was published in 2020 in the Journal of Controlled Release, IF 2020 = 9.78, ranked in D1 (10/275) in the area *PHARMACOLOGY & PHARMACY*

Sign and date:



Ángel Montero Carcaboso (director)

Helena Castillo Ecija (PhD candidate)



“A wife who loses a husband is called a widow. A husband who loses a wife is called a widower. A child who loses his parents is called an orphan. There is no word for a parent who loses a child. That’s how awful the loss is.”

From *An Orphan’s Tale* by Jay Neugeboren (1976).



**INTRODUCTION..... 11**

1. Patient Derived Xenografts (PDX) as preclinical models for the study of solid tumors ..... - 13 -

    1.1. Need and opportunity ..... - 13 -

    1.2. Establishment of the PDXs..... - 13 -

    1.3. Applications of PDXs..... - 17 -

        1.3.1. Tumor biology and tumor heterogeneity ..... - 17 -

        1.3.2. Resistance and progression..... - 17 -

        1.3.3. Patient prognosis ..... - 19 -

        1.3.4. Preclinical research and personalized cancer therapy using mouse avatars-20 -

    1.4. Challenges and limitations of PDX models..... - 25 -

2. Microdialysis sampling ..... - 27 -

    2.1. Microdialysis for *in vivo* investigation..... - 27 -

    2.2. Principle ..... - 27 -

    2.3. Microdialysis as a sampling method for hydrophobic anticancer drugs. - 29 -

    2.4. Compartmental analysis of intratumoral drug distribution..... - 30 -

    2.5. Advantages and challenges of the microdialysis sampling..... - 32 -

3. Tumor chemoresistance ..... - 34 -

4. Childhood cancer ..... - 38 -

    4.1. Ewing sarcoma..... - 40 -

    4.2. Osteosarcoma..... - 42 -

    4.3. Rhabdomyosarcoma ..... - 44 -

5. Camptothecins in the treatment of pediatric sarcomas ..... - 47 -

**HYPOTHESES AND AIMS ..... 53**

**EXPERIMENTAL WORK..... - 59 -**

1. Prognostic value of patient-derived xenograft engraftment in pediatric sarcomas ..... - 61 -

    1.1. Introduction ..... - 63 -

    1.2. Materials and methods ..... - 63 -

        1.2.1. Xenotransplantation of patient samples ..... - 63 -



1.2.2.	Analysis of fusion genes .....	- 64 -
1.2.3.	Histopathology .....	- 65 -
1.2.4.	PDX growth.....	- 65 -
1.2.5.	Analysis of copy number alterations (CNAs).....	- 65 -
1.2.6.	Irinotecan activity <i>in vivo</i> .....	- 65 -
1.2.7.	Prognostic value of positive tumor engraftment .....	- 66 -
1.2.8.	Statistics .....	- 67 -
1.3.	Results .....	- 67 -
1.3.1.	Patients.....	- 67 -
1.3.2.	Biopsies and PDXs .....	- 67 -
1.3.3.	Comparative histopathology of patient tumors and PDX samples .....	- 68 -
1.3.4.	Tumor growth rate.....	- 68 -
1.3.5.	CNA in patient biopsies and corresponding PDXs .....	- 70 -
1.3.6.	Antitumor activity of irinotecan in subcutaneous PDXs .....	- 71 -
1.3.7.	Prognostic value of positive PDX engraftment in mice.....	- 72 -
1.4.	Discussion.....	- 73 -
1.5.	Acknowledgements .....	- 76 -
1.6.	Author contribution statement .....	- 76 -
1.7.	References.....	- 77 -
1.8.	Supplementary material .....	- 81 -
2.	Treatment-driven selection of chemoresistant Ewing sarcoma tumors with limited drug distribution .....	- 105 -
2.1.	Introduction .....	- 107 -
2.2.	Materials and methods.....	- 108 -
2.2.1.	Establishment of paired Ewing sarcoma PDX models .....	- 108 -
2.2.2.	Comparison of paired PDX models by CNA analysis.....	- 108 -
2.2.3.	Drug activity assays .....	- 109 -
2.2.4.	Drug distribution assays.....	- 109 -
2.2.5.	Differential expression of ATP-binding cassette (ABC) transport in PDX pairs .....	- 111 -
2.2.6.	Intracellular accumulation of irinotecan <i>in vitro</i> .....	- 112 -
2.2.7.	Reversal of treatment-induced drug resistance <i>in vitro</i> .....	- 113 -
2.2.8.	Statistics .....	- 113 -

2.3. Results .....	113 -
2.3.1. Paired PDX models and patient clinical exposure to irinotecan .....	113 -
2.3.2. Pairwise comparison of CNAs in PDX derived from early and late tumor biopsies.....	114 -
2.3.3. Comparison of antitumor activity of SN-38/irinotecan in patient-matched early and late PDX models.....	117 -
2.3.4. Intratumor drug distribution in paired early and late xenografts .....	118 -
2.3.5. Comparative expression of efflux transporters and genes related to irinotecan activity in patient-matched early and late PDX .....	120 -
2.3.6. Functional studies of drug uptake in cells derived from paired PDX .....	120 -
2.4. Discussion.....	123 -
2.5. Conclusions.....	124 -
2.6. Declaration of Competing Interest.....	124 -
2.7. Acknowledgements .....	125 -
2.8. References.....	126 -
2.9. Supplementary material .....	132 -

**SUMMARY OF RESULTS ..... 137**

1. Successful establishment and characterization of PDX models established from biopsies and necropsies of pediatric patients.....	139 -
2. Identification of factors favoring PDX engraftment and association between PDX engraftment and prognosis in pediatric patients.....	140 -
3. Changes in anticancer drug activity and intratumoral drug distribution during the evolution of Ewing sarcoma.....	141 -

**DISCUSSION..... 143**

**CONCLUSIONS..... 153**

**REFERENCES..... 159**



# INTRODUCTION

---



### **1. Patient Derived Xenografts (PDX) as preclinical models for the study of solid tumors**

The Dictionary of Cancer Terms of the National Cancer Institute defines PDX as “tumor tissue that has been taken from a patient and implanted into mice for research purposes”. The first reported mouse xenograft tumor model is from 1969, when Rygaard and Povlsen minced a primary colonic adenocarcinoma from a 74-year-old woman patient and inoculated it subcutaneously in nude mice [1]. The tumor engrafted and grew in 40 days up to 2500 mm<sup>3</sup>. Upon successful transplantation of the tumor to new cohorts of mice, they observed no differences in tumor histology during the transfers, regarding degree of differentiation, contents of connective tissue stroma and production of mucoid material [1]. In the 1970s, preclinical investigators studied the potential changes, such as the mitotic index or the heterogeneous histological representation of human adenocarcinoma when serially transferred in mice [2, 3]. Pickard *et al.* observed higher mitotic rate in xenografts compared to human tumors and concluded that this increase could induced greater response rates in mice than in patients. They highlighted the need to study cell kinetics and metabolisms changes when human samples are implanted in mice to use these models in translational research [3]. Among studies from the same period, Selby *et al.* observed a gradual loss of properties of primary testicular teratoma after multiple passages in mice, specifically in the production of human chorionic gonadotropin, but tumors conserved important characteristics of the donor tissue such as histology and differentiation degree [4]. The consistency of PDX models in the clinical research field was studied in the 1980s. Overall, there was good correlation between the response of patients to one specific treatment and the one of their corresponding PDX models [5, 6]. Since then, large collections of PDXs have been developed and used in preclinical research [7].

#### **1.1. Need and opportunity**

One of the main limitations in oncology drug development is the lack of preclinical models that recapitulate the complex heterogeneity of patient tumors. PDXs established from the engraftment of patient biopsies in immunodeficient mice are well-known preclinical tumors models in oncology research [8, 9]. PDXs might better represent human tumors compared to cell line xenografts or *in vitro* models for predicting the efficacy of therapeutics in the clinic [10-12]. These cancer models are used to study tumor biology and tumor progression [8, 10] and they help accelerate the development of anticancer drugs, validation of potential targets and biomarkers in tumor cells [10, 13, 14]. PDXs are becoming the preferred preclinical strategy in both the industry and academia groups [9, 15, 16].

#### **1.2. Establishment of the PDXs**

PDXs are established by direct transplantation of fragments of fresh, primary or metastatic, human solid tumor tissue collected by surgery or biopsy procedures.

The tumor pieces can be implanted either subcutaneously or orthotopically into immunodeficient mice, establishing the first filial generation, also known as F0 [9, 17] (**Figure 1**). PDX models can also be created from tumor cell suspensions obtained from pleural effusions or bone marrow, for instance, and matrigel can be used as vehicle for the cells. Matrigel is a gelatinous protein mixture constituted of structural proteins (such as laminin, nidogen, collagen and heparan sulfate proteoglycans) that resembles the complex extracellular matrix and is used as a substrate for PDX establishment [9, 18, 19]. When the PDX engrafts in mice, it is serially transferred from generation to generation (establishing F1, F2, etc.) [17]. In general, it is accepted that a PDX model is stably established after achieving F2. Most preclinical drug efficacy studies using PDX are performed at early passages, like F3 [16].

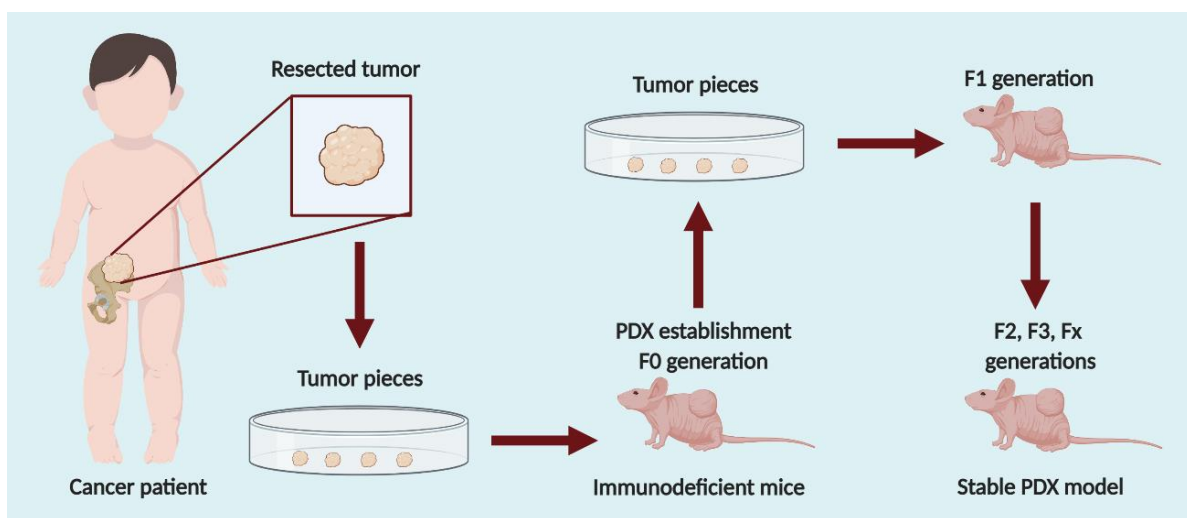


**Figure 1. Protocol for establishing PDXs.** The surgically resected patient tumor is cut into pieces of 3 x 3 x 3 mm. One to two tumor pieces, depending on the size of the original tumor, are implanted subcutaneously into the flank of nude mice to generate the F0. If the tumor engrafts, it is excised and minced into pieces that are subsequently implanted in new mice. This process is serially repeated to maintain and expand a PDX model.

All patient malignancies developed as PDX should be characterized, either after the first engraftment or upon being stabilized (three to five passages), to ensure that they correspond to the expected patient tumor. The analysis of both tumor samples, patient and PDX, include immunohistochemistry markers and molecular features (genetics, gene and protein expression) [8, 16, 20-22]. The underlying hypothesis is that PDX models preserve the original tumor properties better than conventional preclinical models established from cell cultures. Cell lines in culture acquire new properties due to the adaptation process of *in vitro* growth conditions, including higher invasive capabilities [9, 11, 23]. Such changes during culture could explain why conventional cancer models have poor drug efficacy predictive power while PDX models offers the potential for personalizing patient cancer treatment in precision medicine studies [23-25].

To allow xenografting, mice must have a depleted or compromised immune system to avoid tumor rejection [9, 10, 22]. The immune system of immunocompetent mice recognizes human tissue as foreign material and it is rapidly eradicated. To select the most appropriate host mouse strain, we must consider the level of immune suppression as well as the advantages and disadvantages of each strain [9, 26]. A summary table is shown below from Hidalgo *et al.* with the most commonly preferred rodent strains (**Table 1**).

Patient biopsies for engraftment can be obtained from different tissue locations (e.g., primary tumor vs metastasis) and at different times during the evolution of the disease (e.g., diagnosis vs recurrence). It is rare to obtain more than one sample from the same patient during disease progression [27]. Although some formal protocols have addressed PDX sampling from different stages of the disease, most clinical trials only include PDX generation in post-treatment, metastatic or recurrent disease stages but not at diagnosis. For instance, the clinical trial NCT04703244 (launched in January 2021, sponsored by Mayo Clinic) is collecting residual breast cancer samples remaining after chemotherapy to establish PDXs to study the efficacy of new drugs or drug combinations, identify mechanisms of treatment resistance and study the endogenous antitumor immune response. Nevertheless, the use of less invasive surgical approaches, such as fine-needle aspirates or core biopsies, facilitates multiple tumor sampling from the same patient along disease progression (from naïve, resistant and metastatic tumor sites) [10, 28]. Thus, multiple xenografting from individual patients has become a feasible alternative to study tumor evolution and mechanisms involved in therapy resistance [29]. Clinical trial NCT02572778 provides one example of multiple xenografting upon collection of fresh primary and recurrent tumor tissue from patients with squamous cell carcinoma of the head and neck by local biopsy. In my PhD work, I have used paired PDX obtained from Ewing sarcoma patients biopsied at different stages of their disease. Our laboratory is the first to report this unique resource [30]. Establishing tumor pairs was challenging in our hands, given that biopsies at diagnosis result in a lower rate of successful engraftment compared to late biopsies.



**Table 1. Immunodeficient mouse strains.** Summary of the main features of the most common immunodeficient mouse strains used to generate PDX models. Modified from “The Jackson Laboratory” (www.jax.org). Abbreviations are: NK: Natural killer; SCID: severe combined immunodeficiency disorder; NOD/SCID: Non-obese diabetic; NSG: NOD/SCID/IL2 $\lambda$ -receptor null; PBMC: Peripheral blood mononuclear cell.

Mouse Strain	Deficiency	Advantages	Disadvantages	Applications
Nude (nu)	No functional T cells	Well characterized. High take-rate of human tumors. Hairless: improved surgery and tumor monitoring.	Functional B and NK cells. T-cell functionality increases with age.	Transplantation of murine and human (xenogeneic) tumors for imaging, metastasis and new therapies studies.
SCID (scid)	No functional T and B cells	Better engraftment of allogeneic and xenogeneic tumor cells and tissues than in Nude strain.	Functional NK cells. Spontaneous lymphomas.	Transplantation of murine and human (xenogeneic) tumors for imaging, metastasis and new therapies studies. Low levels of engraftment of human PBMC and fetal hematopoietic tissues.
NOD-SCID	No functional T and B cells, NK cells impaired	Well characterized. Low NK cell activity. Very low tendency to produce functional B and T cells (leakiness) with age.	High incidence of lymphomas. Radiosensitive.	Higher levels of engraftment of PBMC and hematopoietic stem cells compared with the SCID strain
NOD-SCID IL2rgnull (NSG)	No functional T, B and NK cells	Lymphoma-resistant. Excellent engraftment of allogeneic and xenogeneic tumor cells and tissues. Suitable for analysis of human cancer stem cells and metastasis.	Not completely characterized.	Increased levels of growth, development and differentiation of human pluripotent stem cells and human tissue engrafted by intravenous, intrahepatic, intraperitoneal and intra-bone marrow injection.

### **1.3. Applications of PDXs**

#### **1.3.1. Tumor biology and tumor heterogeneity**

Tumors are not simply a group of aberrant clonal cells but rather a heterogeneous mixture of cell populations including cancer-associated fibroblasts, pericytes, endothelial cells, tumor-promoting inflammatory cells and progenitor cells of the tumor stroma [31, 32]. Thus, the complexity of the tumor biology and tumor microenvironment (TME) cannot be fully understood without studying all the cellular components, the secreted proteins (such as cytokines), the proteins involved in the formation of the tumor extracellular matrix, and their complex interactions [31]. Tumor cells can be found at different differentiation stages with distinct proliferative potential and tumor-forming ability. This heterogeneity of the tumor cell types leads to variability across surface marker expression, tumor growth rates and response to therapy [33, 34]. Finally, the components of the TME may vary significantly among different patients (inter-patient) and may evolve in the same patient (intra-patient) due to the natural course of cancer pathogenesis or to external factors such as chemotherapy [31, 35].

PDXs recapitulate partially the inter- and intra-tumoral heterogeneity, including both cell-autonomous (genomic and epigenomic heterogeneity) and non-cell-autonomous (stromal heterogeneity) factors (**Figure 2**). In breast cancer, for instance, DeRose *et al.*, Zhang *et al.* and Reyal *et al.* showed that PDXs maintain the essential features of the original tumors such as gland formation and keratin deposition, gene expression profiles, imaging characteristics, clinical biomarkers and drug sensitivity patterns [20, 36, 37]. De Rose *et al.* evaluated DNA copy-number changes of each tumor and the corresponding tumor graft, including different PDX passages, and concluded that xenografts share almost all single-nucleotide variations, with the exception of some specific clusters that are dominant in the PDX but not in the tumor patients [20].

#### **1.3.2. Resistance and progression**

Different response to therapy across the cells of a tumor can lead to the selection of pre-existing clonal tumor cell populations. Such drug resistant cells have a clinical implication in patient-specific responses to therapy that lead to disease progression or metastases [38, 39]. For instance, Diaz *et al.* suggested that the presence of a minor KRAS-mutant clone within a tumor predicts the development of resistance to epidermal growth factor receptor (EGFR) targeted therapy in patients with colorectal cancer [38]. In this context, PDX models can be used to study tumor clonal dynamics and evolution to chemoresistant phenotypes. Bruna *et al.* analyzed 104 samples from 22 PDX models established from patients with breast cancer. Using whole exome sequencing, they studied the clonal architecture in individual samples and clonal dynamics upon engraftment and across different passages [40]. Results showed that clonal heterogeneity present in the patient tumor samples and

their matched PDXs was similar. The preservation of the sub-clonal families in PDXs is crucial to identify the clones at higher risk to show resistance to treatment and, therefore, to develop disease progression in the clinical practice [40, 41]. For instance, Cassidy *et al.* showed that breast cancer PDXs established from patients tumors with multiple sub-clone populations (polygenomical tumors) were more resistant to therapy than tumors with homogenous clonal population (monogenomical tumors) [42].

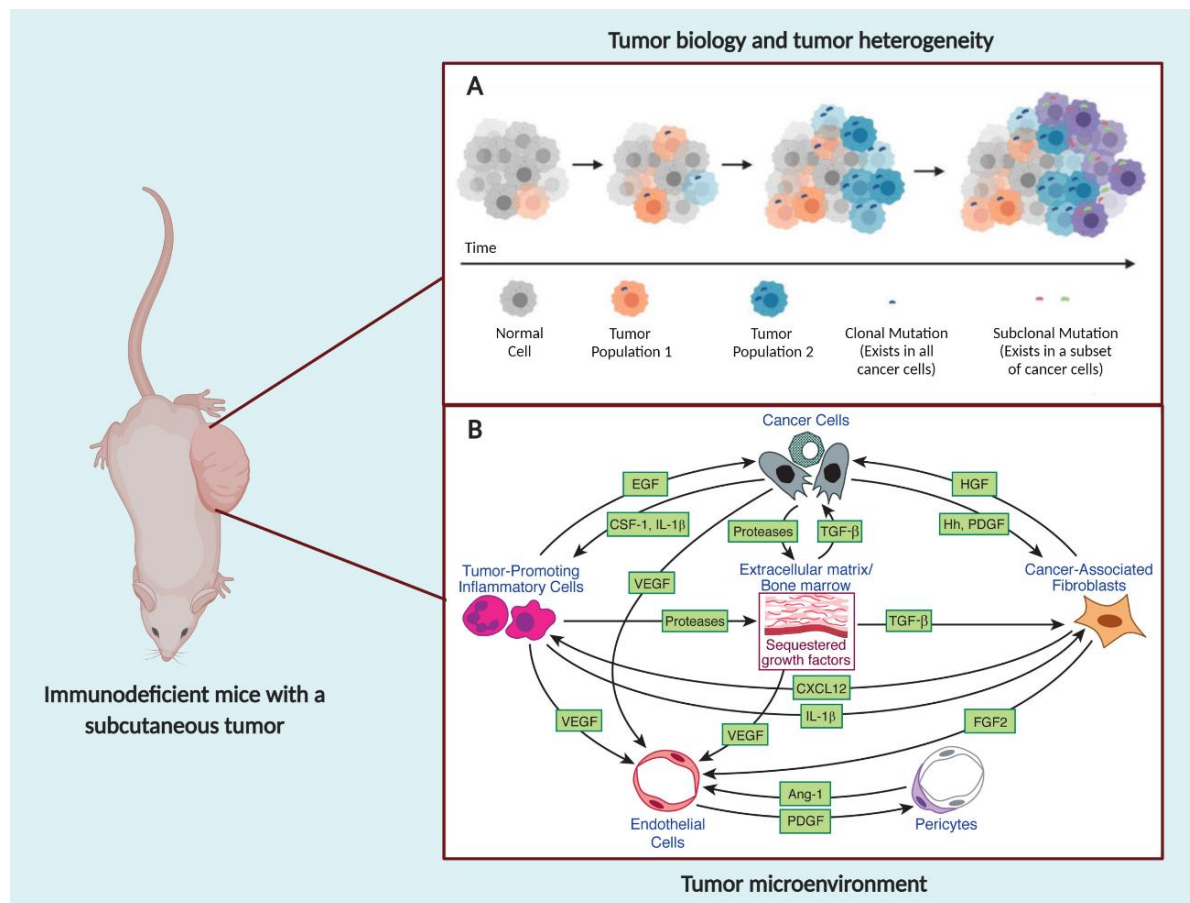


**Figure 2. Heterogeneity of the cellular components of PDXs.** A) Representation of the clonal evolution and development of tumor heterogeneity in tumors. Figure modified from El-Sayes *et al.* [43]. B) Representation of the assembly and collective contribution of assorted cell types constituting the TME, which are orchestrated and maintained by reciprocal heterotypic signaling interactions. Figure modified from Hanahan *et al.* [31].

Another strategy to study drug resistance is to develop laboratory PDX models exposed to chemotherapy at high intensity. In this approach, we select tumors sensitive to a specific drug and treat them with consecutive cycles of the agent to study when and how resistance occurs. Sequencing of such laboratory models (naïve vs resistant) may identify novel mechanisms of resistance. Schueler *et al.* developed three resistant PDXs from one naïve lung cancer PDX model after multiple rounds of treatment with gefitinib, an EGFR inhibitor [44]. They sequenced the exomes of such resistant models and compared them to the original PDX. They found that 85% of the mutations were shared in the four PDXs (504 genes in total).

A smaller subset of mutations was shared by at least two PDXs (26 to 42 mutated genes shared) or was even unique for one specific PDX (26 to 53 unique mutated genes). As a result, the original PDX clustered separately from the three resistant models by hierarchical clustering. Proteomic analysis showed that pathways involved in the newly resistant PDXs were related to DNA topoisomerase type I activity, cell cycle checkpoints, homologous recombination and DNA repair, among others [44].

Acquired resistant PDXs are also useful to evaluate alternative therapies subsequent to chemoresistance. Das Thakur *et al.* developed a melanoma PDX resistant to vemurafenib, a specific inhibitor of V600E-mutated *BRAF*. They proposed that overexpression of mutated *BRAF* caused resistance [45]. They observed *in vivo* that the continuous administration of vemurafenib selected the drug-resistant tumor cells and all tumors grew until endpoint within 100 days. In contrast, mice treated with the intermittent dosage did not develop drug resistance and survived longer than 200 days. These results suggested that continuous administration promoted clonal expansion of drug-resistant cells, while intermittent dosing could eliminate the fitness advantage of the drug-resistant cells in the absence of the drug and, consequently, delayed the progression of the disease [45]. Similarly, Monsma *et al.* developed a resistant alveolar rhabdomyosarcoma PDX after three cycles of ifosfamide, carboplatin, etoposide and paclitaxel therapy (ICE-T) in order to replicate the clinical resistance observed in the patient [46]. Their aim was to identify potentially active therapies in the resistant PDX model in the context of personalized medicine. They tested a series of drugs selected based on tumor transcriptome analysis using a panel of drug prediction algorithms comparing the initial vs resistant PDXs. The drugs selected included ICE-T (as the standard of care treatment for recurrent metastatic alveolar rhabdomyosarcoma), BGJ398 (fibroblast growth factor receptor 2 (FGFR2) inhibitor), sorafenib (multikinase inhibitor), cytarabine (substrate of the equilibrative nucleoside transporter 1 (SLC29A1), which was overexpressed in the resistant model) and sirolimus (mammalian target of rapamycin (mTOR) inhibitor). They observed that the ICE-T resistant PDX and the initial PDX showed similar sensitivity to BGJ398 and sirolimus. Cytarabine was not tested in the initial PDX as the overexpression of SLC29A1 was only observed in the resistant PDX. Cytarabine produced significant regression of the resistant PDX and delayed tumor re-growth after treatment, showing the greatest efficacy of the drugs tested [46]. This work, among others, supports the rational selection of drugs based on the genomic and proteomic profiles of the PDX tumor, both at initial and after acquired resistance as a strategy for precision studies [46-48].

### **1.3.3. Patient prognosis**

Not all tumor biopsy samples from cancer patients engraft successfully in immunodeficient mice, and this may be related to the aggressiveness of the original

tumor [49]. Thus, it is likely that patients whose tumors engraft in mice have poorer prognosis. Preclinical investigations in melanoma, breast, pancreatic and lung cancer demonstrated that successful engraftment is associated with a poorer prognosis in patients [20, 29, 50-53].

Garrido-Laguna et al. found that pancreatic ductal adenocarcinoma tumors engrafting in mice are often SMAD4-mutants, have a metastatic gene expression profile and are associated to worse prognosis. They showed 81% reduction in the risk of death in patients whose tumor samples failed to engraft in mice [53]. Stewart *et al.* showed that successful establishment of PDXs from EGFR-mutant lung cancer was a strong marker of poor prognosis that correlated with higher rates of recurrences. They suggested that the PDX engraftment correlated with more clinically aggressive tumor biology [29]. Nicolle *et al.* showed that the engraftment of pediatric hepatoblastoma was strongly associated with elevated circulating alpha-fetoprotein levels in patients, low rates of necrosis or fibrosis in the tumor specimen after treatment, and gain of chromosome 20. All three characteristics have been described as indicators of resistance to chemotherapy and poor outcome, and therefore, they suggested that the ability of these samples to establish a PDX model was predictive of poor prognosis [54].

Despite the increased use of PDX models in pediatric cancer, few studies have reported the relationship between engraftment of tumor samples and clinical outcome. To address this question, in my PhD work we addressed whether the parameter “PDX engraftment” was useful to identify pediatric sarcomas at risk of relapse. We attempted to establish PDX models from the most frequent pediatric sarcomas and used the available clinical data to calculate median event free survival and overall survival. We compared the survival rates of patients grouped according to the engraftment status (positive or negative) of their tumor biopsies in mice.

#### **1.3.4. Preclinical research and personalized cancer therapy using mouse avatars**

Clinically relevant preclinical oncology models must predict the safety and efficacy of candidate treatments in clinical trials (**Figure 3**). Mouse PDXs help preclinical researchers to identify and evaluate the biological relevance of actionable drug targets and novel biomarkers. PDX can also be used to establish a therapeutic window between efficacy and toxicity of candidate drugs [55]. Prediction of clinical efficacy of novel treatments using PDX is more accurate than using *in vitro* models [16]. Therefore, pharmaceutical companies have generated an extensive collection of PDX models, known as the PDX Encyclopedia at Novartis. The goal of this platform, which currently contains more than 1000 PDX models, is to reduce the number of preclinical anticancer drugs that fail in clinical trials [56]. Also, the US National Cancer Institute decided to stop screening most drugs using the NCI-60,

its panel of 60 human cancer cell lines grown in culture, and replaced them with a new PDX platform [57].

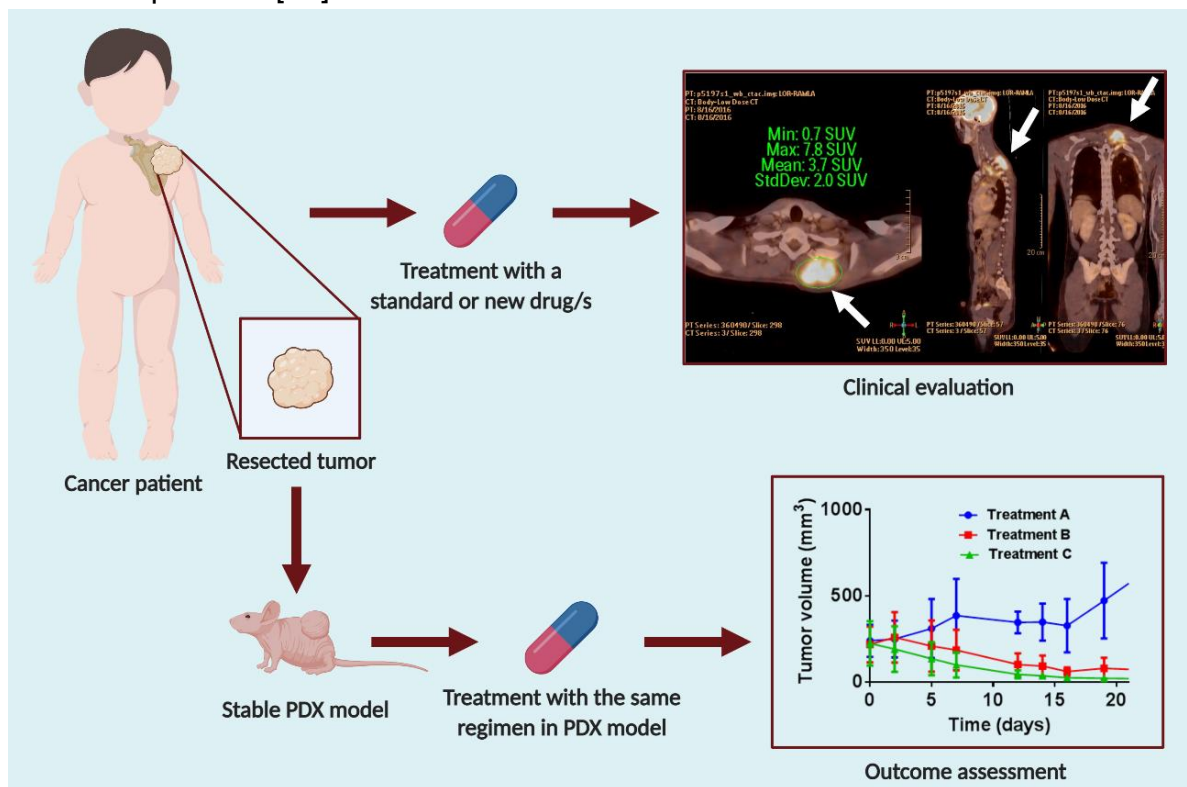


**Figure 3. PDX models to evaluate treatment response.** Scheme showing the parallel use of PDX to test the efficacy of standard or investigational anticancer drugs received by the patient. This approach allows the correlation analysis of treatment in PDX and patient. In the example, response to treatment of an 18 years old patient with a relapsed Ewing sarcoma tumor in the scapula was evaluated by positron emission tomography – computed tomography (PET/CT), while response of his PDX was evaluated by the analyses of tumor volumes upon treatment

Genomic and proteomic analyses of the tumors provide additional support for the rational design of precision medicine studies in the PDXs, which are also known as mouse avatars [13, 58, 59]. The main purpose of this strategy is to identify and develop personalized medicine treatments and to eliminate the toxicities and cost of useless therapies (**Figure 4**) [58]. With the development of personalized programs and the molecular stratification of patients, it is more suitable to deliver the most appropriate therapy at the right dosage [60].

Experiments in individual PDX help evaluate experimental or second line treatments before administration in patients [9, 13, 16]. This ideal scenario is still challenging to apply in the clinical practice, due to the timely and costly process of PDX establishment and propagation for therapy testing. Nevertheless, some clinical trials have applied the concept of individualized PDX models to guide patient therapy at disease relapse [13-15]. For patients with multidrug resistant prostate cancer, there is a clinical trial (NCT03786848, recruiting) whose principal objective is to generate PDXs to select optimal individualized treatment. A similar clinical trial (NCT02732860, recruiting) aims to identify agents with predicted activity in PDXs



from patients with breast, colorectal and ovarian cancer. This trial also performs comprehensive genomic and epigenomic analysis of the tumors. In another example, bevacizumab, a humanized monoclonal antibody that targets VEGF-A, was approved by US Food and Drug Administration in 2004 after years of preclinical development in human PDX models of colorectal and renal carcinoma [61-63]. Similarly, studies using pancreatic cancer PDXs supported that the combination of gemcitabine and nab-paclitaxel modulate tumor stroma and thus increase the intratumoral gemcitabine concentrations. This observation led to phase I-II clinical trials [16, 64, 65].

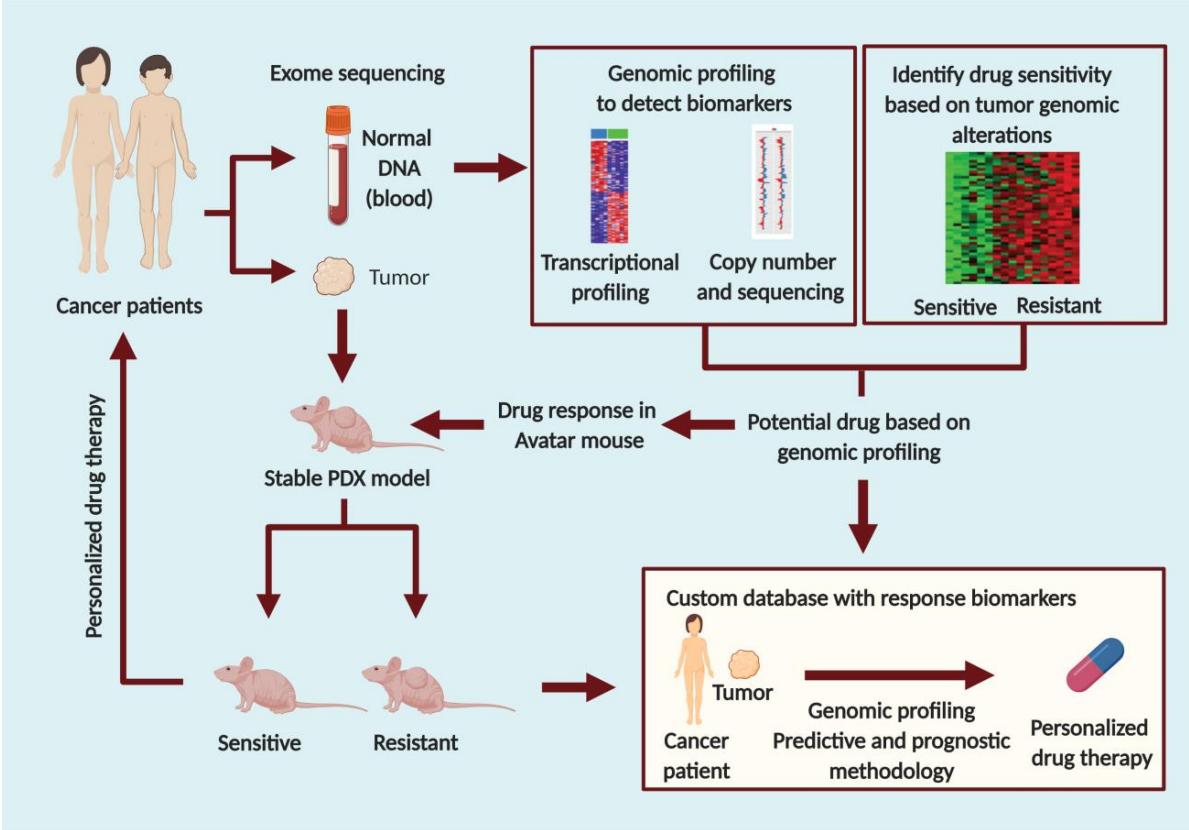


**Figure 4. Precision medicine strategy through the integration of genomic analysis and PDX.** Data from individual precision medicine studies (light blue background) feed databases to establish prospectively biomarkers for therapy response (yellow background). Figure adapted from Hidalgo *et al.* [9].

In published studies, Morelli *et al.* showed a case report of a 29 year old woman with an advanced adenoid cystic carcinoma with brain and liver metastasis that showed resistant to standard of care treatments including surgery, radiation therapy and several lines of conventional treatment such as platinum, anthracyclines and imatinib mesylate [14]. In this study, they generated a PDX from a brain metastasis and treated this model with 22 conventional and experimental treatments. The mouse avatar was sensitive to abraxane, temozolomide, IGF1R, mTOR and FGFR inhibitors. The patient was enrolled in a phase I trial with an IGF1R inhibitor in combination with an EGFR inhibitor that was available at the time of this study and oncologists save the other treatments as opportunities for the future. Treatment

showed good safety profile and resulted in a control of the liver tumor but a progression of the brain lesion. The good correlation observed between the PDX and the patient responses supported the use of this platform to test experimental agents before the administration or the enrollment of patients in clinical trials [14]. Fichtner *et al.* showed similar results in 15 PDX established from colorectal cancer patients treated with 5-fluorouracil, irinotecan or oxaliplatin. Response to chemotherapy in patients agreed with the one in matched corresponding PDXs [66]. Nemati *et al.* demonstrated that response to temozolomide of a cohort of 29 uveal melanoma PDX predicted the clinical efficacy in patients [50]. Pompili *et al.* summarized data from several studies using PDX models established subcutaneously or orthotopically (PDOX) (**Table 2**). Their review supports the use of PDX platforms to test conventional and experimental drugs before the administration into patients or while patients are undergoing initial treatment [67].

Because not all patient biopsies will produce PDX models upon transplantation to mice, new research efforts analyze data from large cohorts of PDX to identify molecular characteristics that stratify patient response to treatments. Hidalgo *et al.* in 2011 tested 63 drugs in 14 PDX models from chemorefractory tumor cells from patients with advanced cancer, resulting in 232 treatment regimens. This approach produced powerful resources to identify suitable personalized treatments in a selected cohort of patients (**Figure 4**). The discovery of predictors of sensitivity and resistance to cetuximab, an inhibitor of the EGFR, provides an example of successful retrospective analysis of PDX data [9].



**Table 2. The predictive value of PDXs for clinical response.** Modified from Pompili *et a* [67].

<b>Tumor histotype</b>	<b>Authors</b>	<b>Model<sup>a</sup></b>	<b>Treatment/Molecular alterations</b>	<b>Correspondence with patients<sup>b</sup></b>
Breast cancer	Marangoni <i>et al.</i> [68]	PDOXs (7)	Docetaxel, 5-fluorouracil, trastuzumab	5/7
	Zhang <i>et al.</i> [36]	PDOXs (10)	Docetaxel, doxorubicin, trastuzumab + lapatinib	10/10
Colorectal cancer	Bertotti <i>et al.</i> [69]	PDXs (85)	Cetuximab, panitumumab	85/85
Ovarian cancer	Ricci <i>et al.</i> [70]	PDXs (11)	Cisplatin	9/11
	Topp <i>et al.</i> [71]	PDXs (10)	Cisplatin	10/10
Small cell lung cancer	Anderson <i>et al.</i> [72]	PDXs (8)	Cisplatin, etoposide	7/8
Colorectal cancer	Nunes <i>et al.</i> [73]	PDXs (52)	WT KRAS (8/52)	8/8 responded to cetuximab
	Bertotti <i>et al.</i> [69]	PDXs (85)	KRAS mutated (18/85)	18/18 not responded to cetuximab
Non-small cell lung cancer	Zhang <i>et al.</i> [74]	PDXs (10)	EGFR mutated (1/10)	1/10 responded to gefitinib

<sup>a</sup> In parenthesis is reported the number of PDXs or PDOXs evaluated

<sup>b</sup> Mice were treated with the same protocol used for the patients and the response was compared

### **1.4. Challenges and limitations of PDX models**

Institutional programs to establish, store, maintain and use PDXs come with several associated challenges. One of them is the immense amount of resources needed to establish (and maintain) the *in vivo* models and to obtain, classify and store their derived samples in a biobank during unlimited time. Sample biobanking, including snap-frozen and cryopreserved samples, is essential, for instance, to develop international collaborations in order to increase the molecular diversity of cancer types representations that would be unlikely to be achieved through a single institution effort [10]. This is especially important in the case of rare cancers, such as pediatric solid tumors. The lack of robust standards for reporting PDX models, including nomenclature, standardized passaging methods, etc., could be a relevant drawback for researchers to find consistent PDX models and their associated data [10, 75]. Meehan *et al.* published in 2017 the PDX minimal information standards (PDX-MI) as a guide to define the “essential” and “desirable” attributes that are required for accurate description and reporting on PDX models [75].

Some samples require prolonged intervals to establish and engraft in mice, frequently months, whereas only a minority grows within a few weeks of implantation [9, 24, 76]. This period for the generation and propagation of PDX is a major limitation for establishing large cohorts of PDX mice for precision medicine testing [13, 53]. A second limitation of the PDX is the replacement of the human tumor stroma components (such as cancer-associated fibroblasts, endothelial cells, tumor associated macrophages and tumor associated lymphocytes) by mouse stroma, affecting predominantly the architecture and function of the TME [7, 16]. This limitation is especially important in studies involving cancer therapies that target the microenvironment, such as anti-VEGF therapies (bevacizumab) and immunotherapies [16]. In this regard, a third limitation is that immunodeficient mice lack an intact immune system, which is necessary to screen immune-modulating drugs or antitumor vaccines [77]. Part of these limitations has been overcome by the development of humanized immune system mice [10].

The fourth limitation arises from the not universal growth of all tumor biopsies in mice. Because tumors are heterogeneous and evolve towards a process of clonal expansions, it becomes important to determine which subclones engraft in patients. PDX would select for treatment-resistant subclones that are present at a minor proportion in the primary tumor and predominate in metastatic disease [78, 79]. Consequently, Collins *et al.* proposed the establishment of multiple PDX models from an individual patient to obtain a better representation of the original tumor heterogeneity [80]. Because the most aggressive tumors are easier to establish and propagate, there is an unbalanced representation of less aggressive tumors in the PDX portfolio [7, 10]. Thus, the study of tumor biology using cohorts of PDX models from different cancer types could be biased and only represent the most aggressive disease subtypes.

A fifth limitation is time. PDXs can show extended latency periods for the establishment and propagation of models, compared to cell lines. Cells in culture provide unlimited supply to inject in mice, with a short latency until tumors are palpable in xenograft mice [17, 81]. Consequently, guiding the therapeutic decision of the patient as first line treatment using the PDX data is difficult to accomplish, because when the efficacy information from the model becomes available, the donor patient could have already undergone multiples rounds of therapy or could have even developed chemoresistance to treatment [82]. To overcome this limitation, recent developments in computational biology, -omics technology and drug development lead to a “PDX-free” targeted therapy approach that selects treatment according to patient-specific genetic aberrations. This strategy is also known as “molecularly guided targeted therapy”. In a phase I clinical trial performed at MD Anderson Cancer Center in patients with advanced cancer, this approach obtained a response rate of 12%, compared to 5% using non-matched therapy [83]. Nevertheless, 12% response rate is still a modest achievement, which could be attributed to the fact that current computational technologies could not distinguish between driver and passenger mutations, and tumors harbor multiple aberrations of both types [84, 85]. Therefore, Pan *et al.* proposed an innovative model that combines the molecularly guided approach with functional analysis in a PDX platform, to select treatments for patients with bladder cancer [82].

The sixth limitation of the PDX is that experimental results of drug efficacy do not always correlate with clinical results, which is likely due to differences in drug pharmacokinetics between humans and mice [13, 86, 87] (**Table 2**). In addition, because personalized medicine studies are still labor intensive and expensive, only a selected and limited number of drugs and combinations can be chosen to test in the PDX. The incorporation of genomic and proteomic analysis of the tumor samples to perform a primary selection of candidate drugs could optimize the selection of candidate treatments to test [88]. However, especially in pediatric patients, the access to certain drugs could be restricted even after being selected as a candidate for personalized medicine [10]. Ethical concerns due to insufficient pediatric data for off-label drugs, or unavailability of age-appropriate oral formulations have hindered several pediatric studies [89].

### 2. Microdialysis sampling

#### 2.1. Microdialysis for *in vivo* investigation

Microdialysis is a minimally invasive sampling technique developed in the beginning of the 1970s [90-92]. This technique allows continuous sampling of both exogenous and endogenous free analytes from interstitial tissue fluid *in vivo* from virtually any tissue [93-95]. The *in vivo* microdialysis technique consists on the insertion of a dialysis probe into an organ or tissue in the body in order to sample protein-unbound analytes in the extracellular fluid (ECF) in awake animals without the need of sacrificing large series of animals [92, 95-98]. Improved restraining methods allow free-mobility of individuals used in the studies, reducing stress and increasing animal wellbeing [92, 94, 99, 100].

#### 2.2. Principle

Microdialysis was originally developed for the measurement of the dynamic release of endogenous compounds with low molecular weight (including neurotransmitters, glucose, lactate or pyruvate), usually in the ECF from animal brains. Sampling of pharmacological agents in pharmacokinetic studies, mostly in rodents, is the second most important use of microdialysis [90, 100]. Recent years have seen an increasing number of studies reporting clinical microdialysis sampling in patients [92, 101]. Initial studies in humans aimed at sampling the subcutaneous adipose tissue, although the technique rapidly evolved to be applied in human brains [97, 102-104].

The procedure involves the insertion of a catheter into a body tissue. In general, the semi-permeable membrane is located at the tip of the catheter, although sometimes it is located in the middle (linear probes). A perfusion fluid, similar in composition to the ECF, is slowly and continuously pumped through the inlet tubing at low flow rates ranging from 0.1 to 5  $\mu\text{L}/\text{min}$ . Under these conditions, analytes that are more concentrated in the ECF than in the perfusate penetrate the microdialysis membrane by concentration gradient-driven diffusion [91, 92, 96, 97]. The dialysate is the solution that exits the probe and contains small organic molecules, inorganic ions, drugs or other molecules that passively diffuse down their concentration gradients (**Figure 5**). In ideal conditions, there is no water exchange between the perfusate and the ECF and the recovered volume should be equal to the perfused one. The dialysate leaking from the outlet tubing of the catheter is collected in vials at regular time intervals, which are chosen based on the desired collection volume, solute of interest, perfusion rate, etc. Finally, the dialysate is sent to analysis [91]. When the analyte of interest is a small molecule, highly sensitive analytical methods such as High-Performance Liquid Chromatography (HPLC) with tandem mass spectrometry detection (MS/MS) are then needed to detect low concentrations in low volumes of the dialysate [96, 105].

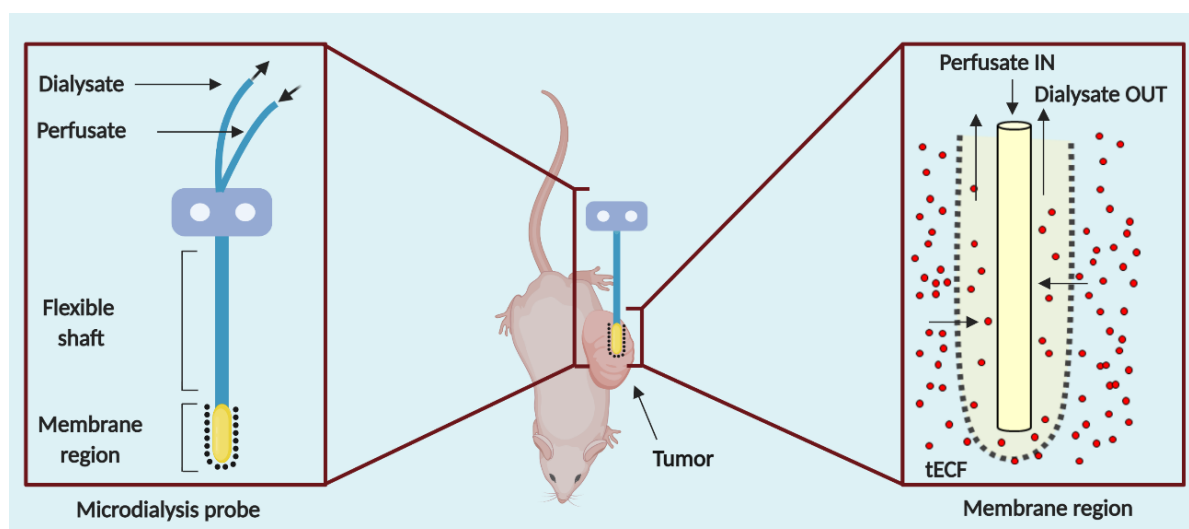


**Figure 5.** Scheme of a microdialysis probe with a semipermeable membrane inserted in a subcutaneous tumor engrafted in one mouse. The semipermeable membrane at the tip of the probe allows the diffusion of analytes along concentration gradients. The perfusate enters the central portion of the probe under a constant flow rate. Then it moves to the outer compartment of the probe where it contacts with the tumor extracellular fluid (tECF) and the solute under investigation (red drops) is collected in the dialysate tubing. The direction of the flow through the probe is indicated with black arrows.

The perfusate flow rates used in microdialysis are low, but they are enough to renew the fluid continuously at the semipermeable membrane, simulating sink conditions. Therefore, the complete equilibrium of concentrations between both sides of the membrane is not reached [92, 93, 96] (**Figure 5**). Using perfusates with physiologic concentrations simulating the composition of the ECF, the analyte concentrations measured in the dialysate are always a fraction of the actual levels in the tissue. Such fraction is known as the relative recovery (RR) and it is defined as the ratio of drug concentrations in the dialysate and in the tissue sampling site. Thus, to measure the real concentration of an analyte in the tissue of interest it is necessary to determine the RR using a calibration method [91, 93, 94, 100].

Several factors affect the RR of the probe *in vivo*, including: (a) perfusate flow rate and composition; (b) composition and dimensions of the material used for microdialysis experiments, such as the probe membrane polymer, probe length, probe membrane permeability or diameter cut-off, tub material and diameter; (c) probe location and tissue temperature; (d) physicochemical properties of the analyte such as molecular weight or molecular charge; and (e) interactions between the analyte of interest and the tissue to be sampled [90-92, 94, 96, 97, 106]. To calibrate probes (i.e., to assess the RR to determine the concentration of any substance in the ECF), the calibration conditions must reproduce, ideally *in vivo*, the properties of the targeted tissue and the factors mentioned above [90, 91, 96, 107]. Some of the most common *in vivo* calibration methods need to be performed at constant (steady-state) concentration of the sampled molecules. These methods are known as “extrapolation to zero flow rate”, “point of no net flux”, and “slow

perfusion method” [92, 94, 97, 108, 109]. At our laboratory, we apply the zero flow rate method for the hydrophobic camptothecin SN-38 (the active metabolite of the prodrug irinotecan), which achieves steady state concentration in the mouse blood upon constant rate subcutaneous perfusion of irinotecan [99]. This method assumes that (i) there is constant ECF concentration of the analyte in plasma (i.e., calibration is performed at the steady state of the analyte in blood) and (ii) there is an exponential relationship between RR and flow rate through the microdialysis probe [99, 100, 108].

The “retrodialysis” is another method to calibrate the probes. In this case, the exogenous analyte is added at a known concentration into the artificial ECF (i.e., the perfusate), and perfused through the microdialysis probe inserted in the sampling tissue. Thus, this is the reverse process of the usual sampling system, because the exogenous compound dissolved in the perfusate diffuses from the probe to the ECF. RR is calculated as the ratio of the compound concentrations in the dialysate and in the perfusate [100]. In order to perform this method, there must be no exogenous analyte present in the tissue, i.e., it must be performed either before the administration of the exogenous analyte to the animal, or after the total clearance of the analyte at the sampling tissue [92, 94].

### **2.3. Microdialysis as a sampling method for hydrophobic anticancer drugs**

The physicochemical properties of a drug of interest affect the diffusion process through the probe membrane and, consequently, modify the RR [93]. Hydrophilic drugs show equal values of RR by dialysis and retrodialysis when diffusing across a microdialysis membrane, while moderate or highly lipophilic drugs have dissimilar RR *in vivo* [93]. Lipophilic compounds bind to microdialysis tubing resulting in a low and usually non-reproducible RR [92, 93]. Loos *et al.* and Whitaker *et al.* showed low or erratic probe recovery due to non-specific binding in studies of the anticancer drugs docetaxel and doxorubicin [110, 111]. Thus, microdialysis experiments are more challenging to set up for hydrophobic drugs [112].

Modifications of the perfusate help overcome this limitation and allow the reproducible microdialysis of selected lipophilic compounds. Adding solubilizers such as 2-hydroxypropyl-beta-cyclodextrin (HPBCD) or albumin in the perfusion fluid prevent the non-specific binding into the tubing system [92, 93, 113, 114]. In a previous work of our laboratory, Carles Monterrubio developed a reproducible method for the assessment of the tumor pharmacokinetics of SN-38 in mice. He studied whether the nonspecific adsorption of SN-38 lactone to the plastic tubing of the microdialysis circuit could be prevented by increasing amounts of HPBCD, from 0% to 10%. The results showed that in the absence of HPBCD SN-38 lactone binds to tubing, while the addition of increasing percentages of HPBCD reduced the binding up to zero at 10% of HPBCD [99].

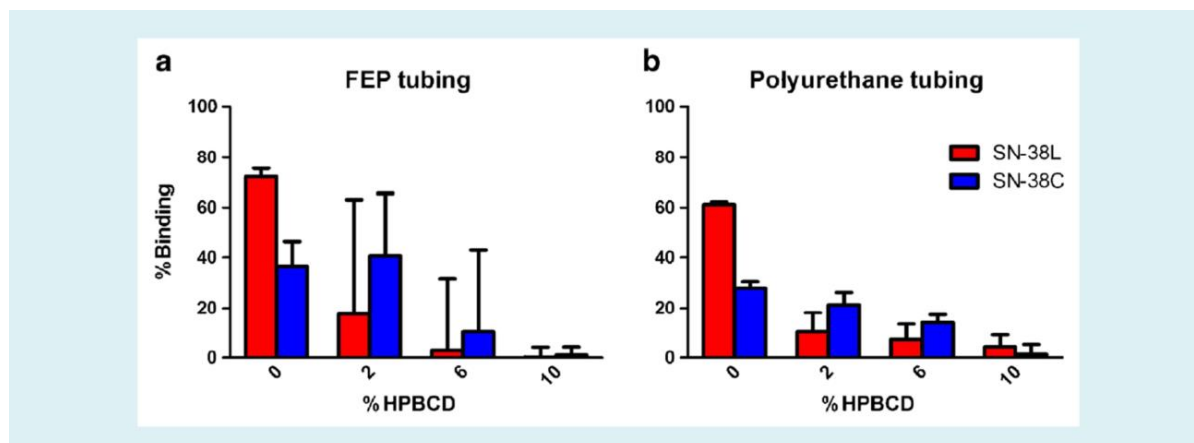


**Figure 6.** Binding of SN-38 C (SN-38 carboxylate; water-soluble) and SN-38 L (SN-38 lactone; insoluble) to (a) FEP (fluorinated ethylene propylene) and (b) polyurethane tubing perfused with SN-38 solution in 0, 2, 6, and 10% HPBCD in PBS. Figure reproduced from Monterrubio *et al.* [99].

The addition of some solubilizers to the perfusate modifies the osmotic pressure in the microdialysis membrane in the tissue under investigation [93, 115]. As a consequence, May *et al.* determined an enhancement effect of cyclodextrins on the uptake of anandamide, a lipophilic compound, when they placed a microdialysis catheter in subcutaneous adipose tissue of 20 healthy volunteers. They suggested that this enhancement could be explained because of the formation of a complex between the hydrophobic compound and the hydrophobic core of the cyclodextrins [116]. In agreement with these results, Monterrubio also described an enhanced relative recovery of the hydrophilic SN-38 lactone ( $f = 1.86$ ), but not of the hydrophilic SN-38 carboxylate ( $f = 1.07$ ), as a result of the use of HPBCD in the perfusate solution. The calculated enhancement factors were used to estimate the real concentration of SN-38 lactone and carboxylate in the tumor extracellular fluid of neuroblastoma PDX models [99]. In my thesis work, I have used this method to study the concentration of both forms of SN-38 lactone and carboxylate in Ewing sarcoma PDXs.

#### 2.4. Compartmental analysis of intratumoral drug distribution

A detailed characterization of the intratumoral drug distribution helps understand the efficacy of anticancer drugs [95, 96]. To exert their anticancer efficacy, therapeutic molecules must reach tumors at sufficient concentration for an adequate period of time [91, 117, 118]. Once in the tumor ECF, most molecules will find their targets intracellularly at the tumor cells. Thus, they need to cross the cell membrane barrier. In order to cross such barriers, molecules need to be unbound, i.e., they need to be free of protein binding at the ECF [95]. Because microdialysis does not allow protein-bound molecules to become dialyzed through the probe, this technique becomes important to determine the relative concentration of molecules at the extracellular and intracellular tumor compartments, when combined with the analysis of the same molecule in the whole tumor homogenate. Our laboratory published this procedure in the work by Monterrubio [99]. Our work was motivated



by previous studies applying intratumoral microdialysis. Zamboni *et al.* reported an intratumoral dose-response relationship between tissue concentration and efficacy using microdialysis experiments in tumor xenografts established from neuroblastoma and colorectal tumors, treated with cisplatin and camptothecins (such as irinotecan and topotecan) [119-121]. Smith *et al.* showed that Lipodox®, the generic equivalent for Doxil®, was less effective in recurrent ovarian cancer patients due to significant changes in doxorubicin pharmacodynamics. They used microdialysis to demonstrate that the distribution of Lipodox® formulation at the tumor tissue was decreased, compared to the one of Doxil®, in human ovarian orthotopic PDXs [122]. Using microdialysis, it is also possible to target different regions within a tumor. Pigatto *et al.* found that etoposide distribution was higher in the periphery than in the tumor center in a mammary solid tumor xenograft. This experiment used two probes simultaneously implanted in a single tumor. They concluded that etoposide plasma concentration is not a good surrogate for tumoral exposure [95].

We set up a technique to analyze the intratumoral drug distribution of the hydrophobic drug SN-38 at the compartmental level, combining the analysis of intratumoral dialysates, tumor homogenates and blood samples [99]. With the analysis of tumor homogenates, we determine total concentration of SN-38, both intra and extracellular, including the content of the vascular compartment. Using microdialysis, we determine the distribution of unbound SN-38 in the ECF. Then, we calculate the unbound drug volume of distribution in tumor ( $V_{u,tumor}$ ), measured in mL/g tumor. We use **equation [1]**, in which  $A_{tot,tumor}$  is the total amount of drug per gram of tumor homogenate (including tumor blood),  $V_{tot,blood}$  is the volume of blood per gram of tumor,  $C_{tot,blood}$  is the total concentration of drug in blood, and  $C_{ss,tumor}$  is the concentration of unbound drug in the tECF at the steady state [99].

[1]

$$V_{u,tumor} = \frac{A_{tot,tumor} - V_{tot,blood} \times C_{tot,blood}}{C_{ss,tumor}}$$

Intuitively, we can interpret that high values of  $V_{u,tumor}$  indicate high distribution of unbound drug in the intracellular compartment whereas low values suggest that the drug is predominantly in the extracellular space (**Figure 7**). Using this methodology, we previously characterized the distribution of SN-38 in tumors using SN-38-loaded nanoparticles or SN-38-loaded local drug delivery systems [99, 123, 124]. We did not use the method combining microdialysis and tumor homogenate, because the delivery systems would have interfered with the analysis. In my PhD work, we applied the combined microdialysis and tumor homogenate method to characterize the compartmental distribution of SN-38 upon administration of irinotecan infusions in paired PDX obtained from patients at different phases of their disease.



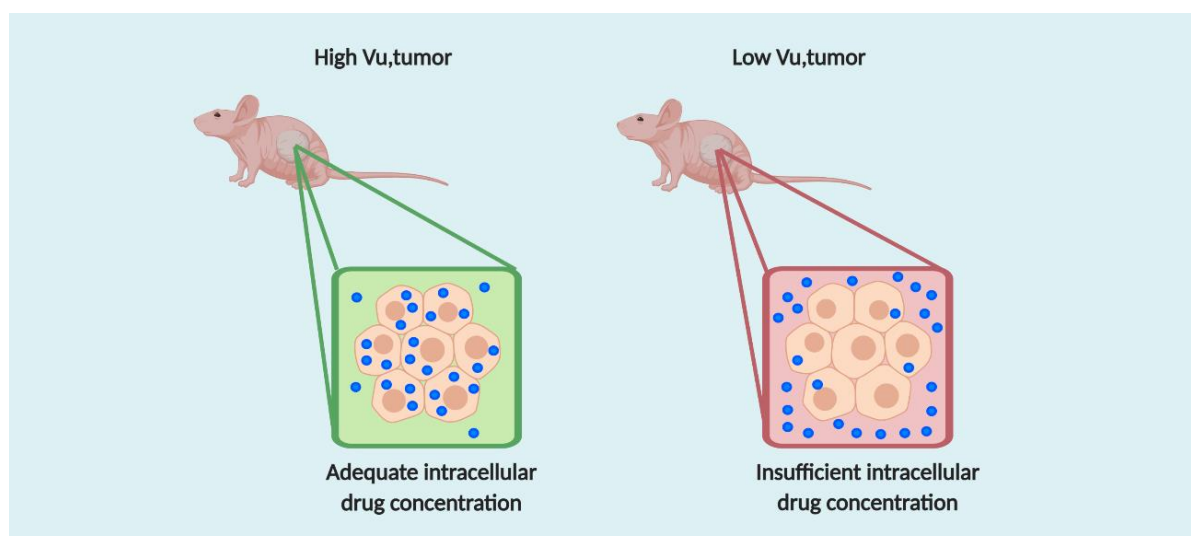


**Figure 7.** Graphical representation of high and low  $V_{u,tumor}$  values obtained with the combined microdialysis-tumor homogenate method. In the subcutaneous tumor with high  $V_{u,tumor}$ , represented in green, the intratumoral drug (blue dots) is mostly intracellular. In contrast, in the tumor with high  $V_{u,tumor}$ , represented in red, the intratumoral drug is mostly placed in the extracellular space.

## 2.5. Advantages and challenges of the microdialysis sampling

One of the main advantages of microdialysis is that dialysates are protein-free, allowing direct analysis of the unbound drug collected in the target tissue without having to apply extraction procedures to the sample [125]. A second important advantage is that dialysates can be collected continuously along hours or even days to obtain profiles of drugs or endogenous compounds over long periods. Consequently, animals needed in such experiments can be reduced to a minimum [92]. A third advantage, related to the long-lasting sampling, is the possibility to detect changes due to treatments applied during the procedure. For example, in previous work by my mentor Angel Carcaboso, microdialysis allowed to determine shifts in the compartmental distribution of topotecan upon the administration of a drug inhibiting drug efflux processes [126].

Tissue trauma caused by the insertion of the probe is one possible drawback of the technique [94]. Groothuis *et al.* suggested that the probe alters the blood brain barrier permeability, perturbing the concentrations of analytes in the extracellular space of the brain [127]. Thus, it becomes important to design appropriate control experiments, in which the technique is equally applied, to account for the effect of the tissue damage. Using the adequate controls of the experiment the technique can be satisfactory and damage to tissue, if any, can be well controlled. Hammarlund-Udenaes described that based on their experience, probes used to obtain analytes from brain should be placed at least 1 day before the experiment whereas in other tissues, such as muscle, tumor or subcutaneously, it is advisable to wait for 1 h in order to minimize the damage made by the insertion [92]. Other studies demonstrate that short waiting times around 1 h are also adequate for CNS sampling studies [128, 129].

The small volumes of dialysate, normally in the microliters range, are another limitation of the method. Thus, sample analysis requests highly sensitive analytical methods, such as HPLC coupled to MS/MS detection. Some laboratories developed a system where microdialysis is directly coupled to such detectors [94]. Alternative methods to the microdialysis addressing drug concentrations in tumor tissue include the non-invasive techniques nuclear magnetic resonance imaging (NMR) and positron emission tomography (PET). Nevertheless, these methods do not totally assess intratumoral drug distribution considering NMR has low spatial resolution and PET is unable to discriminate between bound and unbound drug [96].

### 3. Tumor chemoresistance

Drug resistance or chemoresistance is present in a small proportion of pediatric cancer patients from diagnosis, while a higher proportion acquires resistance to treatment after chemotherapy. In relapsed patients, the evolution of tumors towards a more resistant and aggressive phenotype could be produced due to acquisition of new mutations, adaptive response and natural selection of a drug-resistant tumor clone population [130].

One of the principal mechanisms inducing multiple drug resistance in tumor cells is the up-regulation of drug efflux processes. Multidrug resistance associated proteins (MRPs) are a subgroup of the ATP-binding cassette (ABC) transporter family that utilizes the energy from ATP hydrolysis to transport substrates across the membranes. A wide range of endobiotics (substrates produced in the organisms) and xenobiotics (substrates or chemicals found but not produced in the organisms) can be transported by MRPs. MRPs are not specific of cancer cells as they are also broadly found in normal tissue as the main functions of MRPs may vary from tissue defense to resistance to chemotherapy [131]. In tumors, MRPs mediate the outflow of a range of chemotherapeutic agents such as gemcitabine, doxorubicin, methotrexate, vincristine, etoposide and irinotecan, among others, thereby decreasing the intracellular drug concentration and drug exposure in tumor cells (**Figure 8**) [130-132]. The discovery of ABC transporters like multidrug resistance protein 1 (MRP1), ATP binding cassette subfamily G member 2 (ABCG2), also known as breast cancer resistance protein (BCRP) or P-glycoprotein (P-gp) as proteins responsible of multiple drug resistance identified these MRPs as novel targets for specific inhibitors [133, 134]. Norris *et al.* and Oda *et al.* showed that high-levels of MRP1 expression correlate with poor prognosis in primary neuroblastoma and soft tissue sarcoma [135, 136]. Similarly, Nakanishi *et al.* described that the overexpression of P-gp in a cohort of soft tissue sarcomas was associated with a less favorable prognosis and with high-grade tumors [137].

Zhang *et al.* showed an increment of the intracellular accumulation of chemotherapeutic drugs after inhibition of MRP1 in *in vitro* and *in vivo* studies due to the off-target effect of small molecular inhibitor known as ibrutinib [131]. This drug received the approval of the US FDA for the treatment of chronic lymphocytic leukemia. *In vitro*, ibrutinib effectively blocked the efflux of vincristine and doxorubicin in a leukemia cell line, leading to increased intracellular concentrations of these drugs. In *in vivo* xenografts, the combination of ibrutinib and vincristine resulted in a great inhibitory effect on the tumor growth compared with the treatments in monotherapy [131, 138]. In another study in ovarian carcinoma xenograft models, Ricci *et al.* showed that the specific antagonist of ABCG2, CID1434724, restored chemosensitivity to topotecan when administrated in combination *in vitro* and *in vivo* [133]. Despite intense clinical investigation of ABC transporter inhibitors, results of these trials have not shown significant therapeutic

activity in cancer patients [139]. First generation P-gp inhibitors had potent pharmacologic effects and toxicity whereas third generation seem to have minimal toxicity that is not dose limiting [140]. Tariquidar is a third generation inhibitor of P-gp and ABCG2. In Phase I studies, the coadministration of tariquidar and vinorelbine resulted in no significant side effects or pharmacokinetic interactions [141]. However, a Phase III trial in patients with lung cancer combining first-line chemotherapy such as paclitaxel, carboplatin or vinorelbine with tariquidar, was stopped due to increased toxicity [142]. Not sufficiently restrictive inclusion criteria of clinical trials could explain partially the poor clinical success of MDR modulators. Such trials included patients whose tumors had acquired resistance to chemotherapy through MDR mechanisms, but also due to other mechanisms). A second challenge to interpret clinical data is the modification of drug pharmacokinetics upon combination with MRP inhibitors [139, 142]. Despite these discouraging clinical trial results using MRP inhibitors, MDRs expression are still linked to poor outcome. Further investigation targeting the pathways regulating gene expression of these ABC transporters or using antibodies directly to MRPs will shed light into the clinical meaning of these targets to overcome cell resistance.

In my PhD work, I have studied whether changes in drug distribution within a tumor were related to the expression of some of the mentioned ABC transporters.

A second mechanism inducing chemoresistance is the epithelial to mesenchymal transition (EMT) of tumor cells [143]. Cancer cells acquire a mesenchymal phenotype with associated changes at the genomic and protein levels [130, 132, 144]. Mani *et al.* showed that the induction of EMT in mammary carcinoma cells promotes the acquisition of mesenchymal phenotype and the expression of stem-cell markers, which are able to efficiently generate new mamospheres. In this regard, they observed that this ability could be transmitted through serial passages of mamosphere-forming cells suggesting a heritable and self-renewing state of the EMT [145]. In cancer, EMT promotes cell invasion that leads to tumor cell dissemination to establish secondary tumors [134, 144]. Lawson *et al.* and Rhim *et al.* for instance, showed that circulating pancreatic tumor cells and metastatic breast cancer cells *in vivo* express stem cell markers associated to EMT [146, 147]. Fischer *et al.* and Zheng *et al.* demonstrated that primary and metastatic tumor cells become more resistant to chemotherapy depending on the EMT differentiation state using genetically engineered mice [148, 149]. Lu *et al.* suggested that therapies targeting control mechanisms of cellular plasticity, such as epigenetic regulators of EMT, could sensitize cancer cells to treatment [143]. However, we are still far from completely understanding the complex mechanisms involved in EMT and its pivotal role during tumor initiation, progression, metastasis and treatment resistance.

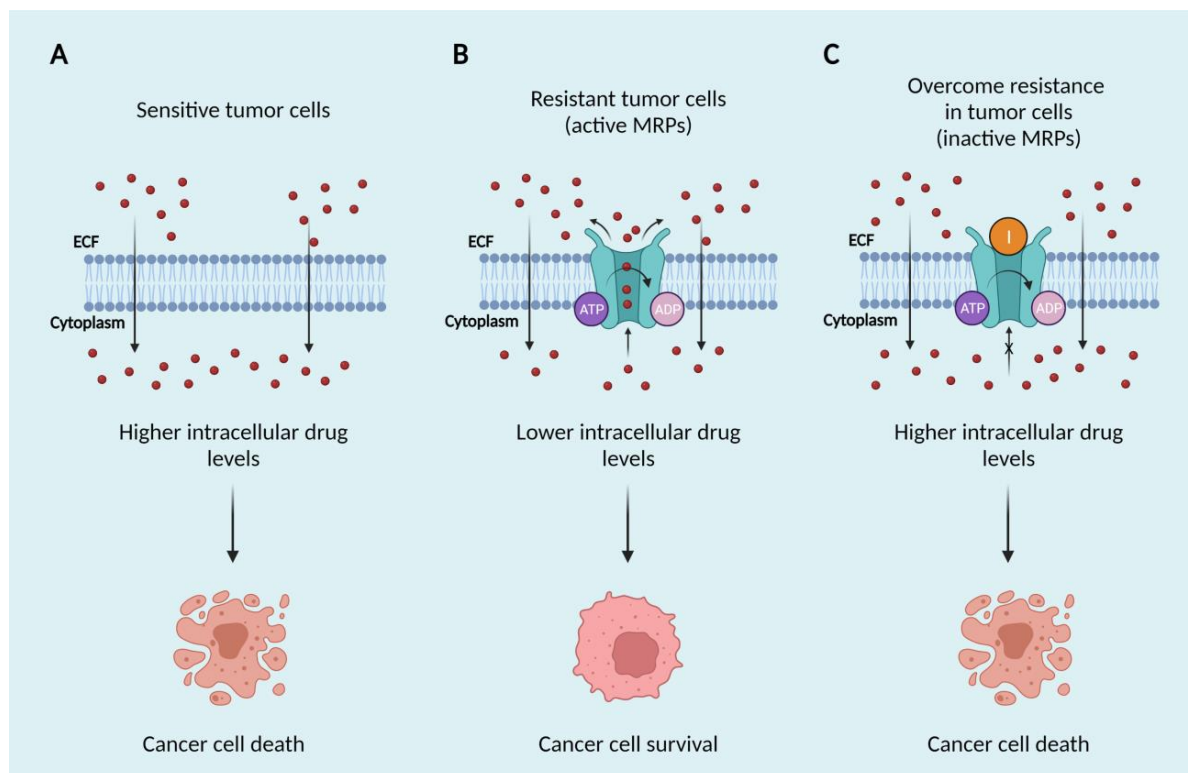


**Figure 8.** Scheme of the process of multidrug resistance acquisition in cancer cells. A) Plasmatic membrane at baseline in drug-sensitive tumor cells. Drug (represented as red dots) crosses the membrane by passive diffusion and accumulates intracellularly. The higher intracellular drug concentration leads to cancer cell death. B) Active MRP is present in resistant tumor cells. Drug crosses the membrane and it is rapidly transported across the MRP to the ECF by active transport when ATP is hydrolyzed to ADP. Drug could not accumulate in the cytoplasm and the lower level of drug intracellularly is not sufficient to cause cancer cell death. C) Inhibitor (represented as orange circle) inactivates MRP at tumor cells to overcome drug resistance. Drug crosses the membrane and is not expelled to the ECF. The inhibition of MRP allows the accumulation of drug intracellularly and drug sensitivity is restored in tumor cells.

A third mechanism leading to drug resistance is the up-regulation of oncogenes related to signaling pathways of tumor development and progression [134]. Liu *et al.* described that drug resistance of ovarian cancer is caused by more than 25 oncogenes that regulate the expression of growth factor receptors, signaling molecules, transcription factors, cell cycle and apoptosis regulators [150]. Apoptosis itself is another important factor associated with drug resistance. For instance, overexpression of anti-apoptotic BCL-2 family members, such as B-cell lymphoma 2 (BCL-2), B-cell lymphoma extra-large (BCL-X<sub>L</sub>) and Myeloid cell leukemia-1 (MCL-1) or downregulation of pro-apoptotic pore-formers factors, such as BCL-2 associated X protein (BAX), BCL-2 homologous antagonist/killer (BAK) and caspases is associated to drug resistance to taxanes and platinum [132, 134, 151, 152]. Campbell *et al.* and Inao *et al.* showed that MCL-1 expression likely contributes to breast cancer chemoresistance and specific MCL-1 inhibitors restored cancer cell sensitivity to doxorubicin [153, 154]. In this regard, the small molecule MCL-1 inhibitor, S63845 showed relevant efficacy *in vitro* and *in vivo* in preclinical mouse models of hematological malignancies [155]. Hassan *et al.*

described other proteins involved in drug chemoresistance, known as inhibitors of apoptosis proteins [132, 156]. These anti-apoptotic factors contribute to cisplatin resistance in ovarian cancer [157].

#### 4. Childhood cancer

Childhood cancer is a rare and heterogeneous group of malignancies that represent a small proportion, approximately 1%, of all cancers diagnosed worldwide each year [158, 159]. However, cancer is the leading cause of disease-related morbidity and mortality in childhood [160]. Pediatric cancers are different diseases with distinct patterns of occurrence, etiology, treatment, survival and risk of acute and long-term side effects with an underlying pathogenesis that in most childhood cancers remains largely unknown [161, 162]. Overall survival has improved from 30% in the 1960s to more than 80% in most high-income countries and around 40% in most low and middle-income ones (**Figure 9**) [158, 159, 163, 164]. Improvement in survival is the consequence of substantial advances in diagnostics, pharmacology, treatment combinations, novel techniques and supportive care during the last decades [158, 165]. However, the outcome of childhood cancer patients not only depends on such improvements but also in the type of malignancy, age, anatomical site, stage of the disease in solid tumor and somatic genetic lesions [161].

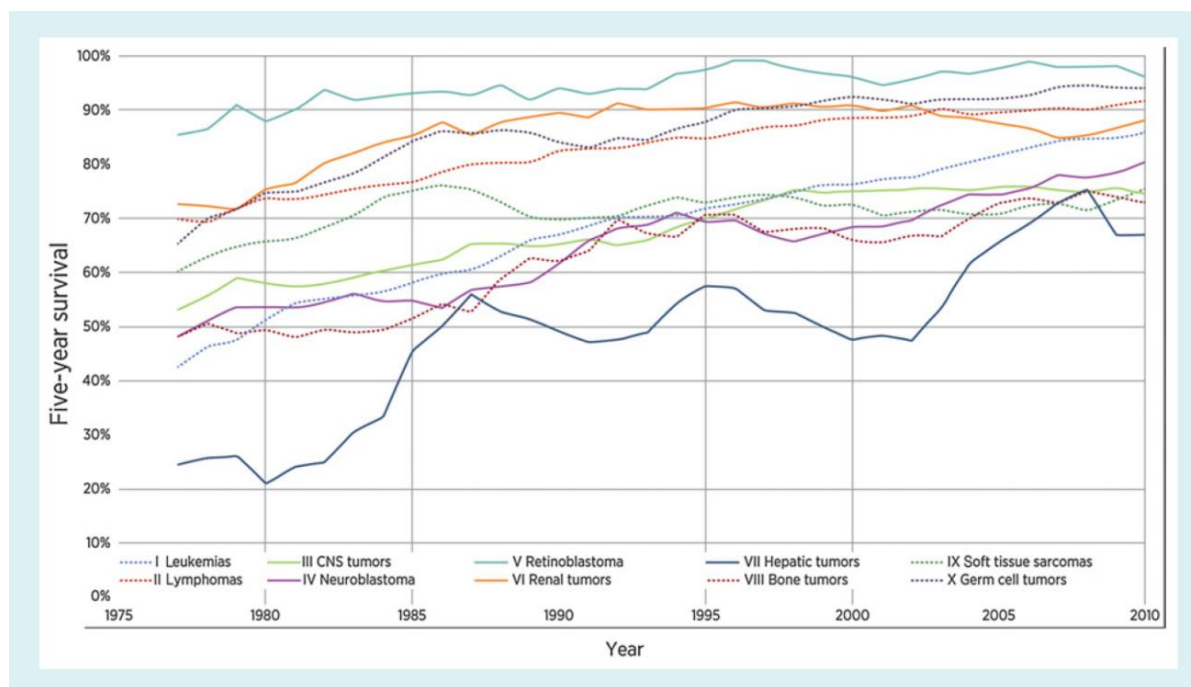


**Figure 9.** Improvements in 5-year survival for childhood cancer in high-income countries, 1975 – 2010. Figure reproduced from Lupo *et al.* [159].

Cancer in children and young adults are fundamentally different from the cancers seen in adults in terms of epidemiology, cellular origin, and response to therapy, among several other factors [158, 166]. Recent pan-cancer next generation sequencing analyses have demonstrated that the mutational burden in most childhood cancers is substantially lower than in adult cancers (**Figure 10**) [159]. Fusion genes are more common in pediatric than in adult malignancies, suggesting



that epigenetic dysregulation is important for the development of many forms of childhood cancer (**Figure 10**) [160, 167, 168].

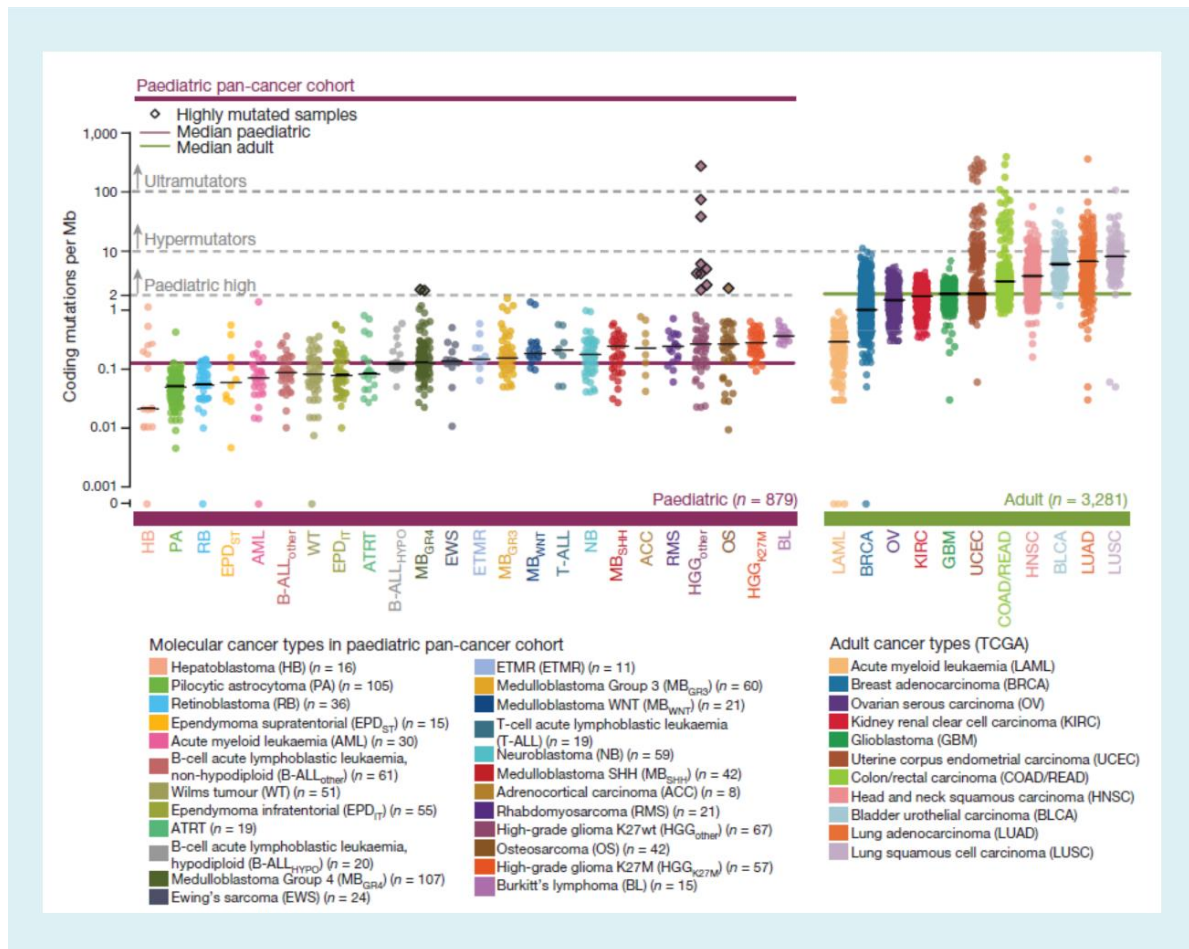


**Figure 10.** Somatic mutations in the pediatric pan-cancer cohort. Somatic coding mutation frequencies in 24 pediatric (n = 879 primary tumors) and 11 adult (n = 3281) cancer types (The Cancer Genome Atlas, TCGA). Hypermutated and highly mutated samples are separated by dashed grey lines and highlighted with black squares. Median mutation loads are shown as solid lines (black, cancer types; purple, all pediatric; green, all adults). Figure reproduced from Grobner *et al.* [167].

Pediatric sarcomas are a group of solid tumors that represent 12-15% of all childhood cancer at diagnosis. There are two main subgroups, bone sarcoma and soft tissue sarcoma [169]. Although each of them has a distinct genetic profile, treatment has historically been similar, consisting in conventional chemotherapy, surgery and irradiation [166]. Among pediatric sarcomas, the most frequent types are Ewing sarcoma, osteosarcoma and rhabdomyosarcoma. In my PhD work, I have addressed questions related to animal modeling and anticancer drug distribution in these diseases, with a principal focus on Ewing sarcoma.



#### 4.1. Ewing sarcoma

Ewing sarcoma is the second most common bone tumor in children and adolescents, commonly arising from the axial skeleton and the diaphysis bones, occurring predominantly in pelvis, femur, tibia and ribs, or in soft-tissue, mainly in thoracic wall, gluteal muscle, pleural cavities and cervical muscles [170, 171] (**Figure 11**). The peak incidence of Ewing sarcoma is around 15 years of age, coinciding with puberty, and males are more affected than females [171, 172]. Metastasis at diagnosis is present in approximately 20-25% of patients, mainly appearing in lung, bones and bone marrow [170, 172, 173].

Current treatment is a multimodal regimen that consist in surgical resection, local radiotherapy and intensive multi-agent chemotherapy, such as regimens containing vincristine, ifosfamide, doxorubicin and etoposide (VIDE) and gemcitabine and docetaxel (G/D), among others [174-176]. Despite this standard of care is effective for treatment of patients with localized disease with a 5-year overall survival of 70-80%, those patients with metastatic diseases at diagnosis or relapsed tumors have poor clinical prognosis, with an overall survival of less than 30% [171-173, 177].

Ewing sarcoma is characterized by a fusion gene encoding Ewing's sarcoma RNA binding protein 1 (*EWSR1*) with variable members of the gene encoding erythroblast transformation-specific (*ETS*) transcription factor family, with 85% being Friend leukemia virus integration 1 proto-oncogene (*FLI1*) and 10% *ETS* related gene (*ERG*) [166, 171, 172, 174]. Delattre *et al.* in 1992 described for the first time the *EWSR1-FLI1* gene fusion in Ewing sarcoma tumors and how the EWS-FLI1 oncoprotein modifies the expression of genes implicated in tumor initiation and progression [178, 179]. Ewing sarcoma has a stable genome with few genomic events, with the exception of *TP53* and stromal antigen 2 (*STAG2*) alterations, which are present in 7% and 20% of cases, respectively, and the depletion of cyclin-dependent kinase inhibitor 2A (*CDKN2A*), which regulates cell proliferation, in 10-22% of cases [171, 172, 174, 180, 181].

A relevant diagnostic marker of Ewing sarcoma is a cell-surface glycoprotein known as CD99, strongly expressed in Ewing sarcoma cell membranes [182, 183]. However, CD99 is not specific for Ewing sarcoma, thus the diagnostic can only be confirmed by molecular pathology using fluorescence *in situ* hybridization (FISH-based) detection of *EWSR1* rearrangements and reverse transcription – polymerase chain reaction (RT-PCR) [184].

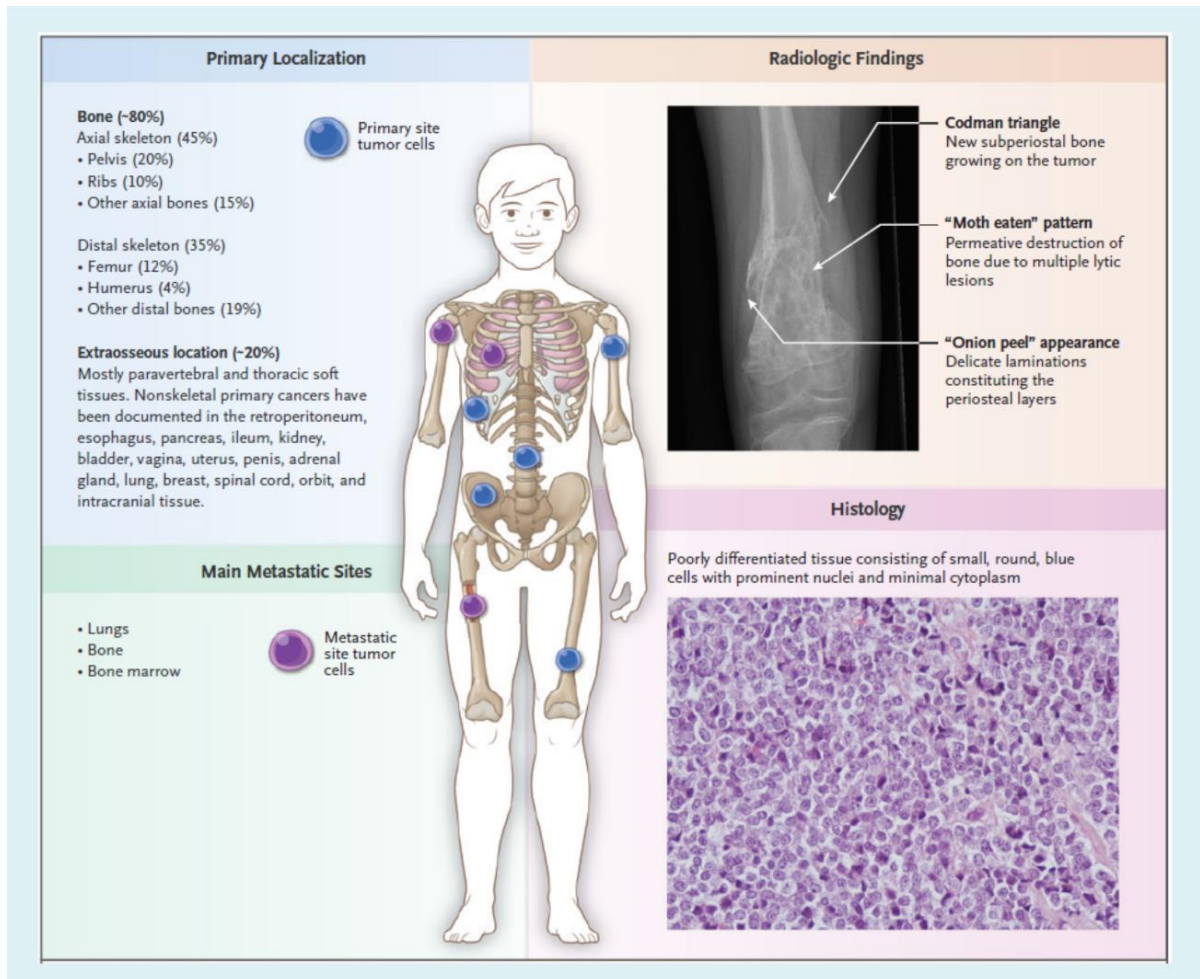


**Figure 11.** Clinical features of Ewing sarcoma: primary localizations, radiologic patterns, histology, and most common main metastatic sites. Figure reproduced from Riggi *et al.* [172].

## 4.2. Osteosarcoma

Osteosarcoma is the most common bone cancer in children and young adults, arising often in long bones such as femur, tibia and fibula, but also in flat bones such as pelvis and skull [170, 185] (**Figure 12**). The peak age at diagnosis of osteosarcoma occurs predominantly during puberty, coinciding with a rapid expansion of large bones, contributing to tumor initiation [186, 187]. Metastasis at diagnosis is present in approximately 20-25% of patients, with the lungs being the most common site [188].

Treatment of osteosarcoma has not changed significantly since established more than 30 years ago [189]. The standard of care includes, similarly to Ewing sarcoma, a surgical resection, local radiotherapy and a combined regimen of chemotherapy that includes doxorubicin, cisplatin, ifosfamide, etoposide and methotrexate [187, 190, 191]. Survival rates for osteosarcoma have remained at 60-70% for localized disease [188, 192]. In those patients who have metastatic disease at diagnosis or who relapse, the 5-year survival rate is below 30% [185, 188, 190, 193, 194]. Despite intensive efforts, no new therapeutic regimens have improved survival in these patients [190].

The genome of osteosarcoma is highly unstable and complex, with a large number of chromosomal breaks leading to structural variations, also known as chromothripsis, and relatively few recurrent point mutations in protein-coding genes [166, 170, 190]. The most frequent molecular alterations in osteosarcoma are the inactivation of the p53 and RB tumor suppressors, in 74% and 64% of cases respectively, as well as gain of function in some of the proteins involved in the PI3K pathway in 56% of cases [190, 192, 195]. This genomic landscape suggests that somatic copy-number variations could play a critical role in the osteosarcoma tumor progression and maintenance [190].

Imaging and biopsy guide the diagnosis of osteosarcoma patients. Imaging techniques include plain radiography followed by magnetic resonance imaging (MRI) or functional studies analyzing glucose metabolism by PET/CT using F-18-FDG [196, 197]. PET/CT provides information for diagnosis of primary lesion and metastasis, and can also be used for histological response to chemotherapy [196]. There is no specific biomarker for osteosarcoma diagnosis, but the presence of osteoid in the tumor biopsies is characteristic of the disease [197].

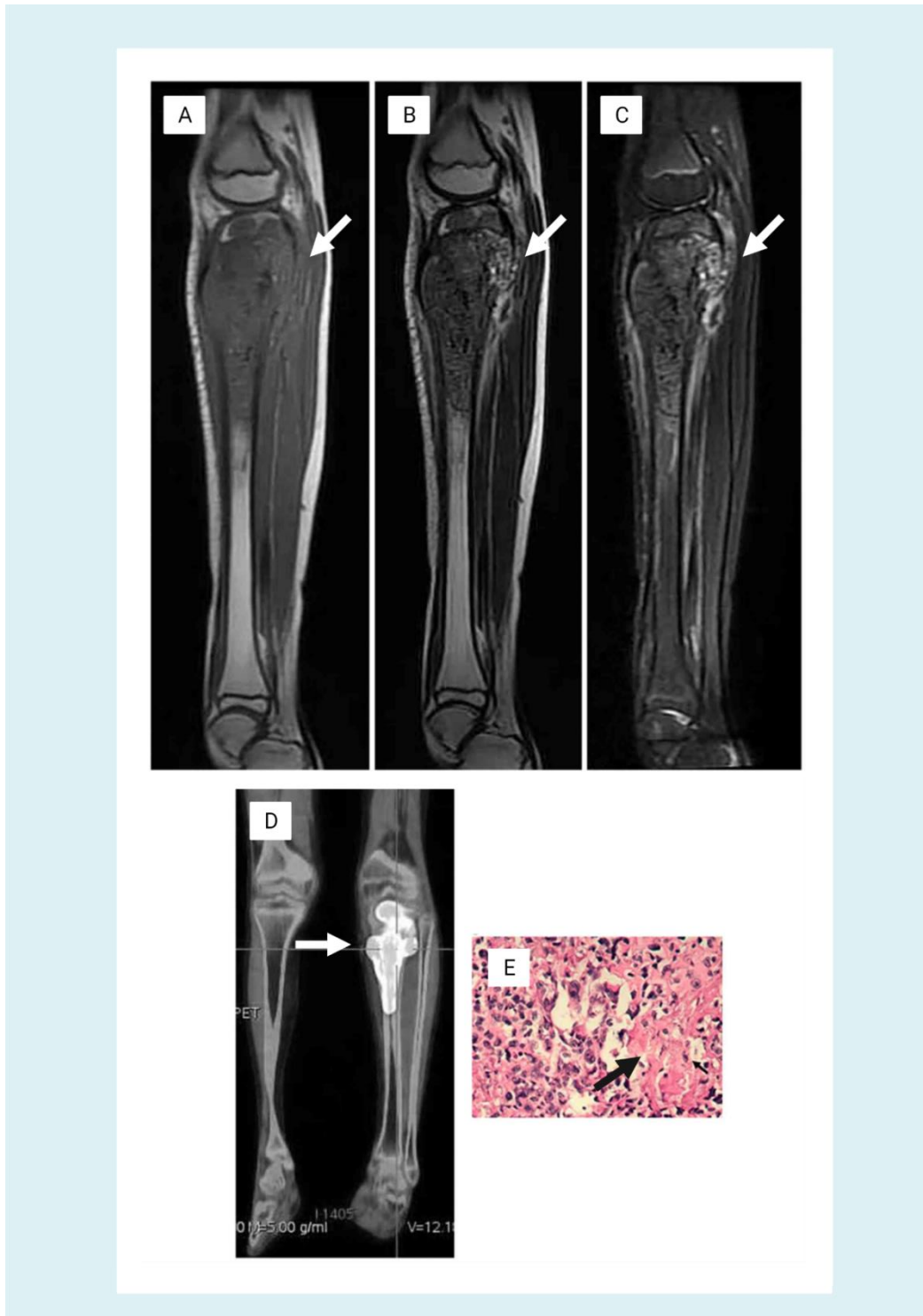


**Figure 12.** Osteosarcoma in the left tibia of a 10 year old female patient. A) Sagittal MRI T1 weighted images (highlight of fat tissue), B) sagittal MRI T2 weighted images (highlight of fat tissue and water), and C) sagittal MRI fat-suppressed T2 weighted images showing low T1/T2 mixed signals of the left tibia. The epiphysis is involved (white arrows). D)  $^{18}\text{F}$ -fluorodeoxyglucose (F-18-FDG) PET/CT metabolic imaging showing increased radionuclide uptake accumulation in the tumor. E) Histologic representation showing patchy distribution of tumor cells, marked nuclear atypia, numerous mitotic figures and osteoid matrix (black arrow) (original magnification, x200; hematoxylin and eosin staining). Figure modified from Sun *et al.* [198].

### 4.3. Rhabdomyosarcoma

Rhabdomyosarcoma is the most common soft-tissue sarcoma of children and adolescents, arising anywhere in the body in association with the musculature [166]. Rhabdomyosarcomas subtypes are denominated alveolar and embryonal. The incidence of the alveolar type is constant throughout childhood and adolescence, while the embryonal type is most common in early childhood [199-201]. Embryonal rhabdomyosarcoma typically arises in the head and neck or in genitourinary sites while alveolar rhabdomyosarcoma arises predominantly at the extremities [166]. Metastasis at diagnosis is present in approximately 20% of children, mainly in lungs, bone and bone marrow [202].

Standard of care is based on controlling the primary tumor by surgical resection, ionizing radiation and eradicating systematic metastatic disease using intensive chemotherapy regimens [174, 203]. Systematic chemotherapy consists in multi-drug regimens including vincristine, actinomycin D and cyclophosphamide (VAC) or ifosfamide, vincristine and actinomycin D (IVA), both combinations showing similar outcomes [200, 203-205]. At our institution, Hospital Sant Joan de Déu, the upfront treatment of the primary tumors in patients with rhabdomyosarcoma consists in irinotecan as monotherapy or combined with carboplatin or vincristine. Globally, 5-year overall survival of rhabdomyosarcoma exceeds 70% [174, 203, 204, 206]. However, patients with alveolar rhabdomyosarcomas have inferior clinical outcomes compared to embryonal rhabdomyosarcomas [170]. Patients with widely metastatic and recurrent disease have poor prognosis, with an overall survival at 3 years of 25-30% [202, 203, 207].

Morphologically, rhabdomyosarcoma cells usually resemble skeletal muscle lineage and the diagnostic of this tumor can be established by immunohistochemistry and molecular studies analyzing the expression of skeletal muscle gene product (muscle-specific actin, myosin, desmin, myoglobin, MYOD1 or MYOG) (**Figure 13**) [208, 209]. Molecularly, alveolar rhabdomyosarcoma is characterized by a fusion gene encoding paired box protein 3 (*PAX3*) or paired box protein 7 (*PAX7*) with forkhead box protein O1 (*FOXO1*) and embryonal rhabdomyosarcoma is fusion-negative [170, 200]. Therefore, the detection of the presence or absence of the fusion gene by molecular analysis, usually by FISH technique or detecting the fusion transcript by RT-PCR assay, is necessary to distinguish between both subtypes [210, 211].

In 1993, Galili *et al.* and Shapiro *et al.* described for the first time the PAX-FOXO fusion as characteristic of alveolar rhabdomyosarcoma tumors [212, 213]. *PAX3* and *PAX7* genes encode highly related members of the paired box transcription factor family, with critical roles during development (maintenance of multipotent state and initiation of differentiation programs, cell migration, proliferation and survival), whereas *FOXO1* encodes a widely expressed member of the forkhead

transcription factor family [203, 214]. The resulting chimeric protein is an activator that increases the expression of downstream target genes related with invasion, migration, proliferation and survival [214]. A small proportion of patients with alveolar rhabdomyosarcoma do not present any of these translocations, and their tumors are biologically and clinically similar to embryonal rhabdomyosarcoma [203].

The overall burden of somatic mutations of rhabdomyosarcomas is very low, as shown by whole-exome and whole-genome sequencing, especially in fusion-positive alveolar rhabdomyosarcoma [215, 216]. Embryonal rhabdomyosarcomas have features of unstable genomes and can present mutation in RAS-family genes, fibroblast growth factor receptor 4 (*FGFR4*), phosphatidylinositol-4,5-bisphosphate 3-kinase catalytic subunit alpha (*PIK3CA*) and the catenin beta 1 (*CTNNB1*) [174, 203, 215, 216].



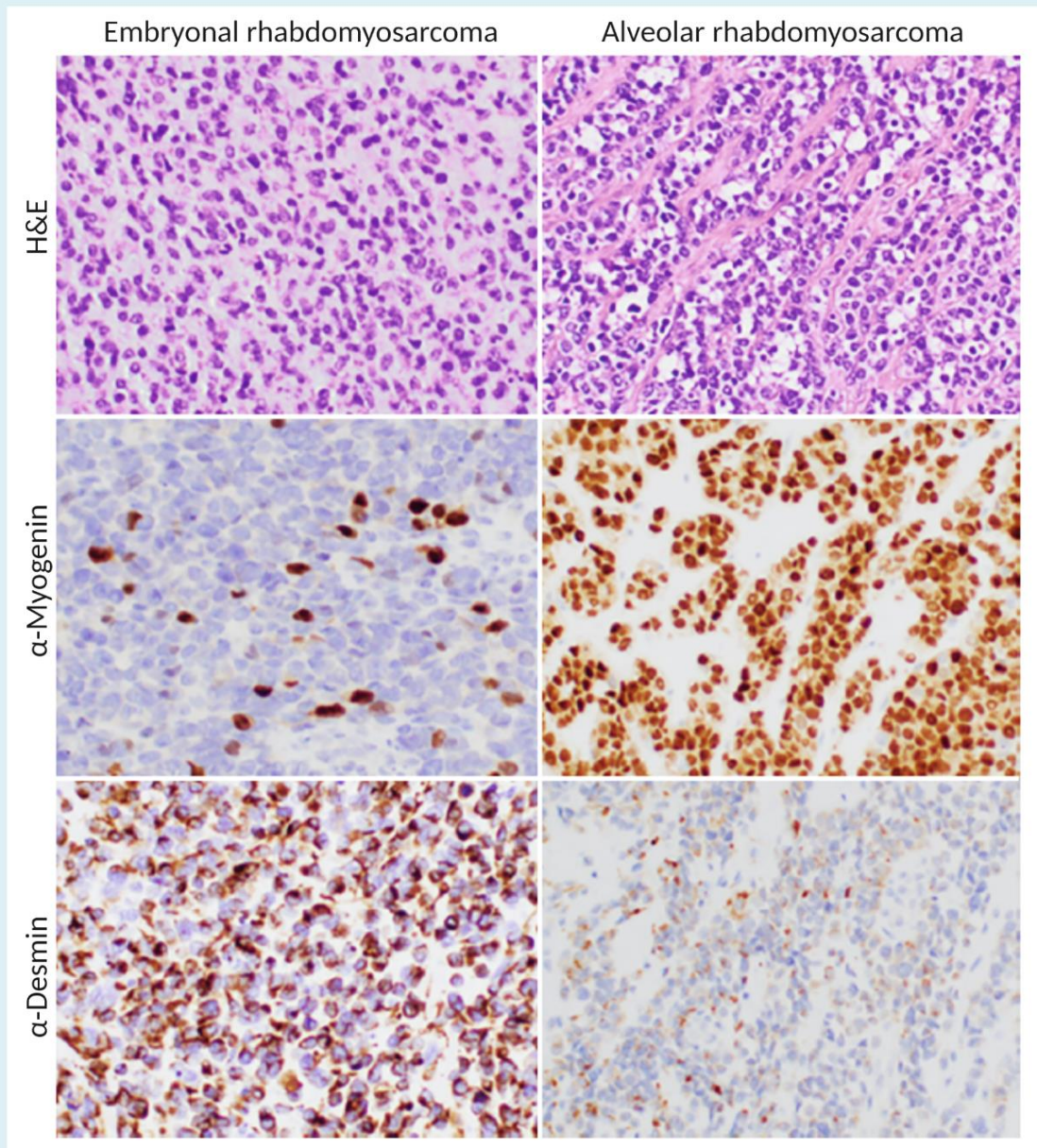


**Figure 13.** Histologic characterization of embryonal and alveolar rhabdomyosarcoma. Immunostaining of  $\alpha$ -myogenin and  $\alpha$ -desmin mark the skeletal muscle lineage. Alveolar pattern is observed with hematoxylin and eosin (H&E) staining in the alveolar rhabdomyosarcoma. Alveolar subtype often, but not always, displays loosely associated tumor cells in clusters resembling pulmonary alveoli and robust immunostaining for  $\alpha$ -myogenin. Original magnification x400. Figure reproduced from Skapek *et al.* [203].

## 5. Camptothecins in the treatment of pediatric sarcomas

Camptothecins are a family of topoisomerase-I inhibitor molecules. Topoisomerases are nuclear enzymes involved in the maintenance of DNA topology and structure during replication and transcription, and they are also implicated in DNA repair [217, 218]. The mechanism of action of camptothecins is by binding to topoisomerase-I and DNA strands forming a non-covalent ternary complex that induces single-strand breaks which are reversible and non-lethal [217, 219]. When the DNA replication fork collides with the ternary complex, single-strand breaks are converted to irreversible double-strand breaks, inducing cell death via apoptosis (**Figure 14**) [219, 220]. Clinically approved camptothecins, topotecan and irinotecan, derive from camptothecin, a potent natural compound extracted from the bush *Camptotheca accuminata*. This compound showed poor solubility and high toxicity due to its chemical structure. Consequently, it was modified to improve its biopharmaceutical properties [218]. Mechanisms of resistance to camptothecins are mainly associated with decreased levels of cellular topoisomerase-I or with gene mutations that downregulate or alter this protein. Another mechanism is to reduce the uptake of camptothecins due to overexpression of the MRPs, including P-gp [218, 220-222] (see section 1.3).

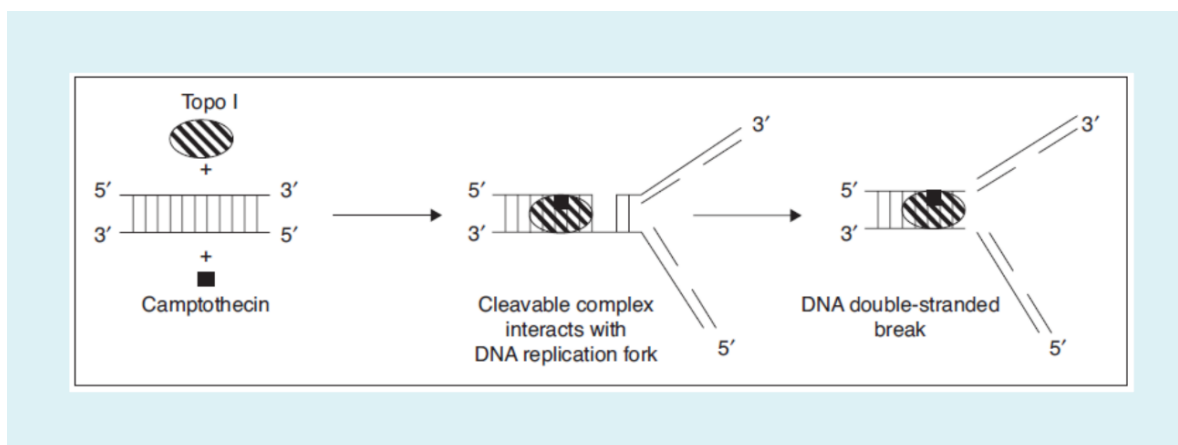


**Figure 14.** Mechanisms of action of camptothecin. Figure reproduced from Bomgaars *et al.* [220].

Irinotecan is one of the best-studied camptothecins. It is a pentacyclic alkaloid chemically conjugated to a bis-piperidine side chain, which contributes to its water solubility [223, 224]. Camptothecins are active only when the lactone ring of the molecule is closed. At acid pH, the lactone is stable. Upon increasing the pH to neutral or basic, the lactone opens to carboxylate and both forms achieve a pH-dependent reversible equilibrium (**Figure 15**) [218, 225]. Only the lactone is active against tumor cells [218, 225]. Thus, camptothecins for parenteral administration to patients are formulated as acid solutions.



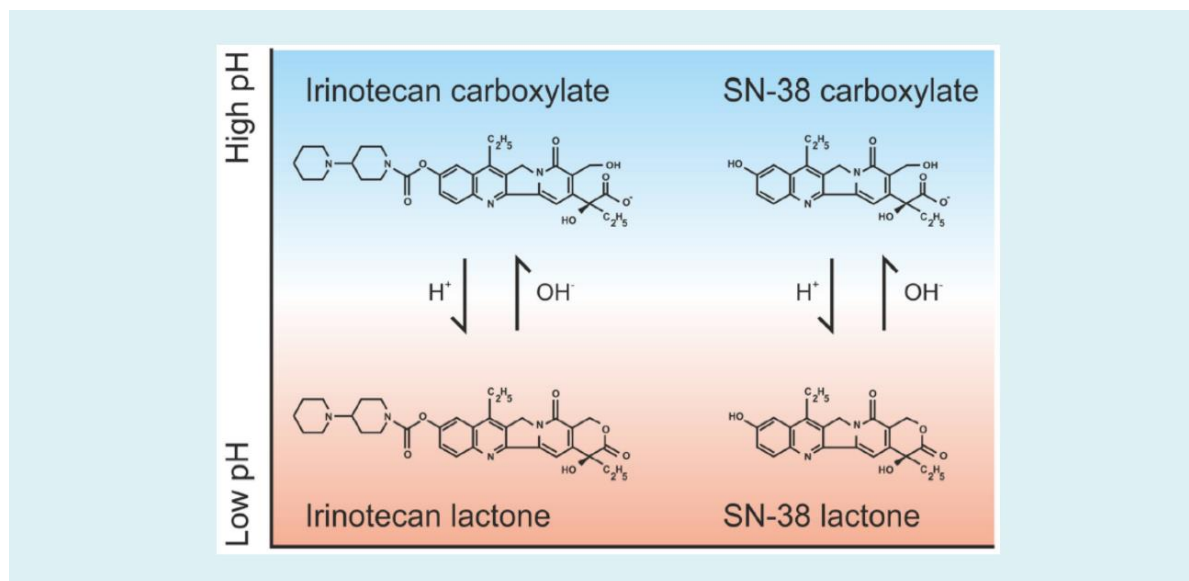


**Figure 15.** pH-dependent equilibrium of irinotecan and SN-38 isoforms. Figure reproduced from de Man *et al.* [225].

Irinotecan is a prodrug that is converted to its active metabolite SN-38 (7-ethyl-10-hydroxycamptothecin) by liver carboxylesterase converting enzymes (CES1/2) and human butyrylcholinesterase (hBChE) in blood plasma [225-227]. SN-38 is highly hydrophobic but very active, especially the lactone form, while the carboxylate presents high aqueous solubility (**Figure 15**) [218, 225]. SN-38 is 100 to 1000-fold more cytotoxic than irinotecan [228]. SN-38 is inactivated by UGT (uridine 5'-diphospho-glucuronosyltransferase) enzymes such as UGT1A1, UGT1A7, UGT1A9 and UGT1A10, which convert SN-38 to glucuronide ( $\beta$ -glucuronide conjugate) promoting the elimination of the drug from the body [218, 225]. Irinotecan pharmacokinetics can be altered by age, sex, dose, administration timing or hepatic function. These processes affect drug clearance and consequently can be related to the appearance of toxicity [225]. The main limitations of irinotecan treatment in monotherapy are hematological and gastrointestinal toxicities associated to neutropenia and severe diarrhea in 16 and 31% of patients respectively [218, 221, 225, 229].

Irinotecan is used in the treatment of several pediatric sarcomas, such as Ewing sarcoma and rhabdomyosarcoma but with less experience in the treatment of osteosarcoma or non-rhabdomyosarcoma soft tissue sarcoma [230]. The first reported pediatric phase I clinical trial of irinotecan was reported by Furman *et al.* in 1999 based on the preclinical observation of improved efficacy when using a protracted multi-day schedule, especially when given for 5 consecutive days 2 weeks in a row (dx5x2 schedule) [230-232]. The objective response observed in patients with relapsed rhabdomyosarcoma and Ewing sarcoma were consistent with the preclinical activity obtained in pediatric sarcoma xenograft models using the same schedule [230, 232]. Irinotecan as a single agent is insufficient for the treatment of pediatric sarcomas, showing response rates in relapsed patients under

10% for both rhabdomyosarcoma and Ewing sarcoma in a phase II trial [233]. Phase II and III clinical studies of irinotecan combinations with other anticancer agents have shown improved activity in pediatric sarcomas, as summarized by Wagner *et al.* [230] (**Table 3**). Chemotherapeutic drugs that have been combined with irinotecan to treat pediatric sarcoma include vincristine [234-238] carboplatin [239], temozolomide [237, 238, 240-242], docetaxel [243] or ifosfamide [244]. The use of irinotecan in combination with other agents is becoming more established for the treatment of intermediate and high-risk rhabdomyosarcoma as well as for relapsed Ewing sarcoma. In my PhD work, I have used irinotecan and SN-38 as model drugs to address questions related to PDX response to therapy, PDX functional stability, tumor evolution towards chemoresistance and drug distribution.

**Table 3.** Key phase II and III studies using irinotecan in pediatric sarcoma patients.

<b>Authors</b>	<b>Phase</b>	<b>Other agents given with irinotecan</b>	<b>Population</b>	<b>Comments</b>
Hawkins DS, <i>et al.</i> [234]	III	Vincristine	Newly-diagnosed intermediate-risk rhabdomyosarcoma	VI <sup>a</sup> alternating with VAC <sup>b</sup> is as efficacious as VAC alone, and may reduce long-term toxicity
Pappo AS, <i>et al.</i> [235]	II	Vincristine	Newly-diagnosed metastatic rhabdomyosarcoma	Response rate to induction rose from 46-70% after addition of vincristine
Dharmarajan KV, <i>et al.</i> [239]	II	Carboplatin, radiation	Newly-diagnosed intermediate or high-risk rhabdomyosarcoma	Local control rate of 89%; reduced mucositis compared to historical controls
Mascarenhas L, <i>et al.</i> [236]	II	Vincristine	Relapsed rhabdomyosarcoma	Similar rates of response and grade 3-4 toxicity between dx5 vs dx5x2 schedule
Mixon BA, <i>et al.</i> [237]	II	Temozolomide, vincristine	Relapsed rhabdomyosarcoma	One complete response in 4 patients
Kurucu N, <i>et al.</i> [240]	II	Temozolomide	Relapsed Ewing sarcoma	Response rate 55%
Wagner LM, <i>et al.</i> [241]	II	Temozolomide	Relapsed Ewing sarcoma	Response rate 29%
Casey DA, <i>et al.</i> [242]	II	Temozolomide	Relapsed Ewing sarcoma	Response rate 63%
Raciborska A, <i>et al.</i> [238]	II	Temozolomide, vincristine	Relapsed Ewing sarcoma	Response rate 68%
Yoon JH, <i>et al.</i> [243]	II	Docetaxel	Relapsed Ewing sarcoma	Response rate 33%
Crews KR, <i>et al.</i> [244]	II	Ifosfamide	Newly-diagnosed high-risk osteosarcoma	Ifosfamide reduced SN-38 exposures

<sup>a</sup> Vincristine plus irinotecan

<sup>b</sup> Vincristine, actinomycin-D and cyclophosphamide





# **HYPOTHESES AND AIMS**

---



Therapy development in cancer involves several consecutive steps including (1) the identification of the unmet medical need (disease or clinical question), (2) the establishment of clinically relevant resources or models to address such need, (3) the evaluation of therapies or experimental questions in the established models, and (4) the design and execution of clinical trials or protocols. The ambition of my PhD work was to follow the mentioned steps to build a body of results with potential clinical impact in the pediatric oncology field. Research at our institution, SJD, focuses on several types of cancers with bad prognosis, such as pediatric sarcomas. These cancers belong to a rare and heterogeneous group of skeletal and soft tissue malignancies accounting for approximately 12% of all childhood solid tumors. The most frequently occurring ones are Ewing sarcoma, osteosarcoma and rhabdomyosarcoma. With the up-to-date treatment modalities, based on surgery, radiation and chemotherapy, the 5-year survival rates of these patients have improved up to 70-80% in the last decades. However, a substantial proportion of patients relapse and do not respond consistently to rescue therapy. Whether the lack of response to therapy of these patients is due to drug delivery issues in resistant tumor cells is not completely understood. The main question I wanted to address in my work was whether patients whose tumors stop responding to anticancer medicines show diminished intratumoral drug distribution. Because this experimental question was challenging to address in the clinical setting, we needed to generate the adequate laboratory models. Thus, we established PDX models in immunodeficient mice. There is compelling evidence suggesting that PDX, at least at initial passages, reproduce the clonal heterogeneity, genetics and histology of several types of cancer. Whether this holds true for pediatric sarcomas was not sufficiently clear. Thus, we embraced an ambitious project to address (1) the identification of clinical and technical factors involved in pediatric sarcoma PDX engraftment, (2) the characterization of the stability of the PDX during initial passages, and (3) the relationship between successful PDX and patient prognosis.

The main hypotheses of my work were:

- (1) PDX models faithfully represent pediatric sarcoma tumors established from patients at different disease stages. PDX conserve the main histology, molecular and functional properties of human tumors over successive passages in mice.
- (2) PDX engraftment correlates with patient prognosis. Successful establishment of PDX models helps identify patients with higher risk of recurrence and disease progression.
- (3) Intratumoral distribution of anticancer drugs becomes restricted due to the evolution of patient disease. Cancer cells in relapsed tumors displace chemotherapeutics from the intracellular to the extracellular tumor compartment.



- (4) The expression of multidrug resistance efflux transporters explains, at least partially, the shift of the intratumoral drug distribution towards the extracellular compartment upon tumor evolution in relapsed patients.

To address my hypotheses, the main objectives of my thesis were:

- (1) To establish and characterize PDX models from biopsies and necropsies of pediatric patients diagnosed with Ewing sarcoma, osteosarcoma and rhabdomyosarcoma. To address this goal, we implanted patient samples obtained at Hospital Sant Joan de Déu in immunodeficient mice. Upon successful engraftment as PDX, we characterized the histology, genomics and response to model therapy (irinotecan) of the established tumor models over time in successive passages in mice.
- (2) To identify factors favoring PDX engraftment and to study the association between PDX engraftment and prognosis in pediatric patients with Ewing sarcoma, osteosarcoma and rhabdomyosarcoma. To address this goal, we collected clinical and technical data from the patients and the PDX, and we studied the relationship between PDX engraftment and several patient and sample factors, including disease stage (diagnosis or relapse) and patient outcome (event free survival and overall survival).
- (3) To detect and characterize changes in anticancer drug activity and intratumoral drug distribution during the evolution of Ewing sarcoma. To address this goal, we established pairs of PDX models from patients at diagnosis and late disease stages. In such paired PDX, we studied the activity and distribution of the model drug irinotecan and its active metabolite, SN-38. We applied the intratumoral microdialysis – tumor homogenate technique to obtain samples of PDX engrafted in mice receiving irinotecan infusions, and we calculated the unbound volume of distribution of SN-38 in the established PDX. We analyzed the expression and function of multidrug resistance efflux transporters, such as P-glycoprotein, as likely cause of the limited drug distribution and acquisition of resistance in relapsed tumors.





# EXPERIMENTAL WORK

---



**1. Prognostic value of patient-derived xenograft engraftment in pediatric sarcomas**

**Article reference:** Journal of Pathology Clinical Research (2021) – DOI: 10.1002/cjp2.210.

Helena Castillo-Ecija<sup>1,2</sup>, Guillem Pascual-Pasto<sup>1,2</sup>, Sara Perez-Jaume<sup>1,2</sup>, Claudia Resa-Pares<sup>1,2</sup>, Monica Vila-Ubach<sup>1,2</sup>, Carles Monterrubio<sup>1,2</sup>, Ana Jimenez-Cabaco<sup>1,2</sup>, Merce Baulenas-Farres<sup>1,2</sup>, Oscar Muñoz-Aznar<sup>1,2</sup>, Noelia Salvador<sup>1,2</sup>, Maria Cuadrado-Vilanova<sup>1,2</sup>, Nagore G. Olaciregui<sup>1,2</sup>, Leire Balaguer-Lluna<sup>1,2</sup>, Victor Burgueño<sup>1,2</sup>, Francisco J. Vicario<sup>1,2,3</sup>, Alejandro Manzanares<sup>1,2,3</sup>, Alicia Castañeda<sup>1,2</sup>, Vicente Santa-Maria<sup>2</sup>, Ofelia Cruz<sup>1,2</sup>, Veronica Celis<sup>1,2</sup>, Andres Morales La Madrid<sup>1,2</sup>, Moira Garraus<sup>1,2</sup>, Maite Gorostegui<sup>2</sup>, Margarita Vancells<sup>3</sup>, Rosalia Carrasco<sup>3</sup>, Lucas Krauel<sup>1,3</sup>, Ferran Torner<sup>4</sup>, Mariona Suñol<sup>5</sup>, Cinzia Lavarino<sup>1,2</sup>, Jaume Mora<sup>1,2</sup>, Angel M. Carcaboso<sup>1,2\*</sup>

<sup>1</sup>Institut de Recerca Sant Joan de Deu, Barcelona, 08950, Spain

<sup>2</sup>Pediatric Oncology, Hospital Sant Joan de Deu, Barcelona, 08950, Spain

<sup>3</sup>Pediatric Surgery, Hospital Sant Joan de Deu, Barcelona, 08950, Spain

<sup>4</sup>Pediatric Orthopedic Surgery, Hospital Sant Joan de Deu, Barcelona, 08950, Spain

<sup>5</sup>Pathology, Hospital Sant Joan de Deu, Barcelona, 08950, Spain

Running title: PDX engraftment predicts bad prognosis in pediatric sarcomas

\*Address for correspondence: Dr AM Carcaboso, Institut de Recerca Sant Joan de Deu, Santa Rosa 39-57, 08950 Esplugues de Llobregat, Barcelona, Spain. Email: amontero@fsjd.org; Tel: +34 936009751 EXT 4420; Fax: +34 936009771

The authors declare no conflict of interest.

Word count: 4270; Number of figures: 5; Number of tables: 1

## **Abstract**

The goals of this work were to identify factors favoring patient-derived xenograft (PDX) engraftment and study the association between PDX engraftment and prognosis in pediatric patients with Ewing sarcoma, osteosarcoma and rhabdomyosarcoma. We used immunodeficient mice to establish 30 subcutaneous PDX from patient tumor biopsies, with a successful engraftment rate of 44%. Age greater than 12 years and relapsed disease were patient factors associated with higher engraftment rate. Tumor type and biopsy location did not associate with engraftment. PDX models retained histology markers and most chromosomal aberrations of patient samples during successive passages in mice. Model treatment with irinotecan resulted in significant activity in 20 of the PDXs and replicated the response of rhabdomyosarcoma patients. Successive generations of PDXs responded similarly to irinotecan, demonstrating functional stability of these models. Importantly, out of 68 tumor samples from 51 patients with a median follow up of 21.2 months, PDX engraftment from newly diagnosed patients was a prognostic factor significantly associated with poor outcome ( $P = 0.040$ ). This association was not significant for relapsed patients. In the subgroup of patients with newly diagnosed Ewing sarcoma classified as standard risk, we found higher risk of relapse or refractory disease associated to those samples that produced stable PDX models ( $P = 0.0357$ ). Overall, our study shows that PDX engraftment predicts worse outcome in newly diagnosed pediatric sarcoma patients.

**Key words:** patient-derived xenograft, Ewing sarcoma, rhabdomyosarcoma, osteosarcoma, prognosis.

### **1.1. Introduction**

Pediatric sarcomas are a rare and heterogeneous group of skeletal and soft tissue malignancies accounting for approximately 12% of all childhood solid tumors (1). The most frequently occurring are Ewing sarcoma, osteosarcoma and rhabdomyosarcoma, altogether representing 13% of all malignant tumors in patients younger than 14 years, and up to 18% of all tumors among patients between 15 and 19 years (2-4). With up-to-date treatment modalities, the five-year survival rates have improved in the last decade to 79% for Ewing sarcoma, 73% for osteosarcoma and 70% for rhabdomyosarcoma (5-7). Unfortunately, intensive and multimodal treatments currently used in pediatric sarcomas have topped their efficacy (1,8,9). A substantial proportion of patients relapse and do not respond consistently to rescue chemotherapies because of tumor evolution into a chemoresistant phenotype (10).

Patient derived xenograft (PDX) tumor models in immunodeficient mice are well-recognized tools for the study of rare tumors and their treatment (11-13). In colorectal cancer, epithelial ovarian cancer and lung adenocarcinoma, for instance, PDXs retain the main properties of the original patient tumor, including histology, genetic and genomic alterations, gene expression profile and heterogeneity (6,11,14,15). Successful engraftment of a patient tumor biopsy in animals might predict the outcome of patients (16). For breast, pancreatic and lung cancers, engraftment in mice associates to worse patient prognosis (15,17,18). Likely, there is a selection process enabling the most aggressive clones to expand and prevail in successive passages in mice (11,13,19-21). PDX models of most pediatric sarcomas are suitable for such establishment (22-24). Whether the parameter “PDX engraftment” could be useful for identifying pediatric sarcoma patients at risk of relapse or refractory disease is not well characterized. To address this question, here we establish PDX models from Ewing sarcoma, osteosarcoma and rhabdomyosarcoma patients and include available clinical data along with the PDX data (25). To characterize this new preclinical platform, we address whether PDX tumors retained the main histologic, genomic and functional properties of patient tumors during successive passages in mice. Sample characterization includes histopathology markers, chromosomal profiles (copy number alteration; CNA) and preclinical treatment assays (efficacy of irinotecan).

### **1.2. Materials and methods**

#### **1.2.1. Xenotransplantation of patient samples**

The appropriate Institutional Review Board approved the research protocol associated with this project (M-1608-C). Patients or their legal guardians signed informed consent at Sant Joan de Déu Hospital (SJD, Barcelona, Spain). Clinical information parameters obtained from patients are listed in supplementary material, Table S1. Patients were biopsied using either a surgical procedure (open surgery or minimally invasive surgery) or percutaneous tissue core biopsy with a Tru-Cut



needle. Biopsies were used fresh or were cryopreserved. For the cryopreservation process, tissues were minced as 2 x 2 x 1 mm pieces with a scalpel on sterile petri dishes. Three to four of these pieces were added to 2 mL cryogenic vials (Corning, Glendale, AZ, USA) containing 1.5 mL of inactivated fetal bovine serum with 10% dimethyl sulfoxide (Life Technologies, Grand Island, NY, USA). Vials were stored overnight in a freezing container (Cool Cell, Corning) at -80 °C, and then transferred to liquid nitrogen for long-term storage.

Work with mice adhered to the European regulations and was approved by the animal experimental ethics committee at the Universitat de Barcelona (animal protocol numbers 135/11 and 134/18). Briefly, we implanted patient tumor biopsies (freshly excised or cryopreserved) subcutaneously in 4-6 week-old female NOD-SCID mice (Envigo, Barcelona, Spain), as previously described (26). Tumors engrafting successfully were named F0 generation. When tumor volume achieved 1000-1500 mm<sup>3</sup>, we performed passage of freshly excised tissue to athymic nude mice (Envigo). We used NOD-SCID mice for the passage of specific rhabdomyosarcoma models. We named subsequent generations with the number of the passage (e.g. F1 was the first filial generation after initial F0 engraftment). Information parameters obtained from successfully engrafted PDX models are listed in supplementary material, Table S2.

To interrogate whether clinical parameters of the patient disease, including the sample collection method (surgical biopsy versus Tru-Cut needle), correlated with the likelihood of successful PDX engraftment, we used mixed effects logistic regression analysis and calculated the odds ratios and their corresponding 95% confidence intervals (CI). To dichotomize age, we computed an optimum threshold by maximizing the Youden index using negative or positive engraftment (27).

### 1.2.2. Analysis of fusion genes

We amplified Ewing sarcoma fusion gene types *EWSR1-ERG* and *EWSR1-FLI1*, and rhabdomyosarcoma fusion genes *PAX3-FKHR* and *PAX7-FKHR* with the polymerase chain reaction (PCR). The sequences of the primers were *EWSR1* forward, 5'- TCCTACAGCCAAGCTCCAAGTC -3'; *FLI1* reverse, 5'- GTGTCAGGCATGGAGGATGGA -3'; *ERG* reverse, 5'- GAGAAGGCATATGGCTGGTGG -3'; *PAX3* forward, 5'- AGGCATGGATTTTCCAGCTATA -3'; *PAX7* forward, 5'- TCTGCCTACGGAGCCCG -3'; and *FKHR* reverse, 5'- GGGACAGATTATGACGAATTGAATT -3'. Ewing sarcoma fusion genes were detected in agarose gels, while rhabdomyosarcoma fusion genes were quantified with a real time quantitative PCR technique, using the probe FAM-5'- CCGGTCAGCAACGGCCTGTCT -3'.

### **1.2.3. Histopathology**

During the process of PDX establishment, the original patient tumors and PDX models at different passages must be characterized and compared (16). First, we compared histology on hematoxylin and eosin (H&E) staining, and the expression of tumor-related proteins in the patient tumor biopsies and derived PDX tumors. To analyze whether protein expression (detected by immunostaining) changed upon successive mouse-to-mouse transplantation, we studied PDX tissues at three different filial generations: F0, as the first generation in mice, and F2 and F5, as early and late successive passages in mice. Tissues were fixed overnight in buffered formalin and embedded in paraffin. To stain human tumor cells in engrafted tumor tissues we used anti-human nuclei primary antibody (1:200, MAB4383, Merck Millipore, Burlington, MA, USA). To detect proliferating cells we used anti-Ki67 antibody (1:200, ACK02, Leica Biosystems, Wetzlar, Germany). We stained proteins highly expressed by specific tumor types, such as CD99 for Ewing sarcoma (1:20, NCL-L-CD99-187, Leica Biosystems), MyoD1 for rhabdomyosarcoma (1:20, M3512 Agilent Technologies, Santa Clara, CA, USA), and the secreted protein acidic and rich in cystein (SPARC) for osteosarcoma (1:80, 35-5500, Invitrogen, Carlsbad, CA, USA).

### **1.2.4. PDX growth**

We measured tumor growth rate as the time needed to achieve the experimental endpoint, i.e. tumor volume of 1500 mm<sup>3</sup>. Tumor volume was calculated as  $(\text{length} \times \text{width}^2)/2$ , length being the longitudinal diameter and width the transverse diameter of the subcutaneous tumor.

### **1.2.5. Analysis of copy number alterations (CNAs)**

We compared the CNA profiles of tumor biopsies and PDX tissue at generations F2 and F5. We performed whole genome analysis using the high-density array CytoScan® HD platform (Affymetrix, Thermo Fisher Scientific, Waltham, MA, USA) as previously described (10). Total DNA from frozen samples was digested, ligated, PCR-amplified and purified, fragmented, biotin-labeled, and hybridized according to manufacturer's instructions. We analyzed the CytoScan® HD Array data with the Chromosome Analysis Suite (ChAS) software (Affymetrix, Thermo Fisher Scientific).

### **1.2.6. Irinotecan activity *in vivo***

We used 20 of the new PDX models to evaluate the activity of irinotecan, as a model drug with established activity against pediatric solid tumors including sarcomas (10,28,29). We reasoned that if the PDXs were truly representative of the patients' diseases, they would likely respond to this drug and such response should remain stable over successive PDX generations. Among the patients from which

these PDX models were established, 11 Ewing sarcoma PDXs resulted from eight patients who received irinotecan as part of their rescue treatment (combined with temozolomide, with or without additional vincristine or trabectedin); seven rhabdomyosarcoma PDXs derived from six patients who received irinotecan as part of the upfront treatment of the primary tumor (either alone or combined with carboplatin or vincristine); and two osteosarcoma PDXs derived from two patients who did not receive irinotecan. To compare responses to treatment of patients and PDXs, we selected newly diagnosed patients treated with irinotecan as upfront treatment and with available PDX models from their primary tumor. We evaluated treatment response in such patients using the responsive evaluation criteria in solid tumors (RECIST) protocol or the metabolic tumor volume (MTV).

For all efficacy studies in mice, we inserted freshly excised PDX tumors (obtained from one mouse of the immediate earlier generation) in both flanks of athymic nude or Nod-Scid mice. Upon engraftment (tumor volumes ranging 100-500 mm<sup>3</sup>), mice were distributed to control or treatment groups, with care that tumor volume means and standard deviations (STDEV) in both groups were similar. Treatment groups received one cycle of 10 mg/kg/day irinotecan (Hospira, Lake City, IL, USA) in a 5-day-on-2-off regimen, intraperitoneal, for two consecutive weeks, as previously described (30). Control groups received saline using the same regimen as treated groups. Tumor volume was measured three times a week, until day 14, in which response to treatment was evaluated as previously described (10). We defined complete response (CR) as tumor mass < 50 mm<sup>3</sup> and > 50% reduction at the end of treatment (day 14); partial response (PR) as tumor volume regression ≥ 50% at day 14 but tumor volume ≥ 50 mm<sup>3</sup>; stable disease (SD) as < 50% regression and ≤ 25% increase in initial volume at day 14; and progressive disease (PD) as < 50% regression from initial volume and > 25% increase in initial volume at day 14.

To address whether the response to the drug changed upon consecutive passages of the PDX in mice, in three of the models we evaluated the response to irinotecan of different filial generations, one early after initial engraftment ( $F \leq 2$ ) and the second one later ( $F \geq 6$ ). After one cycle of irinotecan, we followed up all animals weekly until tumor regrowth to endpoint (1500 mm<sup>3</sup>) or day 100, to build Kaplan-Meier curves and estimate median survival times. We used the log-rank test to compare survival curves between treatments and between different generations from the same PDX model.

### **1.2.7. Prognostic value of positive tumor engraftment**

The main purpose of this work was to address whether successful engraftment in mice of tumor biopsies of newly diagnosed or relapsed Ewing sarcoma, rhabdomyosarcoma and osteosarcoma patients had a prognostic effect on overall survival (OS) and event-free survival (EFS) of these patients.

To assess the prognostic effect of successful PDX engraftment on EFS and OS of the biopsied children, we used Cox models with a robust sandwich variance estimator to account for the correlation of the data. We calculated hazard ratios (HR) and their corresponding 95% CI. We determined median EFS and OS with the Kaplan-Meier method. For each patient, we calculated EFS as the time from biopsy until date of patient recurrence, death or last follow up, and OS as the time from biopsy until patient's death or last follow up.

To address whether PDX engraftment of primary tumors predicted prognosis of patients classified as "standard risk" according to clinical methods, Ewing sarcoma patients whose biopsies were obtained at initial diagnosis (diagnostic cohort) were divided into two groups, standard risk and high risk, according to their risk stratification following the clinical trial GEIS21 (5). For each of such patient groups, we studied the association between the variables PDX engraftment and relapse, using the Fisher exact test.

### **1.2.8. Statistics**

We performed statistical analyses using GraphPad Prism 8 software (La Jolla, CA, USA) and R software version 3.5.2 (Vienna, Austria).

## **1.3. Results**

### **1.3.1. Patients**

We included in this study 51 children, 37 males and 14 females, with newly diagnosed or relapsed Ewing sarcoma (N = 31), osteosarcoma (N = 10) or rhabdomyosarcoma (N = 10, five each embryonal and alveolar), from November 2010 to November 2019. Median age at inclusion was 11.4 years (range 0.52 – 17.9). Most patients (73%) were non-metastatic at diagnosis. Details on tumor types, fusion genes, anatomic location of primary tumors, risk stratification, and presence of metastases are in supplementary material, Tables S3 (Ewing sarcoma), S4 (osteosarcoma) and S5 (rhabdomyosarcoma).

### **1.3.2. Biopsies and PDXs**

We obtained 68 biopsy samples. Engraftment outcomes of individual patient samples are in supplementary material, Table S6. Forty-one tumor samples were Ewing sarcoma, 12 osteosarcoma and 15 rhabdomyosarcoma. In total, 44% samples engrafted efficiently in mice, with engraftment rates for each tumor type shown in Table 1. Age older than 12 years and relapse were factors associated with increased engraftment rate when pooling all diseases together (Table 1). Tumor type, biopsy location and presence of metastases at diagnosis were not associated with engraftment rate. Procedural factors such as sample conservation (freshly excised or cryopreserved) and application of Matrigel to the sample inserted in the

mice did not affect engraftment rate. Biopsies obtained by surgery or by the Tru-Cut method engrafted with a similar success rate (supplemental material, Table S7).

Fifteen of 51 patients had two or more biopsies included in this study. Nine of them produced two stable PDXs. We studied whether the engraftment of a first biopsy from one patient predicted engraftment of successive biopsies of the same patient at more advanced stages of the disease. We found that nine out of 11 of such second biopsies engrafted after a first biopsy with positive PDX engraftment, but the association between first and second engraftments was not statistically significant, likely due to the low number of cases in the study (supplemental material, Table S8).

Because Ewing sarcoma patients were predominant in the study cohort, we also analyzed their data separately. We found that age older than 12 years old was not determinant in this separate analysis, while relapse and the presence of metastases at diagnosis were significantly associated to engraftment (supplemental material, Table S9).

### **1.3.3. Comparative histopathology of patient tumors and PDX samples**

Histopathology of the tumors and expression of tumor markers CD99, SPARC and MyoD1 did not change significantly upon successive mouse-to-mouse passaging in 12 PDX models studied by IHC (Figure 1). The typical small-blue-round-cell tumor and histologic architecture of the original biopsies remained preserved in Ewing sarcoma xenografts at early and late passages. Stroma around Ewing sarcoma and rhabdomyosarcoma tumor cells, and osteoid in osteosarcoma tumors, did not change significantly upon engraftment. Anti-human nuclear antigen staining was positive in all samples (supplementary material, Figure S1). Tumor anatomy and histology markers were similar in PDX pairs established from the same patients (supplemental material, Figure S2).

### **1.3.4. Tumor growth rate**

The number of proliferating cells (% of Ki67-positive nuclei by IHC; representative images in supplementary material, Figure S3A and quantification in supplementary material, Figure S3B) in patient biopsies was  $54\% \pm 26\%$  (mean and STDEV of N = 12 cases). Their corresponding PDX samples at passage F0 showed a lower number of stained cells ( $37\% \pm 19\%$ ). PDX tumors at generations higher than F0 showed increasing number of Ki67-positive cells ( $40\% \pm 23\%$  at F2 and  $44\% \pm 21\%$  at F5; supplementary material, Figure S3B). Although the differences in Ki67 staining were not statistically significant, tumors at F5 achieved endpoint significantly faster ( $53 \pm 21$  days; mean  $\pm$  STDEV of N = 20 cases) than at the earlier stage F2 ( $92 \pm 47$  days; supplementary material, Figure S3C).

**Table 1.** Association of patient factors with engraftment

Factor	No. of Samples	% Engrafted	No. of Engrafted	Odds ratio (95% CI)	P
Age, years					
< 12	36	30.6	11		
≥ 12	32	59.4	19	3.88 (1.1 – 14.3)	0.042
Tumor type					
All	68	44.1	30		
Ewing sarcoma	41	41.5	17		
Osteosarcoma	12	41.7	5	0.99 (0.2 – 5.6) <sup>a</sup>	
Rhabdomyosarcoma	15	53.3	8	1.97 (0.4 – 10.7) <sup>a</sup>	0.69
Alveolar	9	66.7	6		
Embryonal	6	33.3	2		
Timing of surgery					
Diagnosis	31	22.6	7		
Relapse	37	62.2	23	15.4 (1.3 to 182.8)	0.031
Biopsy origin					
Limbs	22	31.8	7		
Head and neck	14	64.3	9	21.1 (0.04 – 11056.5) <sup>b</sup>	
Chest wall and ribs	7	42.9	3	3.4 (0.05 – 215.9) <sup>b</sup>	
Lung or pleura	13	61.5	8	15 (0.07 – 3075.8) <sup>b</sup>	
Pelvic bones	3	33.3	1	1.2 (0.01 – 134.4) <sup>b</sup>	0.17
Muscle	2	100	2	*	
Teste	1	0	0	*	
Vertebral spine	6	0	0	*	
Metastasis at diagnosis					
No	48	37.5	18		
Yes	20	60.0	12	3.62 (0.64 – 20.50)	0.15

\*Excluded from statistical analysis in biopsy of origin for lacking an event in No. of engrafted or in No. of non engrafted.

<sup>a</sup>Compared to Ewing sarcoma.

<sup>b</sup>Compared to limbs.



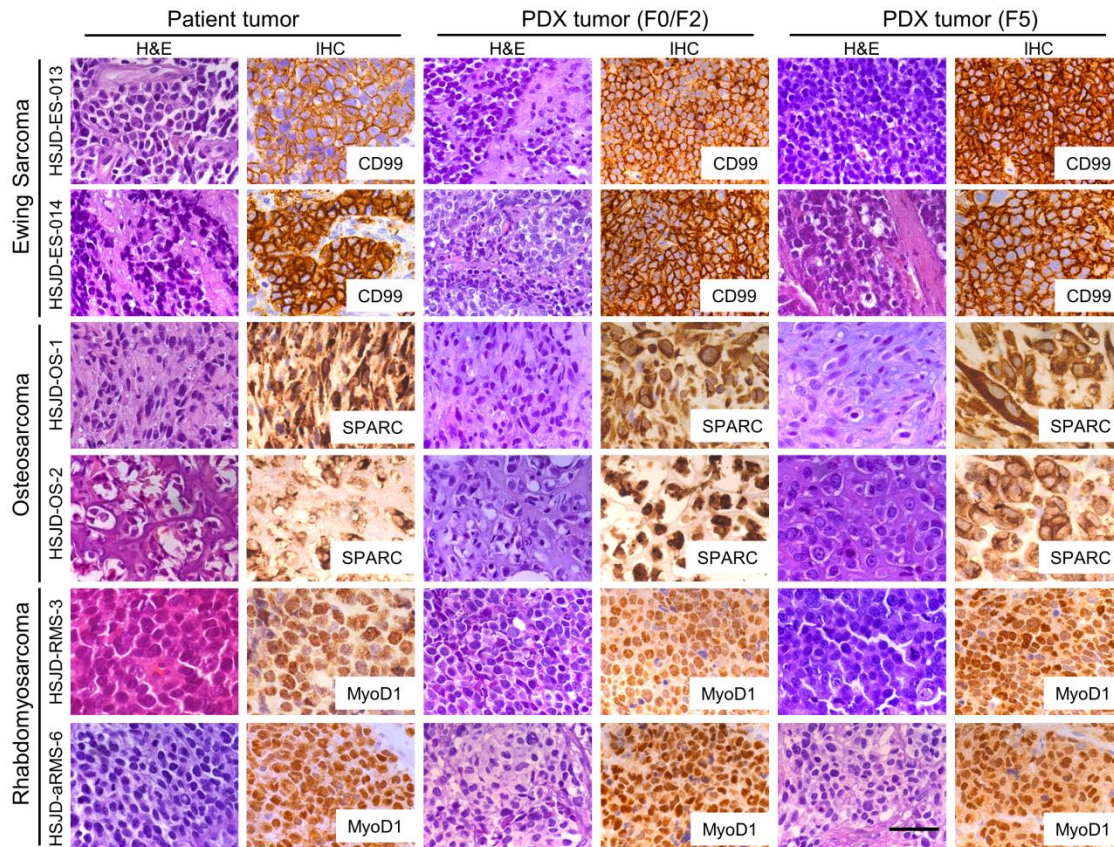


**Figure 1.** Comparative histology (H&E and IHC staining) of six representative cases of original human tumor biopsies and the corresponding patient-derived xenografts (PDX) at early passages (F0/F2) and late passage (F5). CD99 (cell membrane), SPARC (cytoplasm) and MyoD1 (nuclear) are stained in brown. These representative samples were selected from six Ewing sarcomas, three osteosarcomas and three rhabdomyosarcomas with complete histopathology studies. All images were obtained using a microscope at 40x objective magnification. Scale bar represents 50  $\mu$ m.

### 1.3.5. CNA in patient biopsies and corresponding PDXs

We selected one Ewing sarcoma tumor with low CNA alterations, and one rhabdomyosarcoma with highly aberrant chromosomal profile for CNA analyses. Karyotype alterations of Ewing sarcoma (HSJD-ES-012) were equivalent for patient tumor and PDX models at F2 and F5 (10). Ewing sarcoma CNA included a copy-neutral loss of heterogeneity (cnLOH) in chromosome 3p and 20q as previously reported (10) (supplementary material, Figure S4). For rhabdomyosarcoma (HSJD-RMS-4), both PDX models, F2 and F5, shared 90% of the alterations observed in the patient tumor. Chromosomal aberrations shared by the biopsy and the PDX included whole gains in one or two copies of chromosomes 2, 3, 4, 6, 10, 11, 12, 14, 16, 17, 18, 19, 20, 21 and X; partial gain in chromosomes 1, 7, 9 and 13; and whole chromosome loss in chromosome 15. Non-equivalent alterations among biopsy and PDX included gain of two copies of chromosomes 5, 8 and 22 in the tumor biopsy, and partial gains of chromosome 5 and 22 and one copy gain of chromosome 8 in both PDX models (supplementary material, Figure S4).

### 1.3.6. Antitumor activity of irinotecan in subcutaneous PDXs

All PDX models (see identification and clinical details in supplementary material, Table S10) had a measurable response after one cycle of irinotecan (Figure 2A and supplementary material, Table S11). We found that nine of 20 models (45%) achieved CR to treatment and all achieved at least SD (Figure 2B).

We compared responses to treatment of patient and PDX of four newly diagnosed rhabdomyosarcoma patients receiving upfront irinotecan, three combined with carboplatin, and one with vincristine (supplementary material, Table S12). The three patients treated with irinotecan plus carboplatin achieved the same response to treatment as their corresponding PDX models (HSJD-aRMS-7, PR; HSJD-aRMS-10, PR; and HSJD-RMS-11, CR) to irinotecan. The patient treated with irinotecan plus vincristine achieved a lower degree of response (SD) compared to the corresponding PDX (HSJD-RMS-9, CR).

In the PDX models for which irinotecan activity was evaluated at two different filial generations, both tumors at passage  $F \geq 6$  and  $F \leq 2$  showed similar responses to irinotecan (Figure 2C). Upon treatment cessation, the PDXs grew similarly, even those that achieved a complete response, and achieved similar median survivals until endpoint (supplementary material, Table S13).

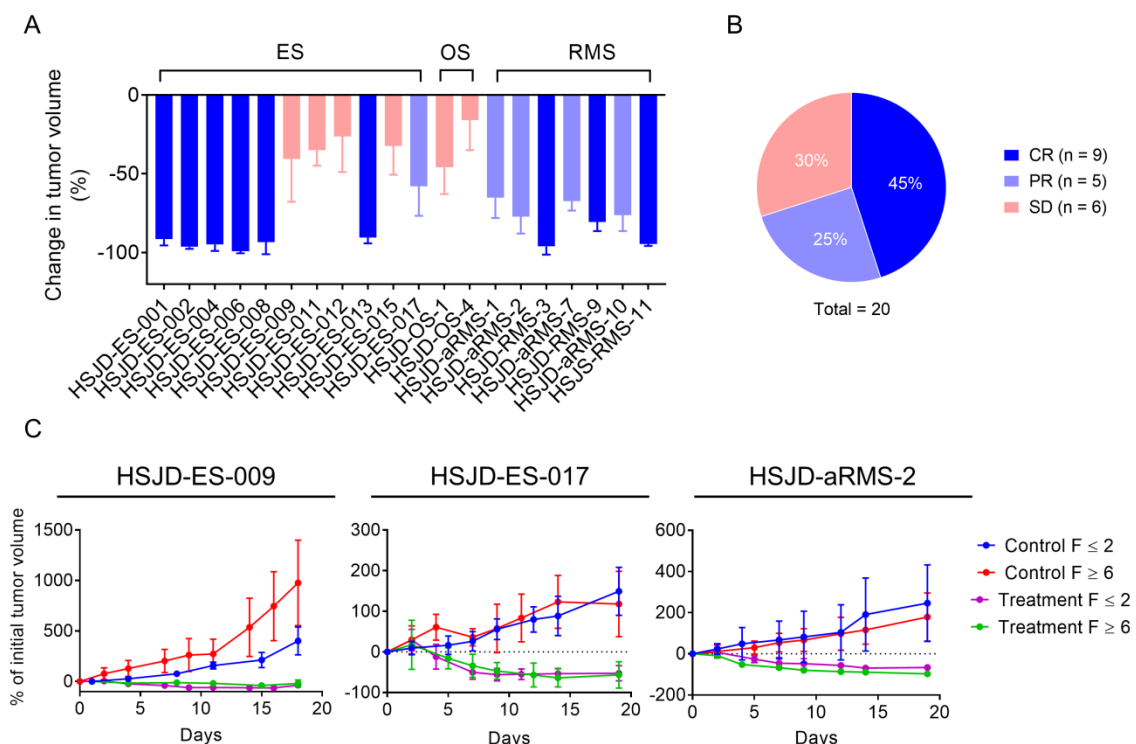


**Figure 2.** Antitumor activity of irinotecan in subcutaneous PDX. (A) Change in tumor volume (mean and STDEV of 3-15 tumors) at the end of irinotecan treatment (day 14). (B) Percentage of tumor models achieving each response. CR, complete response; PR, partial response; SD, stable disease. (C) Tumor volume (% of volume at treatment start) in three PDX pairs at passage  $F \leq 2$  or  $F \geq 6$ , treated with one cycle of irinotecan (Treatment) or not treated (Control). Models and F were HSJD-ES-009 (F2 vs F6), HSJD-ES-017 (F1 vs F8) and HSJD-aRMS-2 (F2 vs F10).



### 1.3.7. Prognostic value of positive PDX engraftment in mice

Patients included in the analysis had a median follow up of 21.2 months (range 2.40 – 101 months). Figure 3 shows the outcome of the study cohort according to engraftment in mice. Median EFS for patients with positive engraftment (7.56 months) was significantly shorter than that of patients with negative engraftment (22.4 months;  $P = 0.00021$ ; HR 3.34; 95% CI: 1.77 to 6.31; Figure 3A). Similarly, median OS was shorter for patients with positive engraftment (19.9 months) compared to that of patients with negative engraftment (42.5 months;  $P = 0.0069$ ; HR 2.51; 95% CI: 1.29 to 4.89; Figure 3B).

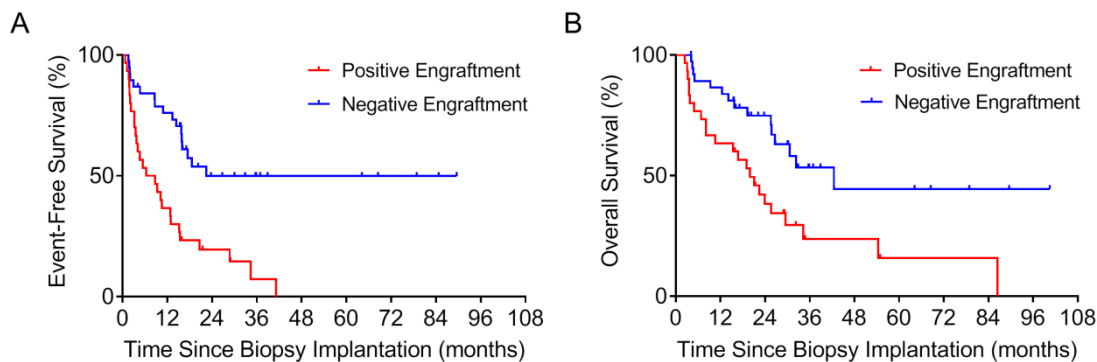


**Figure 3.** Kaplan-Meier estimation of (A) event-free survival and (B) overall survival among all patients with positive ( $n = 30$ ) or negative ( $n = 38$ ) engraftment of their PDX.

Because relapse was associated with increased engraftment rate, we stratified patients into those whose samples were obtained at initial diagnosis (diagnostic cohort) and at relapse (relapse cohort). We further separated each cohort according to positive and negative engraftment. In the diagnostic cohort, positive engraftment associated with shorter median EFS (20.6 months). In contrast, median EFS was not reached for negative engraftment ( $P = 0.040$ ; HR 2.87; 95% CI: 1.05 to 7.85; Figure 4A). In this cohort, patients with positive engraftment also had shorter median OS (34.2 months), although not statistically significant compared to patients with negative engraftment ( $P = 0.19$ ; HR 2.06; 95% CI: 0.70 to 6.0; Figure 4B).

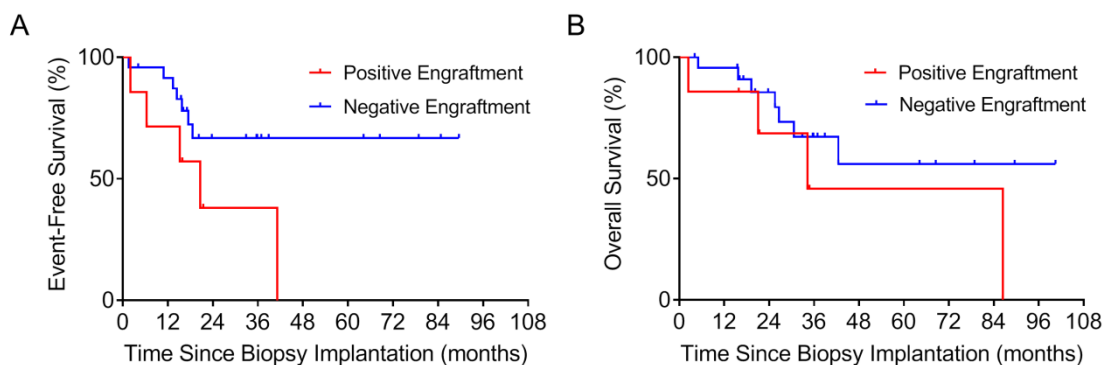


**Figure 4.** Kaplan-Meier estimation of (A) event-free survival and (B) overall survival among patients of the diagnostic cohort with positive ( $n = 7$ ) or negative ( $n = 24$ ) engraftment of their PDX.

In the relapse cohort, we did not find a significant association of positive and negative engraftment with median EFS of 4.56 and 12.2 months, respectively ( $P = 0.17$ ; HR 1.70; 95% CI: 0.80 to 3.63; Figure 5A) and OS of 16.7 and 25.7 months, respectively ( $P = 0.30$ ; HR 1.51; 95% CI: 0.69 to 3.32; Figure 5B).

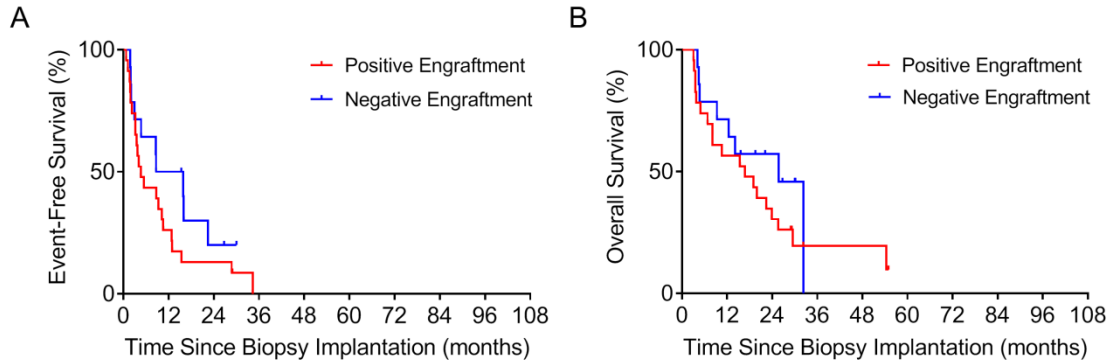


**Figure 5.** Kaplan-Meier estimation of (A) event-free survival and (B) overall survival among patients of the relapse cohort with positive ( $n = 23$ ) or negative ( $n = 14$ ) engraftment of their PDX.

We studied 18 newly diagnosed Ewing sarcoma patients, seven of which were standard risk, and 11 high risk, with follow up times of 15.5 to 101 months. Two out of the seven patients classified as standard risk relapsed and eventually died of disease. Biopsies from these two patients successfully established PDXs in mice, while biopsies from the remaining five standard risk patients did not. In fact, we found that positive PDX engraftment predicted relapse of patients classified as standard risk ( $P = 0.0357$ ; Fisher exact test). Among the 11 newly diagnosed Ewing sarcoma patients classified as high risk, two established PDX models. Both patients relapsed or were refractory to treatment, and eventually died of disease. Among the remaining nine high risk patients, for whom PDX engraftment was unsuccessful, another two relapsed. The association of positive PDX engraftment and relapse was not significant in these high risk patients ( $P = 0.1091$ ).

#### 1.4. Discussion

PDXs are powerful tools for cancer biology and precision cancer medicine studies, and may be useful to predict patient prognosis (17). Determination of prognosis is especially relevant in pediatric patients, 80% of whom will survive cancer and reach adulthood (31). Identification of prognostic factors for these children helps select appropriate treatment for their disease, ensuring maximum clinical benefit along with minimum long-term toxicity (32). In the current study, we show that positive engraftment of tumor biopsies in mice is a prognostic factor related to poorer EFS for newly diagnosed pediatric patients with the most frequent bone or soft tissue sarcomas.

All patients in the diagnostic cohort whose samples engrafted in mice relapsed and died of their disease while we were performing this study. This discovery might be especially relevant for newly diagnosed Ewing sarcoma patients, because PDX

engraftment predicted relapse in patients otherwise classified as standard risk at diagnosis. Thus, our results suggest that PDX engraftment might help unveil patients at higher risk and stratify them accordingly.

The engraftment rate calculated in this study, 44%, is similar to previous studies of pediatric solid malignancies both for primary and relapsed tumors (23,33,34). Patient determinants favoring tumor biopsy engraftment in mice are not yet clear. We show here that age older than 12 years, or relapsed disease, correlate highly with pediatric sarcoma biopsy engraftment. Age and relapsed disease are also determining factors for engraftment of other tumors such as lung adenocarcinoma and hepatoblastoma (15,35). In adult patients, advanced disease stage increases the likelihood of PDX engraftment from patients with lung cancer (36). Also in adult patients, tumor mutations, such as in *EGFR*, *BRCA1/BRCA2* and *SMAD4* genes decrease engraftment rates in adenocarcinoma, breast cancer and pancreatic cancer, respectively (14,15,18).

Other studies have evaluated some of the technical factors addressed in our study, such as sample conservation. In agreement with our results, cryopreserved pancreatic cancer biopsies engrafted efficiently in mice (37). We did not evaluate “engraftment site” as a factor, but the orthotopic site is especially relevant to reproduce the complex microenvironment necessary for the growth of central nervous system tumors (38-40), and could facilitate and accelerate tumor implantation and recapitulate patient tumor characteristics (41,42). However, our selection of the subcutaneous site is justified by its advantages of offering a simple and fast surgical procedure and easier follow up of the mice, as it does not require imaging systems to visualize tumor site implantation (13).

Interestingly, we found that the Tru-Cut technique, a less invasive method than the surgical collection of tumor samples, was successful for the purpose of PDX establishment, and resulted in more rapid patient recovery (43). Patients for whom surgery would constitute an excessive risk or associated morbidity, such as relapsed patients with advanced disease, are more suitable for the Tru-Cut method. On the other hand, the Tru-Cut method is at a disadvantage, due to its resulting smaller sample size and tumor heterogeneity and necrosis in some tumor areas; therefore, the Tru-Cut technique actually can result in greater challenges to pathologists and cancer biologists.

Our studies confirm the similarities of histology and genetics of the PDX and the original biopsy, consistent with previous data showing that CNA variations in patient biopsies were conserved in tumor xenografts of breast cancer and neuroblastoma (17,44). It was not within the scope of our project to perform a comprehensive comparison of paired PDX models coming from the same patient. In a previous study, we compared systematically Ewing sarcoma PDX pairs obtained from the

same patients, finding functional differences among them that we attributed to patient treatments (10).

Other studies have shown changes in tumor architecture and chromosomal stability during successive passages over time that could differ from those arising in patients (13,45). Breast cancer tumors and their corresponding xenografts share mostly all single nucleotide variations, with the exception of some clusters that are dominant in the PDX but not in the tumor patients (17). These results, among others, suggest that there exists clonal selection during xenograft establishment (21,46,47). It is therefore not clear whether such alterations affect the capacity of the PDX to represent the original patient biopsy from the functional perspective, such as response to treatment. Our studies of irinotecan activity in PDX models at different stages of their engraftment partially addressed this question. We confirmed the stability of our models during successive engraftments and their ability to replicate patient response to treatment at the preclinical dosage of 10 mg/kg using the protracted dosing schedule (30). It is likely that this dosage provides a higher SN-38 systemic exposure than the one achievable in humans, due to the better conversion of the prodrug irinotecan in mice (48), which could explain the different response to irinotecan found between the PDX and one of our patients. Nevertheless, our data support that PDX might predict clinical efficacy of personalized medicine while keeping stable tumor architecture and heterogeneity (11-13). Performing drug efficacy studies using the PDX models could aid in the design of personalized therapies for our patients. The main limiting factor is the lag time between the necessary time for the biopsy to engraft (9 – 17 weeks, according to our experience) and the time-critical needs of the patients. Disease progression is usually faster than the time needed to engraft and expand tumors, and not all patients can benefit from this approach. According to our experience, we need at least 28 weeks to obtain preclinical results for candidate individualized treatments. This number is obtained by adding the median times to achieve engraftment of the F0 generation (13 weeks; range 9-17 weeks), median times for expanding the F1 generation in a sufficient number of mice to start candidate treatments (13 weeks; range 6-20 weeks) and times to treat and evaluate treatment activity (2 weeks typically). Although personalized treatments were not within the scope of our work, in our cohort approximately 50% (13) patients with associated stable PDX progressed later than 28 weeks after biopsy, and could have obtained a theoretical benefit from preclinical assays using their PDX.

In conclusion, our study suggests that PDX engraftment at the time of patient diagnosis helps to identify aggressive pediatric sarcoma tumors with poorer prognosis, predicting disease progression. Such PDX models stably represent patient disease, both morphologically and functionally. Whether this systematic study of the PDXs from our patients has future clinical implications for personalized medicine, patient risk classification and intensification of treatments should now be addressed in prospective clinical trials.

## **1.5. Acknowledgements**

Thanks to the Xarxa de Bancs de Tumors de Catalunya (XBTC; sponsored by Pla Director d'Oncologia de Catalunya). The work at Hospital Sant Joan de Deu was generously supported by associations of parents and families of children with cancer, including Asociación Pablo Ugarte. HCE was supported by grant from ISCIII-FEDER (PI19/00138). AMC was supported by grants from AECC Scientific Foundation, MINECO (SAF2011-22660), the European Union Seventh Framework Programme (FP7/2007-2013) under Marie Curie International Reintegration Grant (PIRG-08-GA-2010-276998), ISCIII-FEDER (CP13/00189 and CPII18/00009). This project has received funding from the Innovative Medicines Initiative 2 Joint Undertaking under grant agreement No 116064. This Joint Undertaking receives support from the European Union's Horizon 2020 research and innovation programme and EFPIA.

## **1.6. Author contribution statement**

All authors were involved in data collection and manuscript editing. HC-E, SP-J, CL and AMC analyzed the data. JM and AMC conceived the work, acquired funding and provided resources. HC-E and AMC wrote the original draft and generated the figures. AMC supervised the project.

### 1.7. References

1. Pappo AS, Dirksen U. Rhabdomyosarcoma, Ewing Sarcoma, and Other Round Cell Sarcomas. *J Clin Oncol* 2018; **36**: 168-179.
2. Grunewald TGP, Cidre-Aranaz F, Surdez D, *et al.* Ewing sarcoma. *Nat Rev Dis Primers* 2018; **4**: 5.
3. Kansara M, Teng MW, Smyth MJ, *et al.* Translational biology of osteosarcoma. *Nat Rev Cancer* 2014; **14**: 722-735.
4. Skapek SX, Ferrari A, Gupta AA, *et al.* Rhabdomyosarcoma. *Nat Rev Dis Primers* 2019; **5**: 1.
5. Mora J, Castaneda A, Perez-Jaume S, *et al.* GEIS-21: a multicentric phase II study of intensive chemotherapy including gemcitabine and docetaxel for the treatment of Ewing sarcoma of children and adults: a report from the Spanish sarcoma group (GEIS). *Br J Cancer* 2017; **117**: 767-774.
6. de Alava E. Ewing Sarcoma, an Update on Molecular Pathology with Therapeutic Implications. *Surg Pathol Clin* 2017; **10**: 575-585.
7. Grohar PJ, Janeway KA, Mase LD, *et al.* Advances in the Treatment of Pediatric Bone Sarcomas. *Am Soc Clin Oncol Educ Book* 2017; **37**: 725-735.
8. Crompton BD, Stewart C, Taylor-Weiner A, *et al.* The genomic landscape of pediatric Ewing sarcoma. *Cancer Discov* 2014; **4**: 1326-1341.
9. Whelan JS, Davis LE. Osteosarcoma, Chondrosarcoma, and Chordoma. *J Clin Oncol* 2018; **36**: 188-193.
10. Castillo-Ecija H, Monterrubio C, Pascual-Pasto G, *et al.* Treatment-driven selection of chemoresistant Ewing sarcoma tumors with limited drug distribution. *J Control Release* 2020; **324**: 440-449.
11. Hidalgo M, Amant F, Biankin AV, *et al.* Patient-derived xenograft models: an emerging platform for translational cancer research. *Cancer Discov* 2014; **4**: 998-1013.
12. Gao H, Korn JM, Ferretti S, *et al.* High-throughput screening using patient-derived tumor xenografts to predict clinical trial drug response. *Nat Med* 2015; **21**: 1318-1325.
13. Byrne AT, Alferez DG, Amant F, *et al.* Interrogating open issues in cancer precision medicine with patient-derived xenografts. *Nat Rev Cancer* 2017; **17**: 254-268.
14. Eoh KJ, Chung YS, Lee SH, *et al.* Comparison of Clinical Features and Outcomes in Epithelial Ovarian Cancer according to Tumorigenicity in Patient-Derived Xenograft Models. *Cancer Res Treat* 2018; **50**: 956-963.
15. Stewart EL, Mascaux C, Pham NA, *et al.* Clinical Utility of Patient-Derived Xenografts to Determine Biomarkers of Prognosis and Map Resistance Pathways in EGFR-Mutant Lung Adenocarcinoma. *J Clin Oncol* 2015; **33**: 2472-2480.
16. Kresse SH, Meza-Zepeda LA, Machado I, *et al.* Preclinical xenograft models of human sarcoma show nonrandom loss of aberrations. *Cancer* 2012; **118**: 558-570.

17. DeRose YS, Wang G, Lin YC, *et al.* Tumor grafts derived from women with breast cancer authentically reflect tumor pathology, growth, metastasis and disease outcomes. *Nat Med* 2011; **17**: 1514-1520.
18. Garrido-Laguna I, Uson M, Rajeshkumar NV, *et al.* Tumor Engraftment in Nude Mice and Enrichment in Stroma- Related Gene Pathways Predict Poor Survival and Resistance to Gemcitabine in Patients with Pancreatic Cancer. *Clin Cancer Res* 2011; **17**: 5793-5800.
19. Moon HG, Oh K, Lee J, *et al.* Prognostic and functional importance of the engraftment-associated genes in the patient-derived xenograft models of triple-negative breast cancers. *Breast Cancer Res Treat* 2015; **154**: 13-22.
20. Neale G, Su X, Morton CL, *et al.* Molecular characterization of the pediatric preclinical testing panel. *Clin Cancer Res* 2008; **14**: 4572-4583.
21. Eirew P, Steif A, Khattra J, *et al.* Dynamics of genomic clones in breast cancer patient xenografts at single-cell resolution. *Nature* 2015; **518**: 422-426.
22. Monterrubio C, Pascual-Pasto G, Cano F, *et al.* SN-38-loaded nanofiber matrices for local control of pediatric solid tumors after subtotal resection surgery. *Biomaterials* 2016; **79**: 69-78.
23. Nanni P, Landuzzi L, Manara MC, *et al.* Bone sarcoma patient-derived xenografts are faithful and stable preclinical models for molecular and therapeutic investigations. *Sci Rep* 2019; **9**: 12174.
24. Bukchin A, Pascual-Pasto G, Cuadrado-Vilanova M, *et al.* Glucosylated nanomicelles target glucose-avid pediatric patient-derived sarcomas. *J Control Release* 2018; **276**: 59-71.
25. Meehan TF, Conte N, Goldstein T, *et al.* PDX-MI: Minimal Information for Patient-Derived Tumor Xenograft Models. *Cancer Res* 2017; **77**: e62-e66.
26. Monterrubio C, Paco S, Vila-Ubach M, *et al.* Combined Microdialysis-Tumor Homogenate Method for the Study of the Steady State Compartmental Distribution of a Hydrophobic Anticancer Drug in Patient-Derived Xenografts. *Pharm Res* 2015; **32**: 2889-2900.
27. Skaltsa K, Jover L, Carrasco JL. Estimation of the diagnostic threshold accounting for decision costs and sampling uncertainty. *Biom J* 2010; **52**: 676-697.
28. Monterrubio C, Paco S, Olaciregui NG, *et al.* Targeted drug distribution in tumor extracellular fluid of GD2-expressing neuroblastoma patient-derived xenografts using SN-38-loaded nanoparticles conjugated to the monoclonal antibody 3F8. *J Control Release* 2017; **255**: 108-119.
29. Cosetti M, Wexler LH, Calleja E, *et al.* Irinotecan for pediatric solid tumors: the Memorial Sloan-Kettering experience. *J Pediatr Hematol Oncol* 2002; **24**: 101-105.
30. Thompson J, Zamboni WC, Cheshire PJ, *et al.* Efficacy of systemic administration of irinotecan against neuroblastoma xenografts. *Clin Cancer Res* 1997; **3**: 423-431.



31. Ward ZJ, Yeh JM, Bhakta N, *et al.* Global childhood cancer survival estimates and priority-setting: a simulation-based analysis. *Lancet Oncol* 2019; **20**: 972-983.
32. Winther JF, Kenborg L, Byrne J, *et al.* Childhood cancer survivor cohorts in Europe. *Acta Oncol* 2015; **54**: 655-668.
33. Stewart E, Federico SM, Chen X, *et al.* Orthotopic patient-derived xenografts of paediatric solid tumours. *Nature* 2017; **549**: 96-100.
34. Morton CL, Houghton PJ. Establishment of human tumor xenografts in immunodeficient mice. *Nat Protoc* 2007; **2**: 247-250.
35. Nicolle D, Fabre M, Simon-Coma M, *et al.* Patient-Derived Mouse Xenografts From Pediatric Liver Cancer Predict Tumor Recurrence and Advise Clinical Management. *Hepatology* 2016; **64**: 1121-1135.
36. Chen Y, Zhang R, Wang L, *et al.* Tumor characteristics associated with engraftment of patient-derived non-small cell lung cancer xenografts in immunocompromised mice. *Cancer* 2019; **125**: 3738-3748.
37. Hernandez MC, Yang L, Leiting JL, *et al.* Successful Secondary Engraftment of Pancreatic Ductal Adenocarcinoma and Cholangiocarcinoma Patient-Derived Xenografts After Previous Failed Primary Engraftment. *Transl Oncol* 2019; **12**: 69-75.
38. Brabetz S, Leary SES, Grobner SN, *et al.* A biobank of patient-derived pediatric brain tumor models. *Nat Med* 2018; **24**: 1752-1761.
39. Yu L, Baxter PA, Voicu H, *et al.* A clinically relevant orthotopic xenograft model of ependymoma that maintains the genomic signature of the primary tumor and preserves cancer stem cells in vivo. *Neuro Oncol* 2010; **12**: 580-594.
40. Shu Q, Wong KK, Su JM, *et al.* Direct orthotopic transplantation of fresh surgical specimen preserves CD133+ tumor cells in clinically relevant mouse models of medulloblastoma and glioma. *Stem Cells* 2008; **26**: 1414-1424.
41. Okano M, Oshi M, Butash A, *et al.* Orthotopic Implantation Achieves Better Engraftment and Faster Growth Than Subcutaneous Implantation in Breast Cancer Patient-Derived Xenografts. *J Mammary Gland Biol Neoplasia* 2020; **25**: 27-36.
42. Siolas D, Hannon GJ. Patient-derived tumor xenografts: transforming clinical samples into mouse models. *Cancer Res* 2013; **73**: 5315-5319.
43. Sitt JC, Griffith JF, Lai FM, *et al.* Ultrasound-guided synovial Tru-cut biopsy: indications, technique, and outcome in 111 cases. *Eur Radiol* 2017; **27**: 2002-2010.
44. Braekeveldt N, Wigerup C, Gisselsson D, *et al.* Neuroblastoma patient-derived orthotopic xenografts retain metastatic patterns and geno- and phenotypes of patient tumours. *Int J Cancer* 2015; **136**: E252-E261.
45. Tentler JJ, Tan AC, Weekes CD, *et al.* Patient-derived tumour xenografts as models for oncology drug development. *Nat Rev Clin Oncol* 2012; **9**: 338-350.



46. Ben-David U, Ha G, Tseng YY, *et al.* Patient-derived xenografts undergo mouse-specific tumor evolution. *Nat Genet* 2017; **49**: 1567-1575.
47. Gerlinger M, Rowan AJ, Horswell S, *et al.* Intratumor heterogeneity and branched evolution revealed by multiregion sequencing. *N Engl J Med* 2012; **366**: 883-892.
48. Stewart CF, Zamboni WC, Crom WR, *et al.* Disposition of irinotecan and SN-38 following oral and intravenous irinotecan dosing in mice. *Cancer Chemother Pharmacol* 1997; **40**: 259-265.
49. Mora J, Cruz CO, Parareda A, *et al.* Treatment of relapsed/refractory pediatric sarcomas with gemcitabine and docetaxel. *J Pediatr Hematol Oncol* 2009; **31**: 723-729.
50. Wagner LM, McAllister N, Goldsby RE, *et al.* Temozolomide and intravenous irinotecan for treatment of advanced Ewing sarcoma. *Pediatric Blood Cancer* 2007; **48**: 132-139.
51. Strauss SJ, McTiernan A, Driver D, *et al.* Single center experience of a new intensive induction therapy for ewing's family of tumors: feasibility, toxicity, and stem cell mobilization properties. *J Clin Oncol* 2003; **21**: 2974-2981.
52. Raciborska A, Bilska K, Drabko K, *et al.* Vincristine, irinotecan, and temozolomide in patients with relapsed and refractory Ewing sarcoma. *Pediatric Blood Cancer* 2013; **60**: 1621-1625.
53. Dharmarajan KV, Wexler LH, Wolden SL. Concurrent radiation with irinotecan and carboplatin in intermediate- and high-risk rhabdomyosarcoma: a report on toxicity and efficacy from a prospective pilot phase II study. *Pediatric Blood Cancer* 2013; **60**: 242-247.
54. Meyers PA, Schwartz CL, Krailo MD, *et al.* Osteosarcoma: the addition of muramyl tripeptide to chemotherapy improves overall survival--a report from the Children's Oncology Group. *J Clin Oncol* 2008; **26**: 633-638.
55. Ferrari S, Smeland S, Mercuri M, *et al.* Neoadjuvant chemotherapy with high-dose Ifosfamide, high-dose methotrexate, cisplatin, and doxorubicin for patients with localized osteosarcoma of the extremity: a joint study by the Italian and Scandinavian Sarcoma Groups. *J Clin Oncol* 2005; **23**: 8845-8852.

References 49 – 55 are cited only in the supplementary material.

## 1.8. Supplementary material

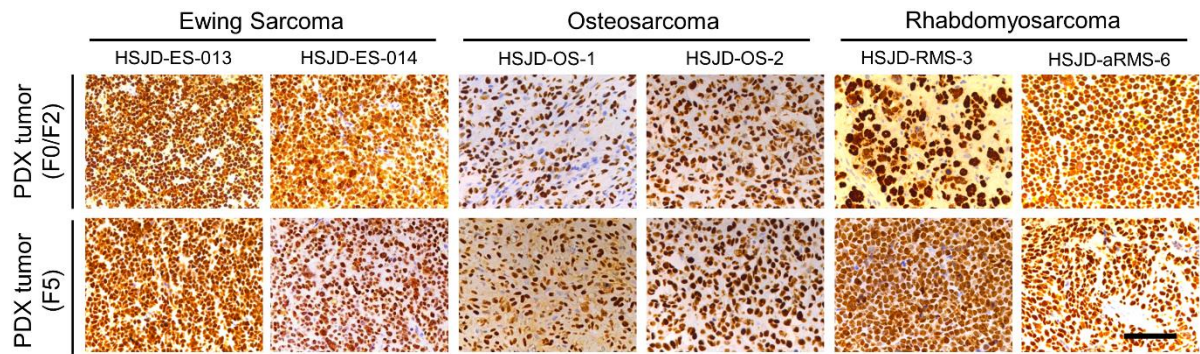


**Figure S1.** Staining of human cells (human nuclei, in brown) in six representative cases of xenografts at early (F0/F2) and late passages (F5). These representative samples were selected among six Ewing sarcoma, three osteosarcoma and three rhabdomyosarcoma with complete histopathology studies. All images were obtained using a microscope with a 20x objective. Scale bar represents 50  $\mu\text{m}$ .

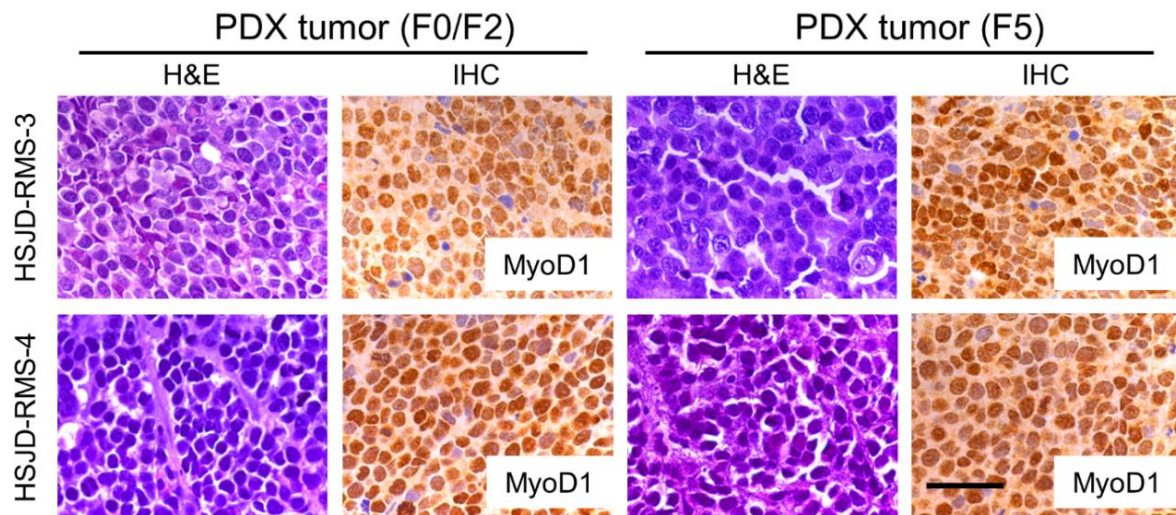


**Figure S2.** Comparative histology (H&E and MyoD1 staining) of two PDX derived from the same rhabdomyosarcoma patient at relapse (HSJD-RMS-3) and necropsy (HSJD-RMS-4). MyoD1 (nuclear) is stained in brown. All images were obtained using a microscope at 40x. Scale bar represents 25  $\mu$ m.

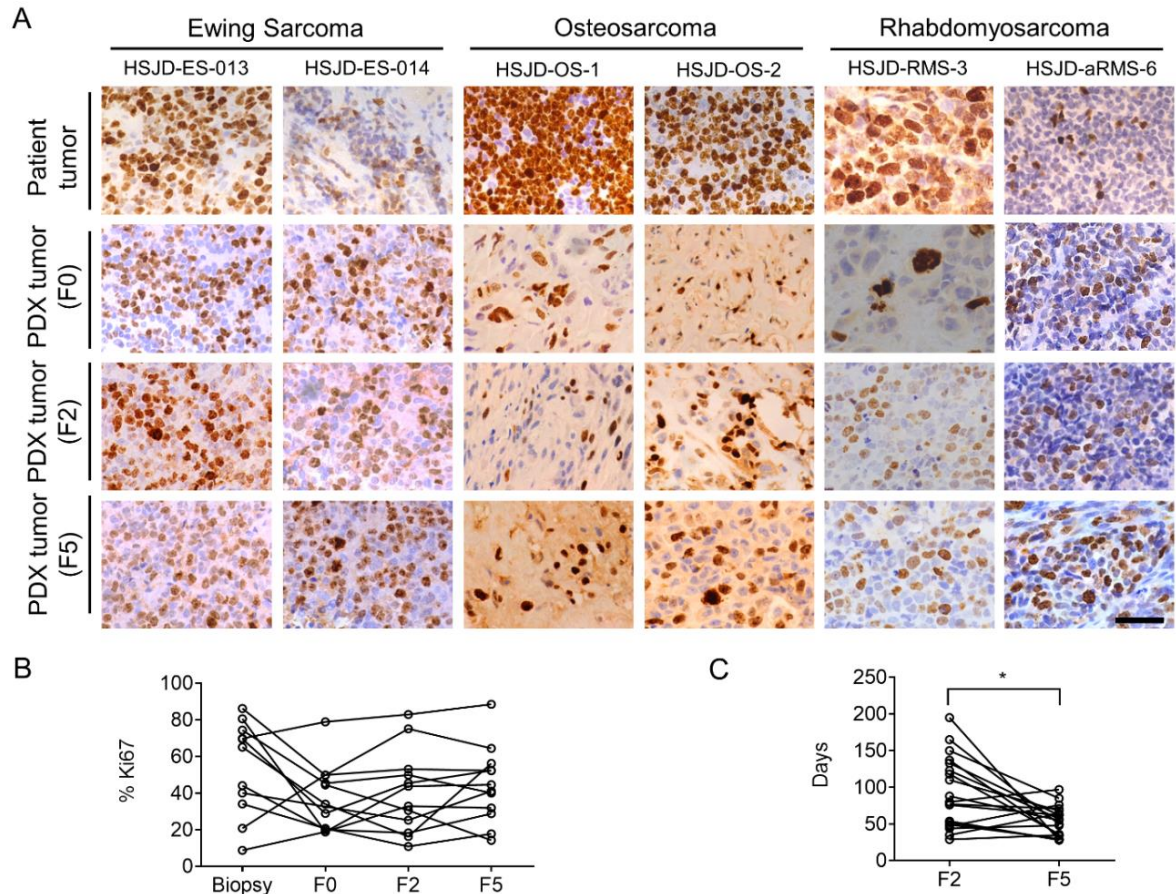


**Figure S3.** Analysis of cell proliferation in human tumor biopsies and their corresponding PDXs. (A) Ki67 histology staining in patient tumor and three PDX generations (F0, F2 and F5) in six representative cases. All images were obtained using a microscope at 40x. Scale bar represents 25  $\mu\text{m}$ . (B) Quantification of Ki67 positive cells (%). These samples were selected among six Ewing sarcoma, three osteosarcoma and three rhabdomyosarcoma with complete histopathology studies. Each point represents the mean of ten slides per tumor and generation. (C) Time in days of tumor growth at F2 and F5 to achieve 1500  $\text{mm}^3$ . \* $P = 0.0042$ , paired  $t$  test, F2 vs F5.



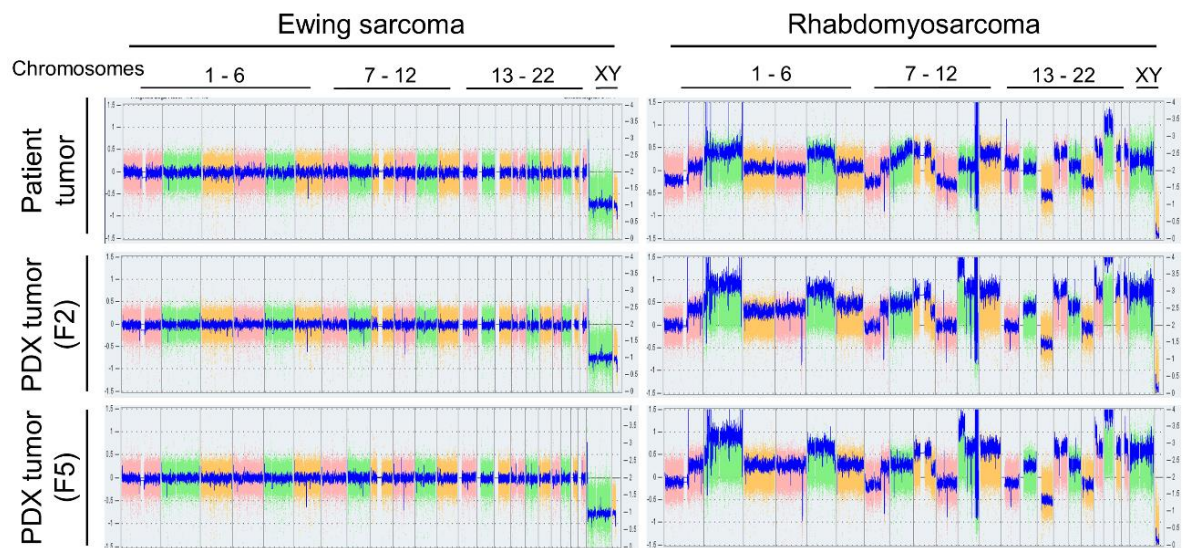


**Figure S4.** Whole genome visualization of the chromosomal profiles of patients with Ewing sarcoma (model named HSJD-ES-012) and rhabdomyosarcoma (HSJD-RMS-4) and their matched PDX models at generations F2 and F5. The log<sub>2</sub> copy number track and the smooth signal indicate the segmental and copy number aberrations observed in the samples. Each column represents a different chromosome.

**Table S1.** Clinical data of patients with Ewing sarcoma, osteosarcoma and rhabdomyosarcoma

<b>Data type</b>	<b>Description</b>	<b>Entry (example)</b>
Patient clinical information	Patient ID	ES-009
	Gender	Male
	Age	12.5 years old
	Diagnosis	Ewing sarcoma
	Relapse, dead or last follow up date	20/10/2010
	Previous treatment	GEIS21
Tumor information	Treatment response	Complete (RECIST protocol)
	Tumor ID	B20-01234
	Biopsy date	01/01/2020
	Primary tumor tissue of origin	Chest wall and ribs
	Timing of surgery	Relapse
	Tissue histology	H&E and IHC panel
	Molecular tissue analysis	Fusion gene <i>EWSR1-FLI1</i>
	Sample collection method	Tru-Cut needle

**Table S2.** Data from patient derived-xenografts (PDX) established from patients with Ewing sarcoma, osteosarcoma and rhabdomyosarcoma

<b>Data type</b>	<b>Description</b>	<b>Entry (example)</b>
Xenograft establishment	PDX ID	HSJD-ES-009
	Mouse strain (source)	NOD-SCID (Envigo)
	Sample conservation	Freshly excised
	Inoculation type and site	Subcutaneous; both flanks
	Use of Matrigel	No
Tumor analysis	Engraftment time	4.2 months
	Tumor characterization technology	Histology and IHC panel
	Anti-human nuclei staining	Positive
Model study	Passage	F0
	Treatment 1	Irinotecan 10 mg/kg/day; 5-day-on-2-off
	Response to treatment 1	CR

**Table S3.** Clinical information from patients with Ewing sarcoma (N = 31; median age 12.3 years; range 0.52 – 17.9 years)

<b>Factor</b>	<b>No. of Patients</b>	<b>%</b>
Gender		
Female	8	25.8
Male	23	74.2
Fusion gene type		
<i>EWSR1-ERG</i>	2	6.5
<i>EWSR1-FLI1</i>	29	93.5
Primary tumor		
Chest wall and ribs	6	19.4
Limbs	12	38.7
Pelvic bones	6	19.4
Vertebral spine	7	22.6
Metastasis at diagnosis		
No	23	74.2
Yes	8	25.8
Risk stratification of newly diagnosed patients <sup>1</sup>		
Standard	7	38.9
High	11	61.1

<sup>1</sup>Of the 31 patients included in this study, 18 were included at disease diagnosis. For such patients, we applied the risk stratification protocol published in reference [5].



**Table S4.** Clinical information from patients with osteosarcoma (N = 10; median age 11.1 years; range 5.67 – 14.7 years)

<b>Factor</b>	<b>No. of Samples</b>	<b>%</b>
Gender		
Female	3	30
Male	7	70
Primary tumor		
Limbs	10	100
Metastasis at diagnosis		
No	8	80
Yes	2	20

**Table S5.** Clinical information from patients with rhabdomyosarcoma (N = 10; median age 9.7 years; range 4.03 – 15.4 years)

<b>Factor</b>	<b>No. of Samples</b>	<b>%</b>
Gender		
Female	3	30
Male	7	70
Tumor type		
Alveolar (aRMS)	5	50
Embryonal (eRMS)	5	50
Fusion gene type		
Absent	5	50
<i>PAX3-FKHR</i>	4	40
<i>PAX7-FKHR</i>	1	10
Primary tumor		
Chest wall and ribs	1	10
Head and neck	3	30
Limbs	3	30
Pelvic bones	1	10
Urogenital region	2	20
Metastasis at diagnosis		
No	6	60
Yes	4	40

**Table S6.** Engraftment outcomes of patient samples

<b>Patient</b>	<b>Disease</b>	<b>Biopsies attempted</b>	<b>Biopsies engrafted</b>	<b>PDX ID</b>
1	Ewing sarcoma	1	1	HSJD-ES-004
2	Ewing sarcoma	1	1	HSJD-ES-003
3	Osteosarcoma	1	0	None
4	Ewing sarcoma	1	0	None
5	Ewing sarcoma	1	0	None
6	Rhabdomyosarcoma	2	1	HSJD-aRMS-5
7	Ewing sarcoma	1	0	None
8	Rhabdomyosarcoma	1	1	HSJD-aRMS-6
9	Ewing sarcoma	2	0	None
10	Rhabdomyosarcoma	3	2	HSJD-aRMS-1, HSJD-aRMS-2
11	Ewing sarcoma	1	0	None
12	Ewing sarcoma	2	0	None
13	Ewing sarcoma	2	2	HSJD-ES-005, HSJD-ES-016
14	Rhabdomyosarcoma	2	1	HSJD-aRMS-7
15	Ewing sarcoma	1	0	None

EXPERIMENTAL WORK

16	Ewing sarcoma	2	2	HSJD-ES-001, HSJD-ES-007
17	Ewing sarcoma	3	0	None
18	Ewing sarcoma	1	0	None
19	Rhabdomyosarcoma	1	0	None
20	Osteosarcoma	2	1	HSJD-OS-4
21	Ewing sarcoma	1	0	None
22	Ewing sarcoma	1	0	None
23	Ewing sarcoma	1	0	None
24	Rhabdomyosarcoma	1	1	HSJD-aRMS-8
25	Ewing sarcoma	2	2	HSJD-ES-002, HSJD-ES-006
26	Ewing sarcoma	1	0	None
27	Ewing sarcoma	1	0	None
28	Ewing sarcoma	2	2	HSJD-ES-009, HSJD-ES-018
29	Osteosarcoma	2	2	HSJD-OS-1, HSJD-OS-5
30	Rhabdomyosarcoma	2	2	HSJD-RMS-3, HSJD-RMS-4
31	Ewing sarcoma	1	0	None
32	Ewing sarcoma	1	1	HSJD-ES-015
33	Ewing sarcoma	1	0	None

34	Ewing sarcoma	2	2	HSJD-ES-008, HSJD-ES-012
35	Osteosarcoma	1	0	None
36	Ewing sarcoma	1	1	None
37	Ewing sarcoma	2	2	HSJD-ES-013, HSJD-ES-017
38	Ewing sarcoma	1	1	HSJD-ES-014
39	Rhabdomyosarcoma	1	0	None
40	Osteosarcoma	1	0	None
41	Ewing sarcoma	1	0	None
42	Osteosarcoma	1	1	HSJD-OS-2
43	Ewing sarcoma	1	0	None
44	Osteosarcoma	1	0	None
45	Osteosarcoma	1	1	HSJD-OS-3
46	Ewing sarcoma	1	0	None
47	Osteosarcoma	1	0	None
48	Osteosarcoma	1	0	None
49	Rhabdomyosarcoma	1	0	None
50	Rhabdomyosarcoma	1	0	None
51	Ewing sarcoma	1	0	None

**Table S7.** Association of technical factors with engraftment

<b>Factor</b>	<b>No. of Samples</b>	<b>% Engrafted</b>	<b>No. of Engrafted</b>	<b>OR (95% CI)</b>	<b>P</b>
Sample conservation					
Freshly excised	56	44.6	25		
Cryopreserved	12	41.7	5	1.28 (0.3 to 6.2)	0.76
Use of Matrigel					
No	41	43.9	18		
Yes	27	44.4	12	1.13 (0.3 to 3.9)	0.84
Biopsy method					
Tru-cut needle	32	31.2	10		
Surgery	35	57.1	20	4.05 (1-17.3)	0.059

**Table S8.** Association of previous biopsy engraftment with the engraftment of the following biopsy obtained from the same patient

<b>Factor</b>	<b>No. of Samples</b>	<b>% Engrafted</b>	<b>No. of Engrafted</b>	<b>OR (95% CI)</b>	<b>P</b>
PDX already established from previous biopsy					
Yes	11	82	9		
No	4	25	1	13.5 (1.13 to 18)	0.0769

**Table S9.** Association of patient factors with engraftment in patients with Ewing sarcoma

Factor	No. of Samples	% Engrafted	No. of Engrafted	Odds ratio (95% CI)	P
Age, years					
< 12	18	22.2	4		
≥ 12	23	56.5	13	4.33 (0.00 – 748.21)	0.70
Timing of surgery					
Diagnosis	18	22.2	4		
Relapse	23	56.5	13	4.76 (4.74 to 4.78)	<0.0001
Biopsy origin					
Limbs	11	36.4	4		
Head and neck	7	71.4	5	$2.44 \cdot 10^9$ (534.56 – $1.11 \cdot 10^{16}$ ) <sup>a</sup>	
Chest wall and ribs	5	40.0	2	$2.86$ ( $9.83 \cdot 10^{-5}$ – $8.29 \cdot 10^4$ ) <sup>a</sup>	
Lung or pleura	9	55.6	5	$6.80 \cdot 10^8$ (2081.25 – $2.22 \cdot 10^{14}$ ) <sup>a</sup>	
Pelvic bones	3	33.3	1	$1.20$ ( $4.65 \cdot 10^{-6}$ – $3.10 \cdot 10^5$ ) <sup>a</sup>	0.52
Muscle	0	0	0	*	
Teste	0	0	0	*	
Vertebral spine	6	0	0	*	
Metastasis at diagnosis					
No	29	31.0	9		
Yes	12	66.7	8	$6.62 \cdot 10^9$ ( $6.59 \cdot 10^4$ – $6.65 \cdot 10^{14}$ )	0.00012

\*Excluded from statistical analysis in biopsy of origin for lacking an event in No. of engrafted or in No. of no engrafted.

<sup>a</sup>Compared to limbs.



**Table S10.** Clinical data from PDX models included in the efficacy study of irinotecan

PDX model ID	Disease stage	Age (years) (g) <sup>a</sup>	Primary	Metastasis at diagnosis	Previous treatment	Biopsy location	Fusion gene type
HSJD-ES-001	Relapse	17.8 (M)	Scapula	Lung, skull, ribs, sternum, bone marrow	G/D <sup>b</sup> , I/T <sup>c</sup> , RT <sup>d</sup> , HIFU <sup>e</sup>	Scapula	<i>EWSR1-FLI1</i> fusion (type II)
HSJD-ES-002	Diagnosis	12.2 (M)	Fibula	None	None	Fibula	<i>EWSR1-FLI1</i> fusion (ex10-ex5)
HSJD-ES-004	Relapse	18 (M)	Mediastinum	None	SEHOP 2001 <sup>f</sup>	Mediastinum	<i>EWSR1-FLI1</i> fusion (type I)
HSJD-ES-006	Relapse	13.5 (M)	Fibula	Pleura, lung	GEIS21 (standard risk) <sup>g</sup>	Pleura	<i>EWSR1-FLI1</i> fusion (ex10-ex5)
HSJD-ES-008	Diagnosis	13 (M)	Humerus	Lung, pleura, lymph node, bone, bone marrow	None	Humerus	<i>EWSR1-FLI1</i> fusion (type I)
HSJD-ES-009	Relapse	10.7 (M)	Chest	None	GEIS 21 (standard risk) <sup>g</sup>	Skull	<i>EWSR1-FLI1</i> fusion (type II)

EXPERIMENTAL WORK

HSJD-ES-011	Relapse	13.9 (F)	Ribs	None	SEHOP 2001 <sup>f</sup> , VIT <sup>h</sup>	Pleura	<i>EWSR1-FLI1</i> fusion (type I)
HSJD-ES-012	Relapse	14.7 (M)	Humerus	Skull	GEIS21 (high risk) <sup>i</sup> ; I/T <sup>c</sup> ; G/D <sup>b</sup>	Skull	<i>EWSR1-FLI1</i> fusion (type I)
HSJD-ES-013	Relapse	18.6 (M)	Pleura	None	GEIS21 (high risk) <sup>i</sup>	Trapezius	<i>EWSR1-FLI1</i> fusion (type I)
HSJD-ES-015	Relapse	18.3 (M)	Tibia	None	GEIS21 (standard risk) <sup>g</sup>	Lung	<i>EWSR1-FLI1</i> fusion (type I)
HSJD-ES-017	Diagnosis	17.9 (M)	Pleura	None	None	Pleura	<i>EWSR1-FLI1</i> fusion (type I)
HSJD-aRMS-1	Relapse	12.3 (M)	Ribs	None	MSKCC <sup>j</sup>	Ribs	<i>PAX3-FKHR</i> fusion
HSJD-aRMS-2	Relapse	14 (M)	Ribs	None	MSKCC <sup>j</sup>	Pleura	<i>PAX3-FKHR</i> fusion
HSJD-RMS-3	Relapse	8.3 (F)	Maxillary bone	Parotid gland, maxillary sinus,	MSKCC <sup>j</sup>	Lymph node	Absent

				orbital bone			
HSJD-aRMS-7	Diagnosis	11.1 (M)	Thigh	None	None	Thigh	<i>PAX7-FKHR</i> fusion
HSJD-RMS-9	Diagnosis	1.4 (M)	Retroperitoneum	None	None	Retroperitoneum	Absent
HSJD-RMS-11	Diagnosis	12.3 (M)	Perianal	Mediastinum, lung, retroperitoneum, lymph node	None	Perianal	Absent
HSJD-OS-1	Relapse	15.5 (M)	Tibia	None	SEHOP-SO-2010 <sup>k</sup>	Lung	-
HSJD-OS-4	Relapse	15.4 (M)	Femur	None	SEHOP-SO-2001 <sup>l</sup>	Thigh	-

<sup>a</sup>g: gender. M: male; F: female.

<sup>b</sup>G/D: clinical protocol including gemcitabine and docetaxel as in reference (49).

<sup>c</sup>I/T: clinical protocol including irinotecan and temozolamide as in reference (50).

<sup>d</sup>RT: radiation therapy.

<sup>e</sup>HIFU: high intensity focused ultrasound.

<sup>f</sup>SEHOP 2001: clinical protocol including six cycles of VIDE chemotherapy (day 1 vincristine followed by day 1 to 3 with doxorubicin, ifosfamide and etoposide) as in reference (51).

<sup>g</sup>GEIS21 (standard risk): clinical protocol including five cycles of mP6 chemotherapy (cycles 1, 2 and 4 with cyclophosphamide, doxorubicin and vincristine; and cycles 3 and 5 with ifosfamide and etoposide); surgery; radiation therapy as in reference (5).

<sup>h</sup>VIT: clinical protocol including vincristine, irinotecan and temozolomide as in reference (52).

<sup>i</sup>GEIS21 (high risk): clinical protocol including gemcitabine/docetaxel (G/D) window phase, followed by five cycles of mP6 chemotherapy; surgery; radiation therapy; followed by G/D maintenance therapy as in reference (5).

<sup>j</sup>MSKCC: clinical protocol at Memorial Sloan-Kettering Cancer Center, including two cycles of carboplatin and irinotecan window phase, followed by three cycles of vincristin, doxorubicin and cyclophosphamide (VAdriaC) induction therapy; radiation therapy and surgery as in reference (53).

<sup>k</sup>SEHOP-SO-2010: clinical protocol including two cycles of high-dose ifosfamide, methotrexate, cisplatin and doxorubicin followed by surgery. After surgery, liposomal-muramyl tripeptide phosphatidyl-ethanolamine (MEPACT) followed by two cycles of doxorubicin and three cycles of high-dose ifosfamide, methotrexate and cisplatin as in reference (54).

<sup>l</sup>SEHOP-SO-2001: clinical protocol including two cycles of high-dose ifosfamide, methotrexate, cisplatin and doxorubicin followed by surgery. Post-surgery treatment consisted in two cycles of doxorubicin and three cycles of high-dose ifosfamide, methotrexate and cisplatin as in reference (55).

**Table S11.** PDX response to treatment with a single cycle of irinotecan

PDX model	Generation	Treatment	N	CR (%)	PR (%)	SD (%)	PD (%)
			(tumors)				
HSJD-ES-001	F6	Control	5	0	0	0	100
		Irinotecan	6	100	0	0	0
HSJD-ES-002	F4	Control	8	0	0	0	100
		Irinotecan	6	100	0	0	0
HSJD-ES-004	F4	Control	6	0	0	0	100
		Irinotecan	7	100	0	0	0
HSJD-ES-006	F3	Control	6	0	0	0	100
		Irinotecan	6	100	0	0	0
HSJD-ES-008	F3	Control	6	0	0	0	100
		Irinotecan	6	100	0	0	0
HSJD-ES-011	F6	Control	3	0	0	0	100
		Irinotecan	7	0	0	100	0
HSJD-ES-012	F4	Control	4	0	0	0	100
		Irinotecan	5	0	0	100	0
HSJD-ES-013	F4	Control	5	0	0	0	100
		Irinotecan	5	100	0	0	0
HSJD-ES-015	F4	Control	7	0	0	0	100
		Irinotecan	7	0	28	72	0
HSJD-aRMS-1	F10	Control	7	0	0	0	100
		Irinotecan	7	14	72	14	0
HSJD-RMS-3	F11	Control	6	0	0	0	100
		Irinotecan	7	100	0	0	0
HSJD-aRMS-7	F5	Control	4	0	0	0	100
		Irinotecan	3	0	100	0	0
HSJD-RMS-9 <sup>a</sup>	F3	Control	7	0	0	0	100

## EXPERIMENTAL WORK

		Irinotecan	7	100	0	0	0
HSJD-RMS-11 <sup>a</sup>	F2	Control	5	0	0	0	100
		Irinotecan	5	100	0	0	0
HSJD-OS-1	F4	Control	5	0	0	0	100
		Irinotecan	9	11	33	56	0
HSJD-OS-4	F1	Control	4	0	0	0	100
		Irinotecan	3	0	0	100	0

<sup>a</sup>Model obtained from patient not included in the PDX engraftment study cohort

**Table S12.** Comparative response to irinotecan-based treatments of rhabdomyosarcoma patients and their corresponding PDX

<b>PDX model ID</b>	<b>Patient Treatment</b>	<b>Clinical response</b>	<b>PDX response to irinotecan</b>
HSJD-aRMS-7	Irinotecan plus carboplatin	PR	PR
HSJD-RMS-9	Irinotecan plus vincristine	SD	CR
HSJD-aRMS-10	Irinotecan plus carboplatin	PR	PR
HSJD-RMS-11	Irinotecan plus carboplatin	CR	CR

**Table S13.** Comparative response to irinotecan treatment and median survival of PDXs at F $\leq$  2 or F  $\geq$  6 passage

PDX model	F(x)	Treatment	N (tumors)	CR (%)	PR (%)	SD (%)	PD (%)	Median survival (days)	P <sup>a</sup>
HSJD-ES-009	F2	Control	6	0	0	0	100	16	0.0008
		Irinotecan	7	14	14	72	0	>30 <sup>b</sup>	
	F6	Control	10	0	0	0	100	21	
		Irinotecan	9	11	22	56	11	44	
HSJD-ES-017	F1	Control	8	0	0	0	100	51.5	0.00014
		Irinotecan	8	50	13	37	0	84	
	F8	Control	5	0	0	0	100	56	
		Irinotecan	7	0	72	28	0	88	
HSJD-aRMS-2	F2	Control	3	0	0	0	100	48	0.0246
		Irinotecan	3	100	0	0	0	86	
	F10	Control	6	0	0	0	100	31	
		Irinotecan	6	33	67	0	0	88.5	

<sup>a</sup>P value, compared to control.<sup>b</sup>This study was ceased at day 30.





## **2. Treatment-driven selection of chemoresistant Ewing sarcoma tumors with limited drug distribution**

**Article reference:** Journal of Controlled Release 324 (2020) 440-449 – DOI: 10.1016/j.conrel.2020.05.032

Helena Castillo-Ecija<sup>1,2§</sup>, Carles Monterrubio<sup>1,2§</sup>, Guillem Pascual-Pasto<sup>1,2</sup>, Soledad Gomez-Gonzalez<sup>1,2</sup>, Daniel J. Garcia-Dominguez<sup>3</sup>, Lourdes Hontecillas-Prieto<sup>3</sup>, Claudia Resa-Pares<sup>1,2</sup>, Víctor Burgueño<sup>1,2</sup>, Sonia Paco<sup>1,2</sup>, Nagore G. Olaciregui<sup>1,2</sup>, Monica Vila-Ubach<sup>1,2</sup>, Camilo Restrepo-Perdomo<sup>1,4</sup>, Maria Cuadrado-Vilanova<sup>1,2</sup>, Leire Balaguer-Lluna<sup>1,2</sup>, Sara Perez-Jaume<sup>1,2</sup>, Alicia Castañeda<sup>1,2</sup>, Vicente Santa-Maria<sup>1,2</sup>, Monica Roldan<sup>1,4,5</sup>, Mariona Suñol<sup>1,4</sup>, Enrique de Alava<sup>3,6</sup>, Jaume Mora<sup>1,2</sup>, Cinzia Lavarino<sup>1,2</sup>, Angel M. Carcaboso<sup>1,2\*</sup>

<sup>1</sup>Institut de Recerca Sant Joan de Deu, Barcelona, 08950, Spain

<sup>2</sup>Pediatric Hematology and Oncology, Hospital Sant Joan de Deu, Barcelona, 08950, Spain

<sup>3</sup>Institute of Biomedicine of Sevilla (IBiS), Virgen del Rocio University Hospital / CSIC / University of Sevilla / CIBERONC, Seville, 41013, Spain

<sup>4</sup>Pathology, Hospital Sant Joan de Deu, Barcelona, 08950, Spain

<sup>5</sup>Confocal Microscopy Unit, Institut Pediàtric de Malalties Rares (IPER), Hospital Sant Joan de Déu, Barcelona, 08950, Spain

<sup>6</sup>Department of Normal and Pathological Cytology and Histology, School of Medicine, University of Seville, Seville, 41009, Spain

\*Address for correspondence: Dr AM Carcaboso, Institut de Recerca Sant Joan de Deu, Santa Rosa 39-57, 08950 Esplugues de Llobregat, Barcelona, Spain. Email: amontero@fsjd.org; Tel: +34 936009751 EXT 4420; Fax: +34 936009771

§Equal contribution

Declaration of interests: none.

Number of figures: 5; Number of tables: 2

## **Abstract**

Ewing sarcoma is a bone and soft tissue tumor predominantly affecting adolescents and young adults. To characterize changes in anticancer drug activity and intratumor drug distribution during the evolution of Ewing sarcomas, we used immunodeficient mice to establish pairs of patient-derived xenografts (PDX) at early (initial diagnosis) and late (relapse or refractory progression) stages of the disease from three patients. Analysis of copy number alterations (CNA) in early passage PDX tissues showed that two tumor pairs established from patients which responded initially to therapy and relapsed more than one year later displayed similar CNAs at early and late stages. For these two patients, PDX established from late tumors were more resistant to chemotherapy (irinotecan) than early counterparts. In contrast, the tumor pair established at refractory progression showed highly dissimilar CNA profiles, and the pattern of response to chemotherapy was discordant with those of relapsed cases. In mice receiving irinotecan infusions, the level of SN-38 (active metabolite of irinotecan) in the intracellular tumor compartment was reduced in tumors at later stages compared to earlier tumors for those pairs bearing similar CNAs, suggesting that distribution of anticancer drug shifted toward the extracellular compartment during clonal tumor evolution. Overexpression of the drug transporter P-glycoprotein in late tumor was likely responsible for this shift in drug distribution in one of the cases.

**Key words:** intratumor drug distribution, SN-38/irinotecan, drug resistance, cancer evolution, tumor microdialysis, Ewing sarcoma

## 2.1. Introduction

Ewing sarcoma is a malignancy of the bone and soft tissue of children, adolescents and young adults [1]. In pediatric patients, these tumors - even those (around 50%) classified as high-risk (i.e., those arising in the pelvis or axial skeleton –around 30-40%- and/or with metastases at diagnosis –around 20-30%) - respond well to first-line intensive high-dose chemotherapy [2-4]. For instance, three cycles of high-dose cyclophosphamide, doxorubicin and vincristine induce greater than 90% tumor necrosis in approximately 70% of high-risk patients [2]. In fact, more than 90% of high-risk Ewing sarcoma patients achieve complete remission upon intensive treatment including chemotherapy, radiotherapy and surgery [2, 3]. However, more than 50% of patients with metastatic disease at diagnosis and 10-25% of patients with localized disease will relapse within five years of diagnosis [2, 4, 5]. Rescue pharmacotherapy regimens include camptothecins (irinotecan or topotecan) in combination with cyclophosphamide, temozolomide, or trabectedin [6-8], or taxane-based regimens [9]. Although these treatments actively slow disease, most relapsed tumors respond poorly (or for the short term) to these anticancer drugs, and long term survival for these patients is poor [2, 5, 10].

The evolution of tumors toward chemoresistance is likely due to the selective pressure of therapies [11-13]. Tumor cells exposed to treatment might be selected to: (i) upregulate oncogenes and downregulate tumor suppressor genes [14]; (ii) alter mitochondrial function to decrease apoptosis [15]; (iii) express drug efflux transporters such as the ATP-binding cassette (ABC) family including ABCB1 (P-glycoprotein/P-gp/MDR1), ABCG2 (Breast Cancer Resistance Protein/BCRP) and ABCC1 (Multidrug Resistance Protein 1/MRP1) [16]; (iv) undergo epithelial to mesenchymal transition [17]; and (v) change tumor dynamics and architecture (blood flow, interstitial fluid pressure, vessel distribution and phenotype, cell density and extracellular matrix) [18]. Some of these mechanisms, especially the expression of drug efflux transporters and changes in tumor dynamics and architecture, may lead to limited drug distribution in tumor cells, which is usually a neglected cause of drug resistance [19].

Whether tumor evolution produces changes in intratumoral drug pharmacokinetics upon intensive treatment in clinically relevant tumor models remains uncharacterized. Therapeutic effect is produced only if the drug can interact with its inner target in the tumor cell at sufficient concentration. However, there has not been in depth *in vivo* evaluation of anticancer drug distribution in the intracellular target and in other tumor compartments (extracellular and vascular) as it is technically challenging to accomplish [20, 21].

To study the compartmental distribution of 7-ethyl-10-hydroxycamptothecin (SN-38), the active metabolite of irinotecan, in subcutaneous (s.c.) neuroblastoma patient-derived xenografts (PDX), we previously used the microdialysis-tumor homogenate method at the steady state (i.e., at constant drug concentration) in blood [22, 23]. *In vivo*, irinotecan requires the action of the carboxylesterases to be rapidly converted to SN-38 in mice. This metabolite remains active in its lactone form, which predominates at acidic pH and coexists with the carboxylate (inactive) form under a pH-dependent equilibrium [22]. Irinotecan activity is known to be higher in mouse tumor models than in human patients, because there is a higher amount of carboxylesterases in mice [24]. Also, irinotecan/SN-38 biodistribution and activity is restrained by the activity of ABC efflux drug transporters in normal organs, such as the brain, and in tumors [25].

For these studies, we established pairs of Ewing sarcoma PDX models from three pediatric patients. One tumor of each pair was established at diagnosis, and the second was obtained upon relapse or refractory disease progression. We compared the chromosomal profile (copy number alterations; CNA) for each pair. Then, we addressed whether tumor evolution under treatment pressure led to changes in the compartmental intratumoral distribution of SN-38 *in vivo*, and in ABC transporter expression. We hypothesized that late tumors evolve to be drug resistant and less susceptible to the penetration of anticancer agents.

## **2.2. Materials and methods**

### **2.2.1. Establishment of paired Ewing sarcoma PDX models**

Tumor biopsies were obtained under an Institutional Review Board-approved protocol at Sant Joan de Déu Hospital (SJD, Barcelona, Spain). Informed consent was obtained from all patients. Samples were obtained from each patient at different stages of treatment, either at diagnosis (early), at advanced (late) relapse or progression refractory stage, in order to establish “early” and “late” patient-matched PDX models. Xenografts were established s.c. in athymic nude mice (Envigo, Barcelona, Spain) by direct insertion of a fresh biopsy, as previously described [22, 26]. Research with mice adhered to European regulations and ARRIVE guidelines and was approved by the animal experimental Ethics Committee at the Universidad de Barcelona (animal protocol number 135/11).

### **2.2.2. Comparison of paired PDX models by CNA analysis**

To study the degree of similarity of early and late tumors, we used the high-density array CytoScan® HD platform (Affymetrix, Thermo Fischer Scientific) which includes more than 2.6 million copy number variation markers (over 740,000 single-nucleotide polymorphism markers and more than 1.9 million nonpolymorphic markers). Total DNA was extracted from fresh or fresh frozen tumor tissue using standard procedures. The wet lab procedures and hybridization steps were

performed according to manufacturer's recommendations. Data analysis was performed using Chromosome Analysis Suite (ChAS) software (Affymetrix Thermo Fisher Scientific). Comparison of CNAs in early and late PDX models was performed as previously described (25).

### **2.2.3. Drug activity assays**

For *in vitro* functional studies, we selected the active metabolite of irinotecan, SN-38 (Carbosynth, Compton, UK), because it is potently active in preclinical Ewing sarcoma models [27]. The lactone form of SN-38 is a substrate of ABC transporters [28] and is suitable to be dialyzed from mouse tumors with intratumoral probes [22]. We established primary cultures of xenograft models by mechanical or enzymatic disaggregation of freshly excised tissue, followed by filtration of cells through a 40  $\mu\text{m}$  cell strainer (Falcon, Corning, NY, USA), as previously described [26]. The antiproliferative activity of SN-38 was evaluated in early passage cultures using a colorimetric assay with MTS tetrazolium compound [3-(4,5-dimethylthiazol-2-yl)-5-(3-carboxymethoxyphenyl)-2-(4-sulfophenyl)-2H-tetrazolium] (Promega, Fitchburg, WI, USA) [26].

We also exposed cells to doxorubicin and etoposide and performed similar *in vitro* experiments. These two drugs are used in the standard of care of Ewing sarcoma and are also substrates of ABC transporters [4].

For *in vivo* activity studies, we used the prodrug, irinotecan, because SN-38 is not suitable for systemic administration due to its poor solubility. For drug efficacy studies, athymic nude mice were inoculated in both flanks with freshly excised viable fragments (10  $\text{mm}^3$  in volume, approximately) of human PDX tumors as previously described [23]. When tumors grew to 100-500  $\text{mm}^3$ , they were randomized to control or treatment groups ( $n = 6-11$ ). Treatment groups received one cycle of intraperitoneal 10 mg/kg/day irinotecan (Hospira, Lake City, IL, USA), five days per week for two consecutive weeks [(dx5) $\times$ 2] [24]. Control groups received saline instead of irinotecan. Tumor volume was measured three times per week with an electronic caliper. Response to treatment was evaluated at the conclusion of drug treatment (day 14). Complete response (CR) was defined as tumor mass  $< 50 \text{ mm}^3$  and  $> 50\%$  reduction at the end of treatment (day 14); partial response (PR) was tumor volume regression  $\geq 50\%$  at day 14 but tumor volume  $\geq 50 \text{ mm}^3$ ; stable disease (SD) was  $< 50\%$  regression and  $\leq 25\%$  increase in initial volume at day 14; and progressive disease (PD) was  $< 50\%$  regression from initial volume and  $> 25\%$  increase in initial volume at day 14.

### **2.2.4. Drug distribution assays**

We evaluated whether tumor evolution from early to late stages resulted in relative changes of intratumor distribution of SN-38, (lactone form) in the following

compartments: tumor extracellular fluid (tECF), tumor cells (intracellular) and blood (vascular) [20, 22]. We used the microdialysis-homogenate method [22, 29] for each tumor sample calculating the unbound drug volume of distribution in tumor ( $V_{u,tumor}$ ; mL/g tumor) at steady state (i.e., at constant concentration) as follows:

$$V_{u,tumor} = \frac{A_{tumor} - V_{blood} \times C_{blood}}{C_{ss,tumor}} \quad (1)$$

where  $A_{tumor}$  is the concentration of SN-38 in the tumor homogenate sample (ng/g) at steady state,  $V_{blood}$  is the volume of blood in tumor at steady state (mL/g; the constant value for each model is calculated by erythrocyte counts in blood and tumor for each xenograft model),  $C_{blood}$  is the concentration of SN-38 in each blood sample (ng/mL), and  $C_{ss,tumor}$  (constant value for each PDX model) is the mean concentration of unbound SN-38 in tECF (ng/mL) obtained by microdialysis sampling at steady state [22]. For each tumor model, we report the mean  $V_{u,tumor}$  ( $\pm$  standard deviation, SD) of 7-18 tumors.

To obtain the experimental values, we inoculated immunodeficient mice s.c. in one flank with freshly excised tumors from the previous generation of the xenograft and performed drug distribution experiments after tumors achieved at least 10 mm diameter. To obtain the  $C_{ss,tumor}$  value, we infused irinotecan to achieve constant concentrations of SN-38 in mouse tissues [22]. The overall design of microdialysis experiments is pictured in **Fig. 1**.

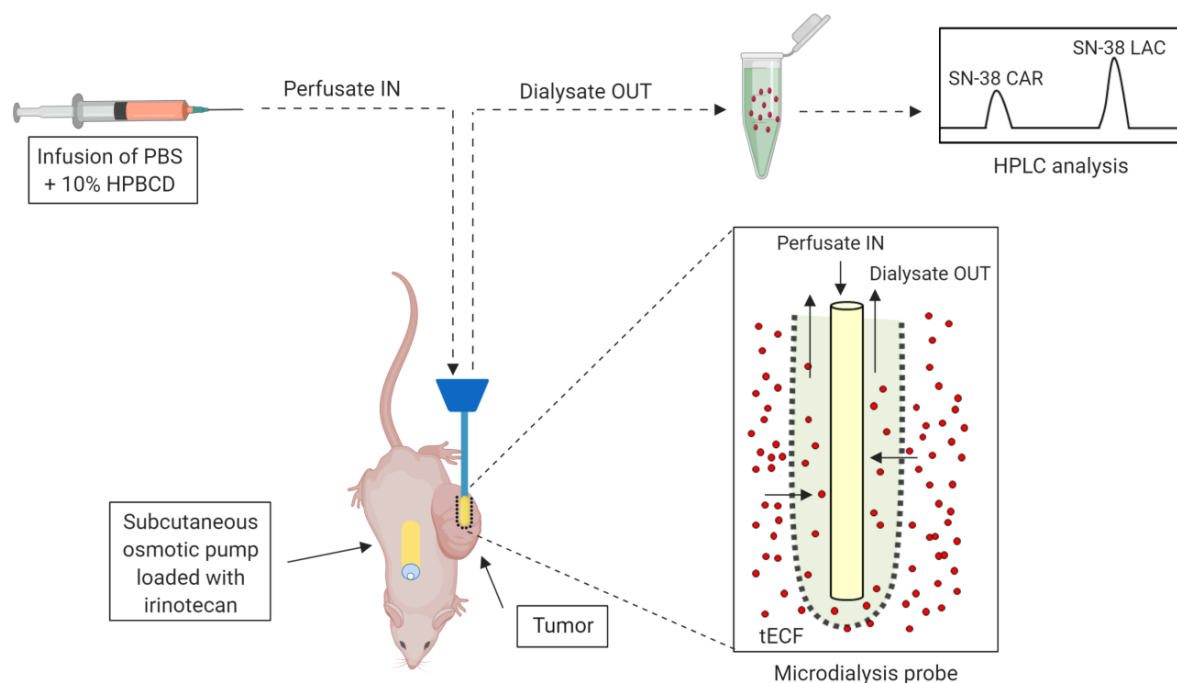


**Figure 1.** Scheme of the microdialysis experiment at steady state. Red dots surrounding the microdialysis probe represent SN-38 molecules in the tECF, dialyzed through the semipermeable membrane. Collected dialysates contain drug molecules analyzed by an HPLC system. Figure created with BioRender.com.

Before the irinotecan infusion, mice were restrained in an infusion cage using an infusion harness (Instech CIH62, Plymouth Meeting, PA, USA). Under brief isoflurane anesthesia, we inserted a 4 mm-length CMA 20 microdialysis probe (CMA, Kista, Sweden) into the tumor of the restrained mouse. The probes were continuously perfused at 0.5  $\mu\text{L}/\text{min}$  with pH 7.4 phosphate buffered saline (PBS) containing 10% hydroxypropyl-beta-cyclodextrin (HPBCD, Sigma-Aldrich, St. Louis, MO, USA) (w/v). After 90 min, mice were anesthetized with isoflurane to insert s.c. Alzet 2001D pumps (Durect, Palo Alto, CA), which were then used to infuse irinotecan at 130  $\mu\text{g}/\text{h}$  for 24 h. We collected tumor dialysates (90 min fractions) overnight in a refrigerated fraction collector which were conserved at  $-80\text{ }^{\circ}\text{C}$  until High Performance Liquid Chromatography (HPLC) analysis of SN-38 lactone and carboxylate forms. The following day, we collected one blood sample from the retroorbital plexus to determine steady state concentration of SN-38 in blood ( $C_{\text{blood}}$ ) by HPLC. We then individually calibrated probes using a previously described zero flow rate method [22]. Following HPLC analysis and recovery correction, we calculated the  $C_{\text{ss,tumor}}$  for each experiment as the mean of three consecutive dialysate samples obtained at steady state. After each microdialysis experiment, mice were euthanized and the tumor terminally collected to process as homogenate. We performed at least three microdialysis experiments of individual mice for each PDX model and calculated  $C_{\text{ss,tumor}}$  as the mean of the individual experiments. In addition to the microdialysis experiments, we collected tumor homogenates and blood samples at steady state from additional mice with tumors which were administered the same irinotecan dose infusion (3-6 mice for each tumor model).

### **2.2.5. Differential expression of ATP-binding cassette (ABC) transport in PDX pairs**

We compared early and late pairs of PDX tissue to observe changes in the expression of drug efflux transporters involved in camptothecin transport [28, 30, 31]. For gene expression analyses, we isolated total RNA from freshly excised engrafted tumors using TRIzol (Life Technologies, Grand Island, NY) and synthesized cDNA from 1  $\mu\text{g}$  of total RNA using the High Capacity Reverse Transcription Kit (Applied Biosystems, Foster City, CA, USA). We performed real-time quantitative polymerase chain reaction (qRT-PCR) with gene-specific fluorescent Taqman probes (Taqman Gene Expression Assays, Applied Biosystems) including probes for ABC transporter genes (*ABCB1/MDR1* (Hs00184500\_m1), *ABCG2* (Hs01053790\_m1), *ABCC1/MRP1* (Hs01561502\_m1), *ABCC2/MRP2* (Hs00166123\_m1) and *ABCC3/MRP3* (Hs00978473\_m1); with *TPT1* (Hs02621289-g1) as an endogenous control to normalize values, as described) [32]. Gene expression was determined using the  $2^{-\Delta\Delta\text{Ct}}$  method [33]. Using the same method, we analyzed the expression of four genes reported to predict response to irinotecan: topoisomerase 1 (*TOP-1*, Hs00243257\_m1), which can be decreased in irinotecan-resistant tumor cells [34]; Schlafen family member



11 (*SLNF11*, Hs00536981\_m1) and retinoblastoma transcriptional corepressor 1 (*RB1*, Hs01078066\_m1), whose high expression and loss, respectively, relate to increased irinotecan activity in triple-negative breast cancers [35]; and carboxylesterase 2 (*CES2*, Hs01077945\_m1), related to the intratumoral activation of irinotecan [36].

For protein expression studies, we performed immunohistochemistry (IHC) of irinotecan/SN-38 efflux transporters, MDR1 (P-gp), BCRP and MRP1, in 4-micron sections of formalin-fixed, paraffin-embedded (FFPE) tissues. Primary antibodies were anti-P-glycoprotein (EPR10363, ab170903; 1:100, Abcam, Cambridge, MA, USA), anti-BCRP/ABCG2 (BXP-21, ab3380; 1:50, Abcam) and anti-MRP1 (MRPm5, ab24102; 1:20, Abcam).

### **2.2.6. Intracellular accumulation of irinotecan *in vitro***

To further characterize changes in intratumor drug distribution due to active drug efflux we analyzed irinotecan accumulation in PDX-derived tumor cells. We used the prodrug irinotecan due to poor solubility of the metabolite SN-38, whose crystals interfere with analyses.

First, we addressed irinotecan accumulation *in vitro* using HPLC. We cultured early passage PDX-derived cells in RPMI supplemented with 10% fetal bovine serum (Life Technologies) until 80% confluence in six well plates. We exposed the cells to irinotecan (20  $\mu$ M), washed them with cold PBS at time points 1 and 5 min, lysed them in water : methanol (20:80), isolated the supernatant by centrifugation and quantified irinotecan (lactone) by HPLC. Proteins were quantified using the bicinchoninic acid protein assay.

Second, we conducted a live cell confocal imaging assay in a Leica TCS SP8 microscope (Leica, Wetzlar, Germany) equipped with resonant scanner. We plated primary cultures of early and late PDX-derived tumor cells in a cell culture imaging dish ( $\mu$ -Dish<sup>35mm,high</sup>, Ibidi GmbH, Martinsried, Germany) and cultured in RPMI medium for 48 h. To improve confocal imaging results, we replaced culture medium with Live Cell Imaging Solution (Thermo Scientific) without phenol red, and then stained cell membranes with Alexa Fluor 568-conjugated wheat germ agglutinin (WGA; 1:200 for ten min; Life Technologies). We performed all experiments at 37 °C and 5% CO<sub>2</sub> using an incubation chamber enclosing the microscope stage and body. Upon selection of a group of cells attached to the plate, irinotecan (final concentration 20  $\mu$ M) was added directly to the dish and images were obtained at a 7.5 s time-lapse mode over 300 s. Time-lapse imaging was performed at 405 and 568 nm excitation and 453 and 597 nm emission wavelengths (irinotecan and WGA, respectively) using a water immersion objective lens (HC PL APO CS2 x40, 1.1 numerical aperture). We observed the total area of transmitted drug autofluorescence inside the cells. To detect and quantify the fluorescence of

irinotecan passing through the cell membrane, we analyzed the mean fluorescence intensity signal in a representative fraction of the cell membrane at the initial time point and at the time of maximum signal intensity. In both scenarios, we used Leica LAS X software for analyses (Leica Microsystems, Wetzlar, Germany).

### **2.2.7. Reversal of treatment-induced drug resistance *in vitro***

Paired PDX tumors showing significantly increased MDR1 expression according to IHC and RT-qPCR analysis in the late xenograft were processed for culture, plated in 96 well plates and exposed to the efflux pump inhibitor elacridar (5  $\mu$ M) 2 h prior to the addition of SN-38 at serial concentrations. After 4 h incubation, we replaced culture medium with fresh medium and performed the MTS assay 72 h later.

### **2.2.8. Statistics**

We used GraphPad Prism 7 (La Jolla, CA, USA) and R software (Vienna, Austria) for statistical analysis and we used EC50 shift analysis to compare IC50 values. We used ANOVA tests to compare gene expression data. Pharmacokinetic data from paired early and late PDX were compared using the Student's *t* test or using the Mann Whitney test for data with non-normal distribution. Aggregate data are presented as mean values  $\pm$  SD.

## **2.3. Results**

### **2.3.1. Paired PDX models and patient clinical exposure to irinotecan**

We established three pairs of Ewing sarcoma PDX models from biopsies obtained at diagnosis (early) and relapse/progressive refractory (late) stage from three individuals with Ewing sarcoma. Clinical data including *EWSR1-FLI1* gene fusions are detailed in **Table 1**. Patients 1 and 2 achieved complete remission after treatment but relapsed more than one year after diagnosis, off treatment. Patient 3 did not achieve remission and a late biopsy was obtained during refractory progression on treatment. Patient 2 received irinotecan (1 h intravenous infusion of 30 mg/m<sup>2</sup> on days 3, 4 and 5 of each cycle, combined with temozolomide infusion at day 1, every 21-28 days, depending on hematology recovery) during his primary treatment (previous to the late/relapse biopsy), with progression of the disease after 4 cycles, which was reversed with gemcitabine and docetaxel (**Table 1**). Patients 1 and 3 received similar irinotecan-temozolomide treatments after the obtention of their late biopsies; patient 1 progressed after 5 cycles, and patient 3 received only one cycle due to rapid progression. All patients eventually died of disease progression.

### 2.3.2. Pairwise comparison of CNAs in PDX derived from early and late tumor biopsies

CNA profiles of early and late PDX pairs are shown in **Fig. 2A**. PDX tissues from patients 1 and 2 showed few CNAs in early and late versions, with most CNA alterations of the early PDX conserved in the paired late tumor. Both PDX from patient 1 presented with gains in chromosome 8 (two copies in the early PDX and one copy in the late PDX) and focal deletion of the *CDKN2A* locus on chromosome 9p21, which are recurrent alterations in Ewing sarcoma [13]. In patient 2, the early PDX showed only a copy neutral loss of heterogeneity (LOH) in chromosome 3 and 20, while the late PDX conserved such alteration with no additional changes. In contrast, patient 3 showed substantially different CNA profiles in both PDX models. While the early PDX showed important alterations in chromosomes 7, 9, 10, 12 and 15 (involving the loss of *CDKN2A* locus), 80% of these alterations were not shared by the late PDX, which additionally showed CNAs in regions of chromosomes 8, 14 and 17 that include loss of *TP53*, *STAT3* and *BRAC1* genes.

These findings suggest that late tumors likely evolved clonally from the early tumor cells in patients 1 and 2, while tumors from patient 3 are of different clonal origin (**Fig. 2B**).

**Table 1.** Clinical data of the paired Ewing sarcoma PDX models.

Patient (g <sup>a</sup> )	Disease stage	Age (years)	Primary	Metastasis	Previous treatment	Biopsy location	PDX model ID	PDX stage	Molecular diagnosis
1 (M)	Diagnosis	12.2	Fibula	None	None	Fibula	HSJD-ES-002	Early	<i>EWSR1-FLI1</i> fusion
	Relapse	13.5	No	Pleura, lung	GEIS21 (SR) <sup>b</sup>	Pleura	HSJD-ES-006	Late	<i>EWSR1-FLI1</i> fusion
2 (M)	Diagnosis	13.0	Humerus	Lung, pleura, lymph node, bone, bone marrow	None	Humerus	HSJD-ES-008	Early	<i>EWSR1-FLI1</i> fusion
	Relapse	14.7	No	Skull	GEIS21 (HR) <sup>c</sup> ; I/T <sup>d</sup> ; G/D <sup>e</sup>	Skull	HSJD-ES-012	Late	<i>EWSR1-FLI1</i> fusion
3 (M)	Diagnosis	17.9	Pleura	None	None	Pleura	HSJD-ES-017	Early	<i>EWSR1-FLI1</i> fusion
	Progression on treatment	18.6	Pleura	None	GEIS21 (HR) <sup>c</sup>	Trapezius	HSJD-ES-013	Late	<i>EWSR1-FLI1</i> fusion

<sup>a</sup>g: gender. M: male; F: female.

<sup>b</sup>GEIS21 (standard risk, SR): five cycles of mP6 chemotherapy (Cycles 1, 2 and 4 with cyclophosphamide, doxorubicin and vincristine; and cycles 3 and 5 with ifosfamide and etoposide); surgery; radiation therapy [4].

<sup>c</sup>GEIS21 (high risk, HR): gemcitabine/docetaxel (G/D) window phase, followed by five cycles of mP6 chemotherapy; surgery; radiation therapy; followed by G/D maintenance therapy [4].

<sup>d</sup>I/T: irinotecan and temozolomide [6].

<sup>e</sup>G/D: gemcitabine and docetaxel [9].

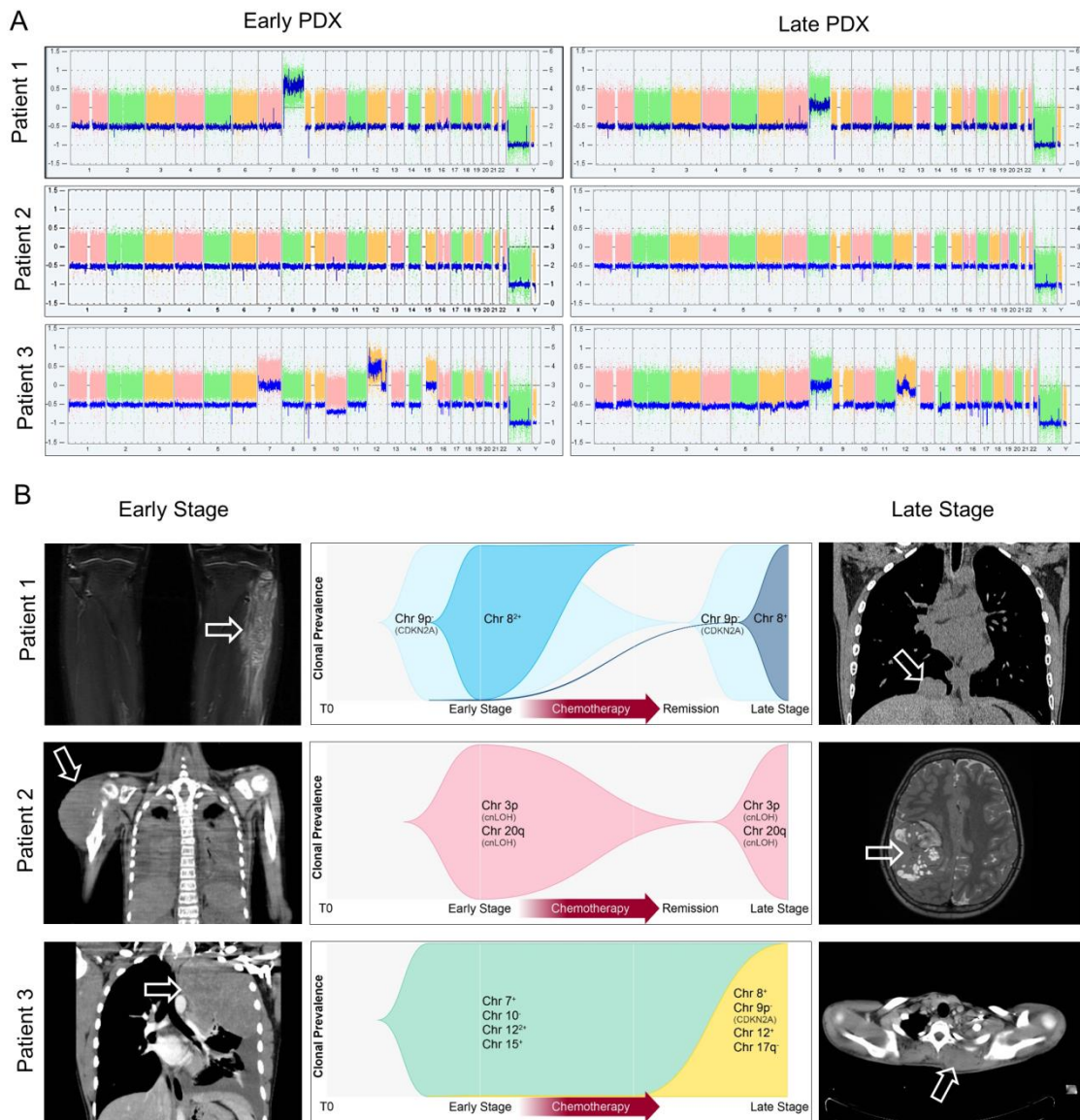


**Figure 2.** Chromosomal analyses of paired PDX models. A) Whole genome representation of the chromosomal profiles of paired early and late PDX models of patients 1, 2 and 3. Each colored column represents a different chromosome. Passage number in mice (F) of the analyzed early and late PDX were three and one (patient 1), three and four (patient 2) and one and zero (patient 3), respectively. B) Representation of the clonal evolution of tumors of patients 1, 2 and 3. Clonal prevalence (y axes) at each time point (x axes) is represented in colors. Arrows in images show the location of primary (early stage) and relapsed/progression refractory (late stage) tumors. Images displayed for patient 1 are fibula (magnetic resonance) and pleura (computed tomography scan), for patient 2 are humerus (computed tomography scan) and skull (magnetic resonance), and for patient 3 are lung (magnetic resonance) and trapezius (computed tomography scan), for early and late stage tumors, respectively.

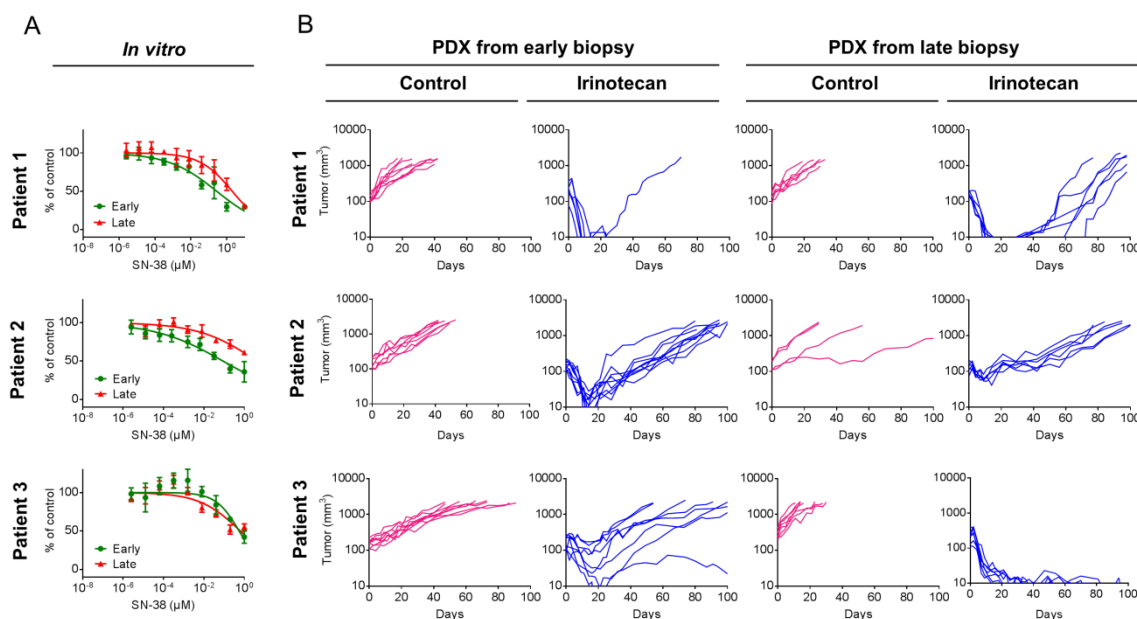


**Figure 3.** Activity of SN-38/irinotecan in paired PDX models. A) *In vitro* antiproliferative activity curves of SN-38 in PDX-derived cells in culture show % of MTS signal (mean and SD of six experimental values) compared to control untreated cells that were considered 100%. B) *In vivo* antitumor activity curves of irinotecan in PDX models (right columns) show volumes of individual tumors of untreated (control) or treated (irinotecan) mice. Note that mice with successful engraftment in both flanks produced two individual tumor curves in the graphics. Passage number in mice of the treated early and late PDXs were four and three (patient 1), three and four (patient 2) and one and four (patient 3), respectively.

### 2.3.3. Comparison of antitumor activity of SN-38/irinotecan in patient-matched early and late PDX models

To evaluate whether treatment led to increased chemoresistance in the late PDX, we treated low passage PDX-derived cells with SN-38, and s.c. tumors engrafted in mice with systemic irinotecan [26] (**Fig. 3A and B**). For those patients achieving complete remission after therapy (patients 1 and 2), drug resistance in PDX-derived primary cells increased in later-stage tumors compared to their early counterparts. IC<sub>50</sub> values of the late cells were five to ten-fold higher compared to early cells, increasing from 0.30 (0.15-0.45)  $\mu\text{M}$  to 2.00 (1.30-3.10)  $\mu\text{M}$ , and from 0.100 (0.050-0.150)  $\mu\text{M}$  to 4.20 (2.00-11.5)  $\mu\text{M}$  for patients 1 and 2, respectively (means and 95% confidence intervals;  $P < 0.0001$ , EC<sub>50</sub> shift analysis) (**Fig. 3A**). Similar results showing higher IC<sub>50</sub> values for the late cells were obtained for doxorubicin and etoposide (**Fig. S1**). In both PDX pairs, irinotecan treatment led to inferior tumor control in mice bearing the late PDX, which relapsed more rapidly upon treatment cessation (patient 1) or had a poorer response during treatment (patient 2) (**Fig. 3B** and **Table S1**).

In contrast, for PDX tumors of patient 3, there was no increased resistance to the same treatment at late stage (**Fig. 3B**). IC<sub>50</sub> values for SN-38 were similar, specifically 0.557 (0.359-0.941)  $\mu\text{M}$  (early model) and 0.637 (0.350-1.440)  $\mu\text{M}$  (late

model). Similar results showing no changes in cell drug sensitivity were obtained for doxorubicin and etoposide (**Fig. S1**). *In vivo*, the late PDX of patient 3 was significantly more sensitive to therapy than the early PDX (**Fig. 3B** and **Table S1**).

#### 2.3.4. Intratumor drug distribution in paired early and late xenografts

At steady state, experimental values for  $C_{ss,tumor}$  (i.e., SN-38 concentrations in tECF samples obtained by microdialysis) were constant (**Fig. S2A**). These values were higher in late tumor samples of patients 1 and 2 than in patient-matched early tumor samples (**Fig. S2A**). The ratio of lactone-to-carboxylate SN-38 concentrations in tECF was higher in late tumors of patient 2, compared to patient-matched early pairs (**Fig S2B**). We analyzed tECF data, together with SN-38 concentrations in blood samples and tumor homogenates at steady state, to calculate  $V_{u,tumor}$  for each PDX model (**Table 2**). High values for  $V_{u,tumor}$  indicate high distribution of the drug in the intracellular compartment of the tumor (or nonspecifically bound to tumor tissue components), whereas low values suggest that the drug is predominantly distributed in the extracellular space [20]. As reported in **Table 2**, we observed significantly lower  $V_{u,tumor}$  values in late PDX from paired tumors of patients 1 and 2 compared to early ones. Thus, at earlier stages during treatment, a greater proportion of SN-38 was intracellular rather than unbound in tECF. For patient 3, whose tumor was refractory to initial treatment, we did not observe the same shift in compartmental distribution of the drug, and  $V_{u,tumor}$  was higher in the late xenograft (**Table 2**). Overall, these findings suggest that anticancer agents are displaced from the intracellular compartment upon clonal tumor selection by treatment.



**Table 2.** Results of intratumor SN-38 distribution experiments - matched tumor pairs receiving s.c. infusions of irinotecan. Data is represented as mean  $\pm$  SD. Values in parentheses are the number of individual data available to calculate means.

Patient	Tumor model	Disease stage	$C_{ss,tumor}^a$ (ng/mL)	$A_{tot,tumor}^b$ (ng/g tumor)	$C_{tot,blood}^c$ (ng/mL)	$V_{tot,blood}^d$ (mL/g tumor)	$V_{u,tumor}^e$	<i>P</i> value <sup>f</sup>
1	HSJD-ES-002	Early	3.2 $\pm$ 1.8 (3)	28.3 $\pm$ 14.1 (8)	3.5 $\pm$ 1.0 (8)	0.03	8.8 $\pm$ 4.4 (8)	0.0128
	HSJD-ES-006	Late	5.0 $\pm$ 2.5 (3)	17.6 $\pm$ 10.5 (7)	4.0 $\pm$ 3.2 (7)	0.02	3.5 $\pm$ 3.1 (7)	
2	HSJD-ES-008	Early	6.5 $\pm$ 3.5 (5)	31.5 $\pm$ 9.4 (14)	3.8 $\pm$ 0.5 (6)	0.00	4.8 $\pm$ 1.4 (14)	< 0.0001
	HSJD-ES-012	Late	13.7 $\pm$ 5.0 (5)	31.7 $\pm$ 17.2 (18)	4.5 $\pm$ 0.9 (6)	0.00	2.3 $\pm$ 1.3 (18)	
3	HSJD-ES-017	Early	12.8 $\pm$ 7.5 (5)	29.9 $\pm$ 14.1 (12)	4.0 $\pm$ 1.2 (5)	0.00	2.3 $\pm$ 1.1 (12)	0.0010
	HSJD-ES-013	Late	12.1 $\pm$ 7.0 (5)	55.5 $\pm$ 22.9 (16)	5.2 $\pm$ 1.3 (5)	0.00	4.6 $\pm$ 1.9 (16)	

<sup>a</sup>Probe recovery-corrected concentration of unbound SN-38 in tECF obtained by microdialysis sampling at steady state.

<sup>b</sup>Concentration of SN-38 in the tumor homogenate samples at steady state,

<sup>c</sup>Concentration of SN-38 in blood samples.

<sup>d</sup>Volume of blood in tumor

<sup>e</sup>Unbound drug volume of distribution in tumor, calculated from Equation (1).

<sup>f</sup>*P* value of “early *versus* late”  $V_{u,tumor}$  parameter comparison.



### 2.3.5. Comparative expression of efflux transporters and genes related to irinotecan activity in patient-matched early and late PDX

Because the increased expression and activity of ABC transporters at the tumor cell membrane would partially explain the shift in SN-38 distribution toward the extracellular compartment [20], we addressed the presence of these proteins using PCR and IHC. Our PCR results demonstrated remarkable overexpression (9500-fold) of the *ABCB1* gene (*MDR1*) in the late PDX of patient 2 (**Fig. 4A**). Gene expression correlated well with increased protein expression (IHC staining) of MDR1/P-gp in tumor cell membranes in the late patient biopsy and its corresponding PDX, compared to no detectable expression in the paired samples at early stage (**Fig. 4B**). Changes in ABC transporter gene expression for patients 1 and 3 (**Fig. 4A**) did not correlate with increases or decreases in protein expression as analyzed using IHC (**Fig. S3**). Thus, in these patients we could not explain changes in intratumoral drug distribution with the study of these selected ABC transporters. Changes in gene expression of proteins related to irinotecan activity were detected during the evolution of tumor pairs (**Fig. S4**), but the real impact of these changes in drug activity was not experimentally addressed in our study. Increased activity of irinotecan against late tumor of patient 3 could be partially explained by highest expression of *CES2* in this tumor (**Fig. S4**; 7-fold;  $P < 0.0001$ ; ANOVA test).

### 2.3.6. Functional studies of drug uptake in cells derived from paired PDX

Early and late PDX-derived cells from patient 2 were selected to characterize intracellular irinotecan uptake and accumulation through *in vitro* assays and live cell imaging. These cell models were selected based on their highly differential expression of P-gp. As expected, intracellular irinotecan accumulation was diminished (up to 53% lower at one min) in late PDX-derived cells (**Fig. 5A**). The concentration of SN-38 in cells exposed to irinotecan was almost negligible (data not shown), which is consistent with the low expression of *CES2* by this tumor. Upon exposure of cultured cells to irinotecan, intracellular fluorescence due to drug accumulation increased faster in early PDX-derived cells (early cells), compared to late PDX cells (late cells) (**Fig. 5B**). We observed a lag time of 45 s at which time point, irinotecan fluorescence in the intracellular compartment of tumor cells was not detectable (**Fig. 5C**). A peak of intracellular irinotecan appeared at the time of maximum fluorescence in early cells ( $t = 108$  s), but not in late ones (**Fig. 5C, Suppl. Videos 1 and 2**). Increased resistance of late cells to SN-38 reversed following co-incubation with elacridar (P-gp inhibitor) (**Fig. 5D**). Overall, these findings support the shift of irinotecan distribution toward the extracellular compartment upon clonal selection by treatment.

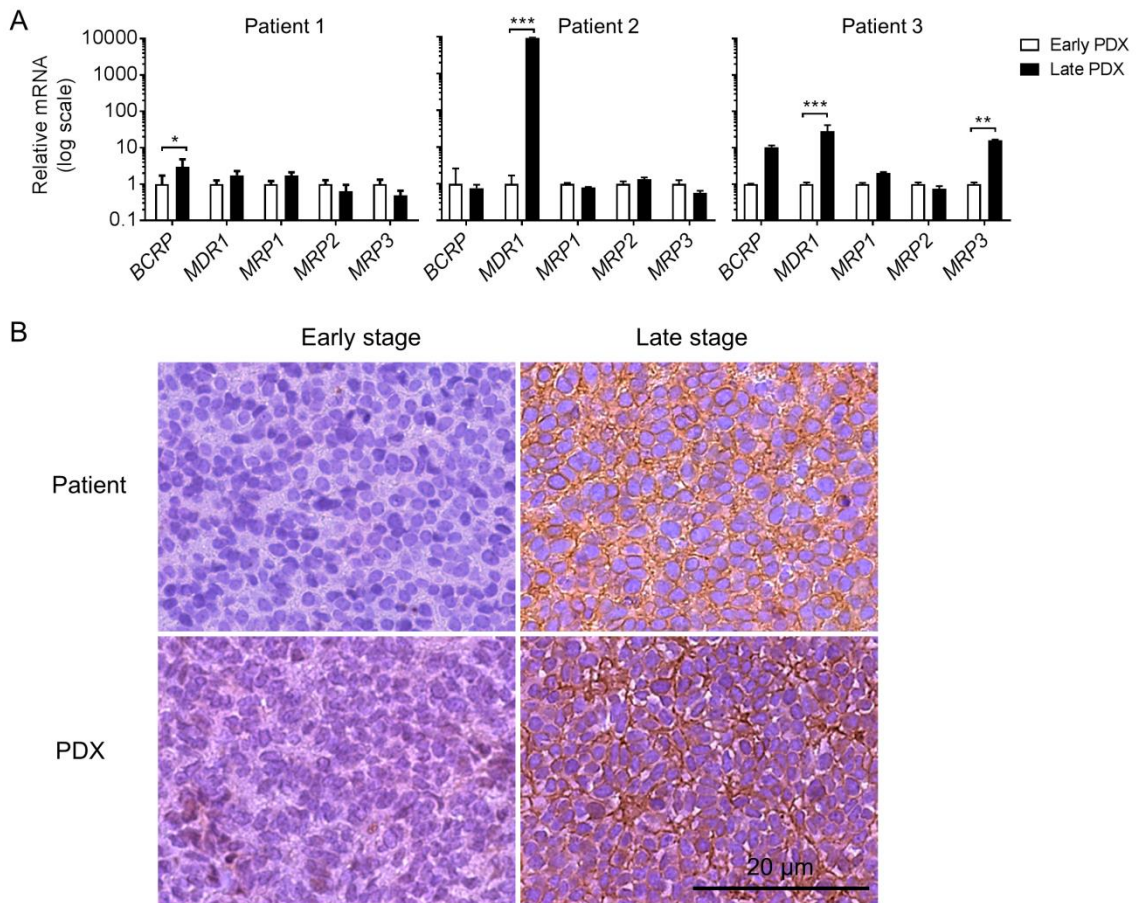


**Figure 4.** Expression of ABC transporters in paired PDX models and patient biopsies. A) Expression of ABC transporter genes in early and late PDX tissue samples from patients 1-3. Values are relative to gene expression in the early PDX sample. \* $P = 0.0119$ ; \*\* $P = 0.0017$ ; \*\*\* $P < 0.0001$  (ANOVA test with Sidak correction for multiple comparisons). B) IHC staining of P-gp (brown color in cell membranes) in patient and PDX samples obtained from patient 2.

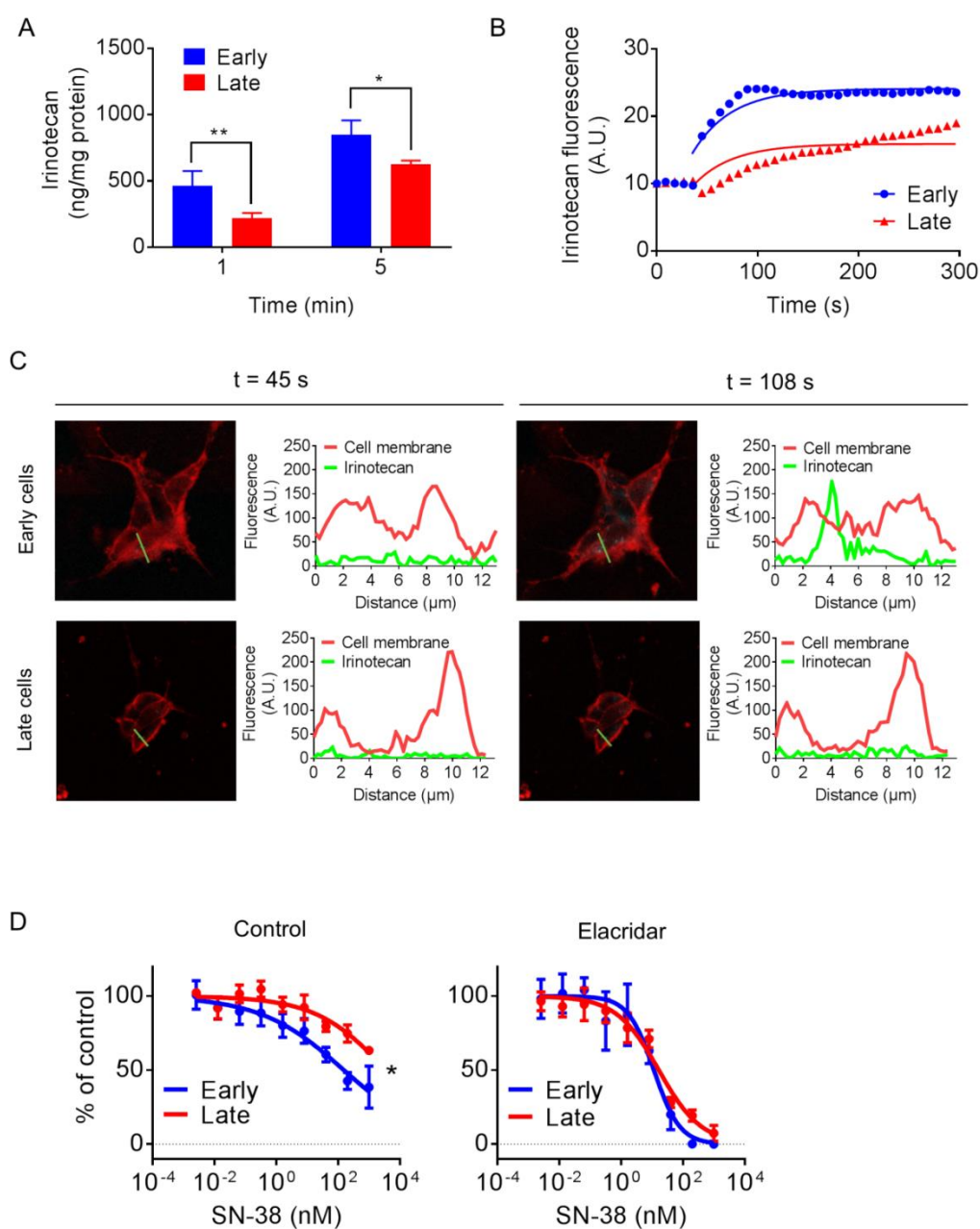


**Figure 5.** Differential uptake of SN-38 and irinotecan in PDX-derived cells of patient 2. A) Intracellular accumulation of irinotecan lactone;  $*P = 0.0258$ ,  $**P = 0.0226$ ,  $t$  test. B) Live cell confocal imaging showing irinotecan uptake in selected groups of cells. A.U.: arbitrary units. C) Fluorescence intensities of irinotecan and cell membrane (Alexa Fluor 568-WGA) in delimited sections (green lines) passing through two membranes of one Ewing sarcoma cell. D) Activity of elacridar at sub-cytotoxic concentration (1  $\mu$ M) to reverse resistance of late PDX-derived cells to irinotecan.  $*P < 0.0001$ , EC<sub>50</sub> shift analysis.

## 2.4. Discussion

Our studies in patient-matched pairs of PDX models of Ewing sarcoma addressed questions related to changes in drug efficacy and pharmacokinetics within tumor compartments upon tumor evolution. Tumor pairs from patients 1 and 2 after relapse showed the same fusion genes and subtle chromosomic changes compared to early tumor pairs, but were more prone to become chemoresistant and less susceptible to intracellular drug distribution. The patient-matched tumor pair obtained from primary refractory progression in patient 3 showed the same fusion gene but with significantly different CNA composition and a different pharmacodynamic evolution profile. The complex karyotype of the refractory tumor of patient 3 may explain its poor clinical response to therapy, as previously reported [37].

Proposed models of clonal evolution in Ewing sarcoma progression suggest that early clones are driven by the canonical fusion genes *EWSR1-FLI1* or *EWSR1-ERG* and give rise to primary and metastatic tumors that diverge early and evolve independently [38]. Tumor clones may contain significant differences in their CNA and mutation status, but yet not in the fusion gene [13,38]. From our results, we infer that if both early and late tumors have similar CNA profiles, it is likely that late tumors will be resistant to previously efficacious therapies, due in part to clonal evolution leading to restricted intracellular drug concentrations in tumor cells. In contrast, late tumor pairs with substantially different CNA might be equally responsive to therapies used during early stages of the disease.

In one of our cases, we identified overexpression of P-gp/MDR1 in the late tumor as a probable cause for chemoresistance and lower intracellular drug concentrations. This transporter was likely responsible for the shift of drug distribution towards tECF (extracellular compartment) in the late tumor model, presenting a hurdle for intracellular drug penetration [20]. Further supporting active efflux from tumor cells, *in vivo* microdialysis results showed higher lactone-to-carboxylate ratio in tECF of late stage tumor, which is consistent with selectivity of P-gp for transport of lactone - but not carboxylate - camptothecins from the intracellular compartment towards tECF [39].

P-gp is involved in the efflux transport of several chemotherapy agents and its expression in solid tumors is regulated by exposure to chemotherapy [40]. Chemotherapy increases the expression of MDR1 and MRP1 proteins in pediatric soft tissue sarcomas [41]; fifty percent of Ewing sarcoma patients show negative immunostaining of MDR1/P-gp before treatment, becoming positive after treatment [42]. Several other pediatric solid tumors also increase the expression of P-gp upon exposure to chemotherapy [43].

This study provides a novel approach to understanding intratumor drug pharmacokinetics during tumor evolution, using PDX as a valuable tool for the study of functional tumor evolution. Limitations of this study include the small number of cases, the different anatomic location of primary and relapsed tumors in patients 1 and 2, and the possible selection of the most aggressive clones during engraftment in mice. Regarding the number of cases, this is justified by the lower rate of successful engraftment of tumor biopsies at diagnosis compared to late (relapse or refractory) biopsies, which precludes the establishment of matched PDX pairs in most cases. Regarding the possible selection of the most aggressive clones in xenografts, recent studies have demonstrated that PDX maintain the same gene expression and CNA patterns of the original tumors [44, 45]. Another possible limitation is the absence of DNA sequencing to detect somatic mutations. In this regard, previous whole genome sequencing and CNA analyses demonstrated that relapsed Ewing sarcoma samples are enriched in somatic aberrancies, including a three-fold increase in the frequency of mutations in genes involved in chemoresistance and malignancy, such as *TP53* and *STAG2* [13, 38]. Similar findings upon tumor evolution have been described in high grade glioma recurrences compared to matched early tumor pairs [11].

An important clinical implication of our compartmental pharmacokinetic study is that novel pharmacological approaches inhibiting physiologic or tumor barriers, or novel drug delivery systems which increase intracellular drug concentrations in tumors, might improve antitumor efficacy in relapsed tumors. For instance, tyrosine kinase inhibitor gefitinib can increase intracellular concentration of topotecan in orthotopic glioma xenografts, likely through the inhibition of the barrier function of ABC transporters expressed by the tumor cells [20].

## **2.5. Conclusions**

In summary, using a unique set of clinically relevant patient-derived xenograft pairs established at early and late tumor stages, we have identified that drug concentration in Ewing sarcoma tumor cells becomes restricted during tumor evolution under treatment pressure. We observed this in two cases in which CNAs in early and late xenografts were similar, suggesting a common clonal origin. Our results should be taken cautiously due to the low number of cases, but they might be clinically relevant to predict response of relapsed tumors to chemotherapy and to justify novel treatments that enhance drug delivery in the tumors at relapse.

## **2.6. Declaration of Competing Interest**

None.

## **2.7. Acknowledgements**

The work at Hospital Sant Joan de Deu was supported by associations of parents and families of children with cancer. The work of EdA was supported by the AECC Scientific Foundation (GCB13-1578), ISCIII-FEDER (PI14/01466 and PI17/00464), CIBERONC (CB16/12/00361), Asociación Pablo Ugarte and Fundación María García Estrada. The work of JM was supported by the AECC Scientific Foundation (GCB13-1578) and Asociación Pablo Ugarte. The work of AMC was supported by grants from the AECC Scientific Foundation, MINECO (SAF2011-22660), Fundacion BBVA, the European Union Seventh Framework Programme (FP7/2007-2013) under Marie Curie International Reintegration Grant (PIRG-08-GA-2010-276998) and ISCIII-FEDER (CP13/00189 and CPII18/00009).

## 2.8. References

- [1] T.G.P. Grunewald, F. Cidre-Aranaz, D. Surdez, E.M. Tomazou, E. de Alava, H. Kovar, P.H. Sorensen, O. Delattre, U. Dirksen, Ewing sarcoma, *Nat Rev Dis Primers*, 4 (2018) 5.
- [2] E.A. Kolb, B.H. Kushner, R. Gorlick, C. Laverdiere, J.H. Healey, M.P. LaQuaglia, A.G. Huvos, J. Qin, H.T. Vu, L. Wexler, S. Wolden, P.A. Meyers, Long-term event-free survival after intensive chemotherapy for Ewing's family of tumors in children and young adults, *J Clin Oncol*, 21 (2003) 3423-3430.
- [3] G.M. Milano, R. Cozza, I. Ilari, L. De Sio, R. Boldrini, A. Jenkner, M. De Ioris, A. Inserra, C. Dominici, A. Donfrancesco, High histologic and overall response to dose intensification of ifosfamide, carboplatin, and etoposide with cyclophosphamide, doxorubicin, and vincristine in patients with high-risk ewing sarcoma family tumors, *Cancer*, 106 (2006) 1838-1845.
- [4] J. Mora, A. Castaneda, S. Perez-Jaume, A. Lopez-Pousa, E. Maradiegue, C. Valverde, J. Martin-Broto, X. Garcia Del Muro, O. Cruz, J. Cruz, J. Martinez-Trufero, J. Maurel, M.A. Vaz, E. de Alava, C. de Torres, GEIS-21: a multicentric phase II study of intensive chemotherapy including gemcitabine and docetaxel for the treatment of Ewing sarcoma of children and adults: a report from the Spanish sarcoma group (GEIS), *Br J Cancer*, 117 (2017) 767-774.
- [5] J.S. Miser, M.D. Krailo, N.J. Tarbell, M.P. Link, C.J. Fryer, D.J. Pritchard, M.C. Gebhardt, P.S. Dickman, E.J. Perlman, P.A. Meyers, S.S. Donaldson, S. Moore, A.R. Rausen, T.J. Vietti, H.E. Grier, Treatment of metastatic Ewing's sarcoma or primitive neuroectodermal tumor of bone: evaluation of combination ifosfamide and etoposide--a Children's Cancer Group and Pediatric Oncology Group study, *J Clin Oncol*, 22 (2004) 2873-2876.
- [6] L.M. Wagner, N. McAllister, R.E. Goldsby, A.R. Rausen, R.Y. McNall-Knapp, M.B. McCarville, K. Albritton, Temozolomide and intravenous irinotecan for treatment of advanced Ewing sarcoma, *Pediatr Blood Cancer*, 48 (2007) 132-139.
- [7] J. Herzog, F. von Klot-Heydenfeldt, S. Jabar, A. Ranft, C. Rossig, U. Dirksen, J. Van den Brande, M. D'Incalci, I. von Luettichau, P.J. Grohar, W.E. Berdel, S. Burdach, Trabectedin Followed by Irinotecan Can Stabilize Disease in Advanced Translocation-Positive Sarcomas with Acceptable Toxicity, *Sarcoma*, 2016 (2016) 7461783.

- [8] R.L. Saylor, 3rd, K.C. Stine, J. Sullivan, J.L. Kepner, D.A. Wall, M.L. Bernstein, M.B. Harris, R. Hayashi, T.J. Vietti, Cyclophosphamide plus topotecan in children with recurrent or refractory solid tumors: a Pediatric Oncology Group phase II study, *J Clin Oncol*, 19 (2001) 3463-3469.
- [9] J. Mora, C.O. Cruz, A. Parareda, C. de Torres, Treatment of relapsed/refractory pediatric sarcomas with gemcitabine and docetaxel, *J Pediatr Hematol Oncol*, 31 (2009) 723-729.
- [10] C. Rodriguez-Galindo, C.A. Billups, L.E. Kun, B.N. Rao, C.B. Pratt, T.E. Merchant, V.M. Santana, A.S. Pappo, Survival after recurrence of Ewing Tumors, *Cancer*, 94 (2002) 561-569.
- [11] B.E. Johnson, T. Mazor, C. Hong, M. Barnes, K. Aihara, C.Y. McLean, S.D. Fouse, S. Yamamoto, H. Ueda, K. Tatsuno, S. Asthana, L.E. Jalbert, S.J. Nelson, A.W. Bollen, W.C. Gustafson, E. Charron, W.A. Weiss, I.V. Smirnov, J.S. Song, A.B. Olshen, S. Cha, Y. Zhao, R.A. Moore, A.J. Mungall, S.J. Jones, M. Hirst, M.A. Marra, N. Saito, H. Aburatani, A. Mukasa, M.S. Berger, S.M. Chang, B.S. Taylor, J.F. Costello, Mutational analysis reveals the origin and therapy-driven evolution of recurrent glioma, *Science*, 343 (2014) 189-193.
- [12] A. Schramm, J. Koster, Y. Assenov, K. Althoff, M. Peifer, E. Mahlow, A. Odersky, D. Beisser, C. Ernst, A.G. Henssen, H. Stephan, C. Schroder, L. Heukamp, A. Engesser, Y. Kahlert, J. Theissen, B. Hero, F. Roels, J. Altmuller, P. Nurnberg, K. Astrahantseff, C. Gloeckner, K. De Preter, C. Plass, S. Lee, H.N. Lode, K.-O. Henrich, M. Gartlgruber, F. Speleman, P. Schmezer, F. Westermann, S. Rahmann, M. Fischer, A. Eggert, J.H. Schulte, Mutational dynamics between primary and relapse neuroblastomas, *Nat Genet*, 47 (2015) 872-877.
- [13] B.D. Crompton, C. Stewart, A. Taylor-Weiner, G. Alexe, K.C. Kurek, M.L. Calicchio, A. Kiezun, S.L. Carter, S.A. Shukla, S.S. Mehta, A.R. Thorner, C. de Torres, C. Lavarino, M. Sunol, A. McKenna, A. Sivachenko, K. Cibulskis, M.S. Lawrence, P. Stojanov, M. Rosenberg, L. Ambrogio, D. Auclair, S. Seepo, B. Blumenstiel, M. DeFelice, I. Imaz-Rosshandler, Y.C.A. Schwarz-Cruz, M.N. Rivera, C. Rodriguez-Galindo, M.D. Fleming, T.R. Golub, G. Getz, J. Mora, K. Stegmaier, The genomic landscape of pediatric Ewing sarcoma, *Cancer Discov*, 4 (2014) 1326-1341.
- [14] H.Y. Huang, P.B. Illei, Z. Zhao, M. Mazumdar, A.G. Huvos, J.H. Healey, L.H. Wexler, R. Gorlick, P. Meyers, M. Ladanyi, Ewing sarcomas with p53 mutation or



p16/p14ARF homozygous deletion: a highly lethal subset associated with poor chemoresponse, *J Clin Oncol*, 23 (2005) 548-558.

[15] H. Brahmabhatt, S. Oppermann, E.J. Osterlund, B. Leber, D.W. Andrews, Molecular Pathways: Leveraging the BCL-2 Interactome to Kill Cancer Cells-- Mitochondrial Outer Membrane Permeabilization and Beyond, *Clin Cancer Res*, 21 (2015) 2671-2676.

[16] J.I. Fletcher, R.T. Williams, M.J. Henderson, M.D. Norris, M. Haber, ABC transporters as mediators of drug resistance and contributors to cancer cell biology, *Drug Resist Updat*, 26 (2016) 1-9.

[17] S. Lamouille, J. Xu, R. Derynck, Molecular mechanisms of epithelial-mesenchymal transition, *Nat Rev Mol Cell Biol*, 15 (2014) 178-196.

[18] K.J. Patel, O. Tredan, I.F. Tannock, Distribution of the anticancer drugs doxorubicin, mitoxantrone and topotecan in tumors and normal tissues, *Cancer Chemother Pharmacol*, 72 (2013) 127-138.

[19] A.I. Minchinton, I.F. Tannock, Drug penetration in solid tumours, *Nat Rev Cancer*, 6 (2006) 583-592.

[20] A.M. Carcaboso, M.A. Elmeliegy, J. Shen, S.J. Juel, Z.M. Zhang, C. Calabrese, L. Tracey, C.M. Waters, C.F. Stewart, Tyrosine kinase inhibitor gefitinib enhances topotecan penetration of gliomas, *Cancer research*, 70 (2010) 4499-4508.

[21] O. Langer, R. Karch, U. Muller, G. Dobrozemsky, A. Abraham, M. Zeitlinger, E. Lackner, C. Joukhadar, R. Dudczak, K. Kletter, M. Muller, M. Brunner, Combined PET and microdialysis for in vivo assessment of intracellular drug pharmacokinetics in humans, *J Nucl Med*, 46 (2005) 1835-1841.

[22] C. Monterrubio, S. Paco, M. Vila-Ubach, E. Rodriguez, R. Glisoni, C. Lavarino, P. Schaiquevich, A. Sosnik, J. Mora, A.M. Carcaboso, Combined Microdialysis-Tumor Homogenate Method for the Study of the Steady State Compartmental Distribution of a Hydrophobic Anticancer Drug in Patient-Derived Xenografts, *Pharm Res*, 32 (2015) 2889-2900.

[23] C. Monterrubio, S. Paco, N.G. Olaciregui, G. Pascual-Pasto, M. Vila-Ubach, M. Cuadrado-Vilanova, M.M. Ferrandiz, H. Castillo-Ecija, R. Glisoni, N. Kuplennik, A. Jungbluth, C. de Torres, C. Lavarino, N.V. Cheung, J. Mora, A. Sosnik, A.M. Carcaboso, Targeted drug distribution in tumor extracellular fluid of GD2-expressing neuroblastoma patient-derived xenografts using SN-38-loaded nanoparticles

conjugated to the monoclonal antibody 3F8, *J Control Release*, 255 (2017) 108-119.

[24] J. Thompson, W.C. Zamboni, P.J. Cheshire, L. Lutz, X. Luo, Y. Li, J.A. Houghton, C.F. Stewart, P.J. Houghton, Efficacy of systemic administration of irinotecan against neuroblastoma xenografts, *Clin Cancer Res*, 3 (1997) 423-431.

[25] C.F. Stewart, M. Leggas, J.D. Schuetz, J.C. Panetta, P.J. Cheshire, J. Peterson, N. Daw, J.J. Jenkins, III, R. Gilbertson, G.S. Germain, F.C. Harwood, P.J. Houghton, Gefitinib enhances the antitumor activity and oral bioavailability of irinotecan in mice, *Cancer Res.*, 64 (2004) 7491-7499.

[26] C. Monterrubio, G. Pascual-Pasto, F. Cano, M. Vila-Ubach, A. Manzanares, P. Schaiquevich, J.A. Tornero, A. Sosnik, J. Mora, A.M. Carcaboso, SN-38-loaded nanofiber matrices for local control of pediatric solid tumors after subtotal resection surgery, *Biomaterials*, 79 (2016) 69-78.

[27] P.J. Grohar, L.E. Segars, C. Yeung, Y. Pommier, M. D'Incalci, A. Mendoza, L.J. Helman, Dual targeting of EWS-FLI1 activity and the associated DNA damage response with trabectedin and SN38 synergistically inhibits Ewing sarcoma cell growth, *Clin Cancer Res*, 20 (2014) 1190-1203.

[28] P.J. Houghton, G.S. Germain, F.C. Harwood, J.D. Schuetz, C.F. Stewart, E. Buchdunger, P. Traxler, Imatinib mesylate is a potent inhibitor of the ABCG2 (BCRP) transporter and reverses resistance to topotecan and SN-38 in vitro, *Cancer research*, 64 (2004) 2333-2337.

[29] Y. Wang, D.F. Welty, The simultaneous estimation of the influx and efflux blood-brain barrier permeabilities of gabapentin using a microdialysis-pharmacokinetic approach, *Pharm Res*, 13 (1996) 398-403.

[30] F.R. Luo, P.V. Paranjpe, A. Guo, E. Rubin, P. Sinko, Intestinal transport of irinotecan in Caco-2 cells and MDCK II cells overexpressing efflux transporters Pgp, cMOAT, and MRP1, *Drug Metab Dispos*, 30 (2002) 763-770.

[31] E.A. Abdallah, M.F. Fanelli, E.S.V. Souza, M.C. Machado Netto, J.L. Gasparini Junior, D.V. Araujo, L.M. Ocea, M.E. Buim, M.S. Tariki, S. Alves Vda, V. Piana de Andrade, A.L. Dettino, C. Abdon Lopes de Mello, L.T. Chinen, MRP1 expression in CTCs confers resistance to irinotecan-based chemotherapy in metastatic colorectal cancer, *Int J Cancer*, 139 (2016) 890-898.

[32] L. Hontecillas-Prieto, D.J. Garcia-Dominguez, D.P. Vaca, R. Garcia-Mejias, D. Marcilla, G.L. Ramirez-Villar, C. Saez, E. de Álava, Multidrug resistance transporter

profile reveals MDR3 as a marker for stratification of blastemal Wilms tumour patients, *Oncotarget*, 8 (2017) 11173-11186.

[33] K.J. Livak, T.D. Schmittgen, Analysis of relative gene expression data using real-time quantitative PCR and the 2(-Delta Delta C(T)) Method, *Methods*, 25 (2001) 402-408.

[34] Y. Sugimoto, S. Tsukahara, T. Oh-hara, T. Isoe, T. Tsuruo, Decreased expression of DNA topoisomerase I in camptothecin-resistant tumor cell lines as determined by a monoclonal antibody, *Cancer research*, 50 (1990) 6925-6930.

[35] F. Coussy, R. El-Botty, S. Chateau-Joubert, A. Dahmani, E. Montaudon, S. Leboucher, L. Morisset, P. Painsec, L. Sourd, L. Huguet, F. Nemati, J.L. Servely, T. Larcher, S. Vacher, A. Briaux, C. Reyes, P. La Rosa, G. Lucotte, T. Popova, P. Foidart, N.E. Sounni, A. Noel, D. Decaudin, L. Fuhrmann, A. Salomon, F. Reyal, C. Mueller, P. Ter Brugge, J. Jonkers, M.F. Poupon, M.H. Stern, I. Bieche, Y. Pommier, E. Marangoni, BRCAness, SLFN11, and RB1 loss predict response to topoisomerase I inhibitors in triple-negative breast cancers, *Sci Transl Med*, 12 (2020).

[36] M. Capello, M. Lee, H. Wang, I. Babel, M.H. Katz, J.B. Fleming, A. Maitra, H. Wang, W. Tian, A. Taguchi, S.M. Hanash, Carboxylesterase 2 as a Determinant of Response to Irinotecan and Neoadjuvant FOLFIRINOX Therapy in Pancreatic Ductal Adenocarcinoma, *Journal of the National Cancer Institute*, 107 (2015).

[37] P. Roberts, S.A. Burchill, S. Brownhill, C.J. Cullinane, C. Johnston, M.J. Griffiths, D.J. McMullan, N.P. Bown, S.P. Morris, I.J. Lewis, Ploidy and karyotype complexity are powerful prognostic indicators in the Ewing's sarcoma family of tumors: a study by the United Kingdom Cancer Cytogenetics and the Children's Cancer and Leukaemia Group, *Genes Chromosomes Cancer*, 47 (2008) 207-220.

[38] N.D. Anderson, R. de Borja, M.D. Young, F. Fuligni, A. Rosic, N.D. Roberts, S. Hajjar, M. Layeghifard, A. Novokmet, P.E. Kowalski, M. Anaka, S. Davidson, M. Zarrei, B. Id Said, L.C. Schreiner, R. Marchand, J. Sitter, N. Gokgoz, L. Brunga, G.T. Graham, A. Fullam, N. Pillay, J.A. Toretsky, A. Yoshida, T. Shibata, M. Metzler, G.R. Somers, S.W. Scherer, A.M. Flanagan, P.J. Campbell, J.D. Schiffman, M. Shago, L.B. Alexandrov, J.S. Wunder, I.L. Andrulis, D. Malkin, S. Behjati, A. Shlien, Rearrangement bursts generate canonical gene fusions in bone and soft tissue tumors, *Science*, 361 (2018).

- [39] J. Shen, A.M. Carcaboso, K.E. Hubbard, M. Tagen, H.G. Wynn, J.C. Panetta, C.M. Waters, M.A. Elmeliogy, C.F. Stewart, Compartment-specific roles of ATP-binding cassette transporters define differential topotecan distribution in brain parenchyma and cerebrospinal fluid, *Cancer research*, 69 (2009) 5885-5892.
- [40] Y. Tada, M. Wada, K. Kuroiwa, N. Kinugawa, T. Harada, J. Nagayama, M. Nakagawa, S. Naito, M. Kuwano, MDR1 Gene Overexpression and Altered Degree of Methylation at the Promoter Region in Bladder Cancer during Chemotherapeutic Treatment, *Clinical Cancer Research*, 6 (2000) 4618-4627.
- [41] A. Citti, R. Boldrini, A. Inserra, A. Alisi, R. Pessolano, A. Mastronuzzi, A. Zin, L. De Sio, A. Rosolen, F. Locatelli, D. Fruci, Expression of multidrug resistance-associated proteins in paediatric soft tissue sarcomas before and after chemotherapy, *Int J Oncol*, 41 (2012) 117-124.
- [42] Y.M. Hijazi, C.A. Axiotis, S. Navarro, S.M. Steinberg, M.E. Horowitz, M. Tsokos, Immunohistochemical detection of P-glycoprotein in Ewing's sarcoma and peripheral primitive neuroectodermal tumors before and after chemotherapy, *Am J Clin Pathol*, 102 (1994) 61-67.
- [43] T. Oue, A. Yoneda, S. Uehara, H. Yamanaka, M. Fukuzawa, Increased expression of multidrug resistance-associated genes after chemotherapy in pediatric solid malignancies, *J Pediatr Surg*, 44 (2009) 377-380.
- [44] Y.S. DeRose, G. Wang, Y.C. Lin, P.S. Bernard, S.S. Buys, M.T. Ebbert, R. Factor, C. Matsen, B.A. Milash, E. Nelson, L. Neumayer, R.L. Randall, I.J. Stijleman, B.E. Welm, A.L. Welm, Tumor grafts derived from women with breast cancer authentically reflect tumor pathology, growth, metastasis and disease outcomes, *Nat Med*, 17 (2011) 1514-1520.
- [45] N. Braekeveldt, C. Wigerup, D. Gisselsson, S. Mohlin, M. Merselius, S. Beckman, T. Jonson, A. Borjesson, T. Backman, I. Tadeo, A.P. Berbegall, I. Ora, S. Navarro, R. Noguera, S. Pahlman, D. Bexell, Neuroblastoma patient-derived orthotopic xenografts retain metastatic patterns and geno- and phenotypes of patient tumours, *Int J Cancer*, 136 (2015) E252-261.

## 2.9. Supplementary material

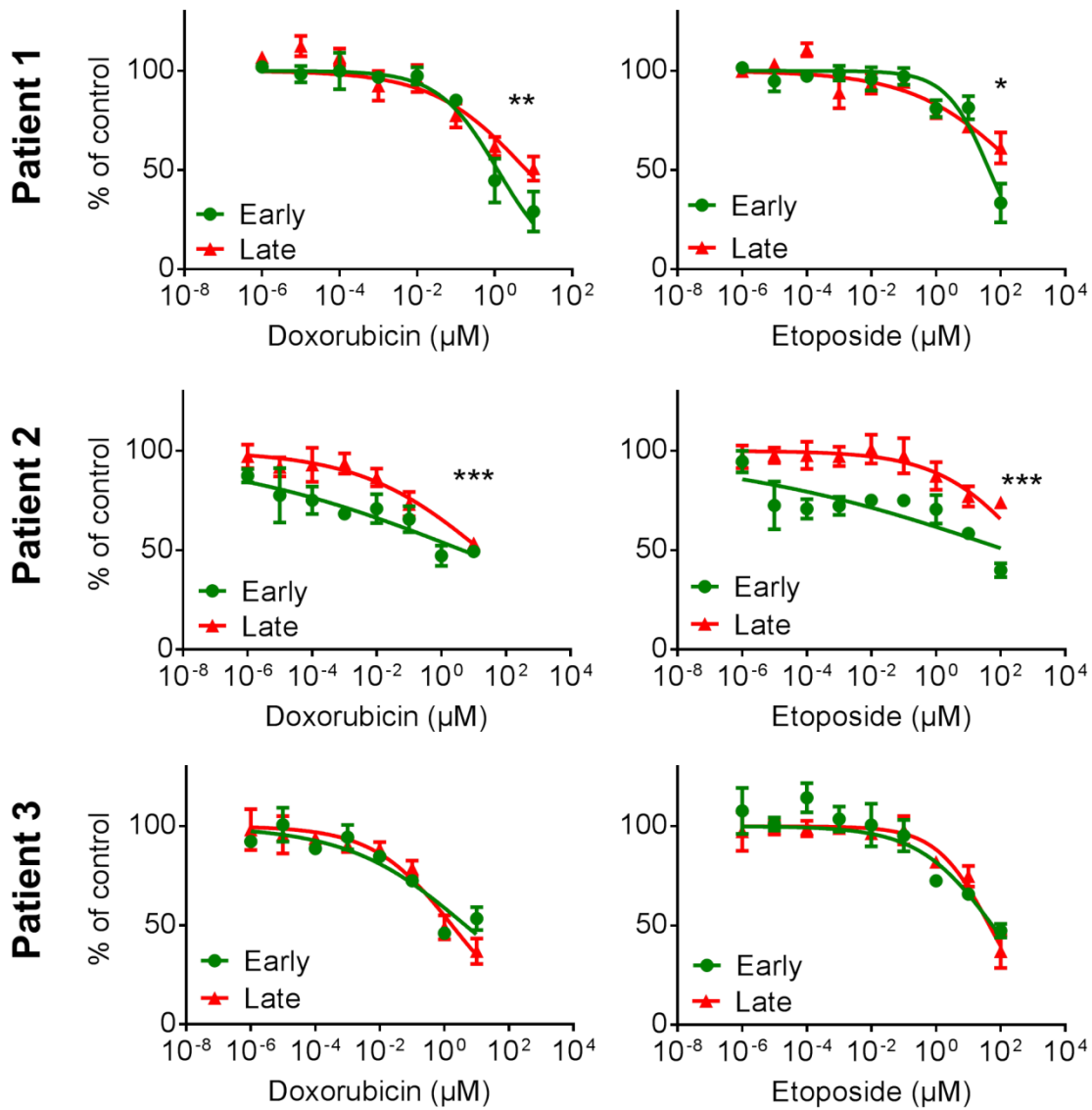


**Figure S1.** Activity of doxorubicin and etoposide in paired PDX models. *In vitro* antiproliferative activity curves of both drugs in PDX-derived cells in culture show % of MTS signal (mean and SD of six experimental values) compared to control untreated cells that were considered 100%. \* $P = 0.0456$ ; \*\* $P = 0.0031$ ; \*\*\* $P < 0.0001$ , late vs early cell IC<sub>50</sub> values; EC<sub>50</sub> shift analysis.

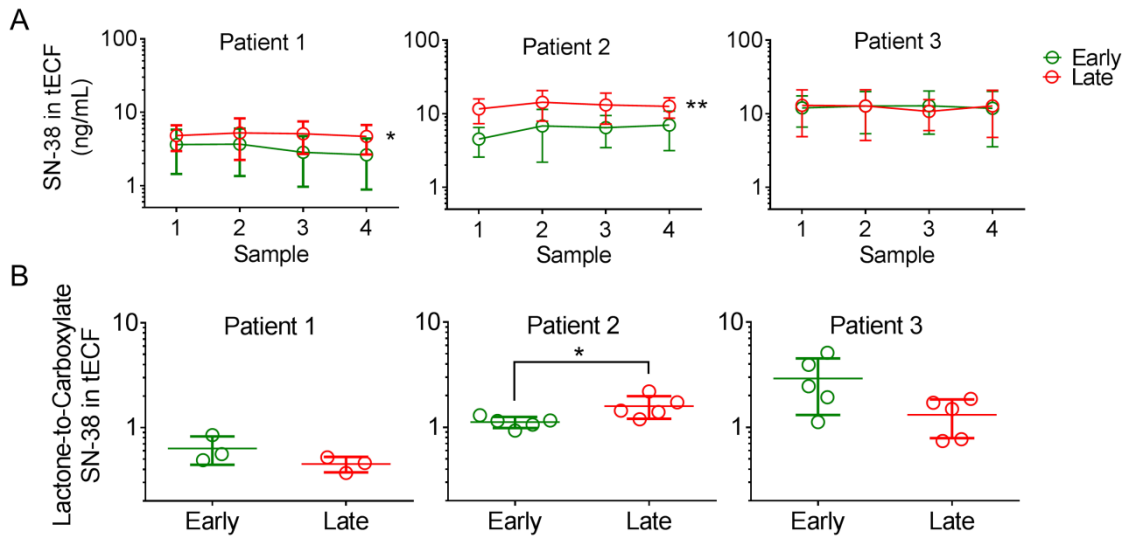


**Figure S2.** SN-38 concentrations in tECF at steady state. A) SN-38 lactone concentrations in tECF during four consecutive 90 min intervals (1 to 4) (mean  $\pm$  SD of 3-5 experiments). \* $P = 0.002$ , \*\* $P = 0.0001$ ,  $t$  test, early vs late samples. B) Lactone-to-carboxylate ratio of SN-38 concentrations in tECF at steady state. Dots represent value of each experiment, calculated as the ratio of SN-38 lactone and carboxylate concentrations (means of three consecutive dialysate samples at the steady state). \* $P = 0.0335$ ,  $t$  test.



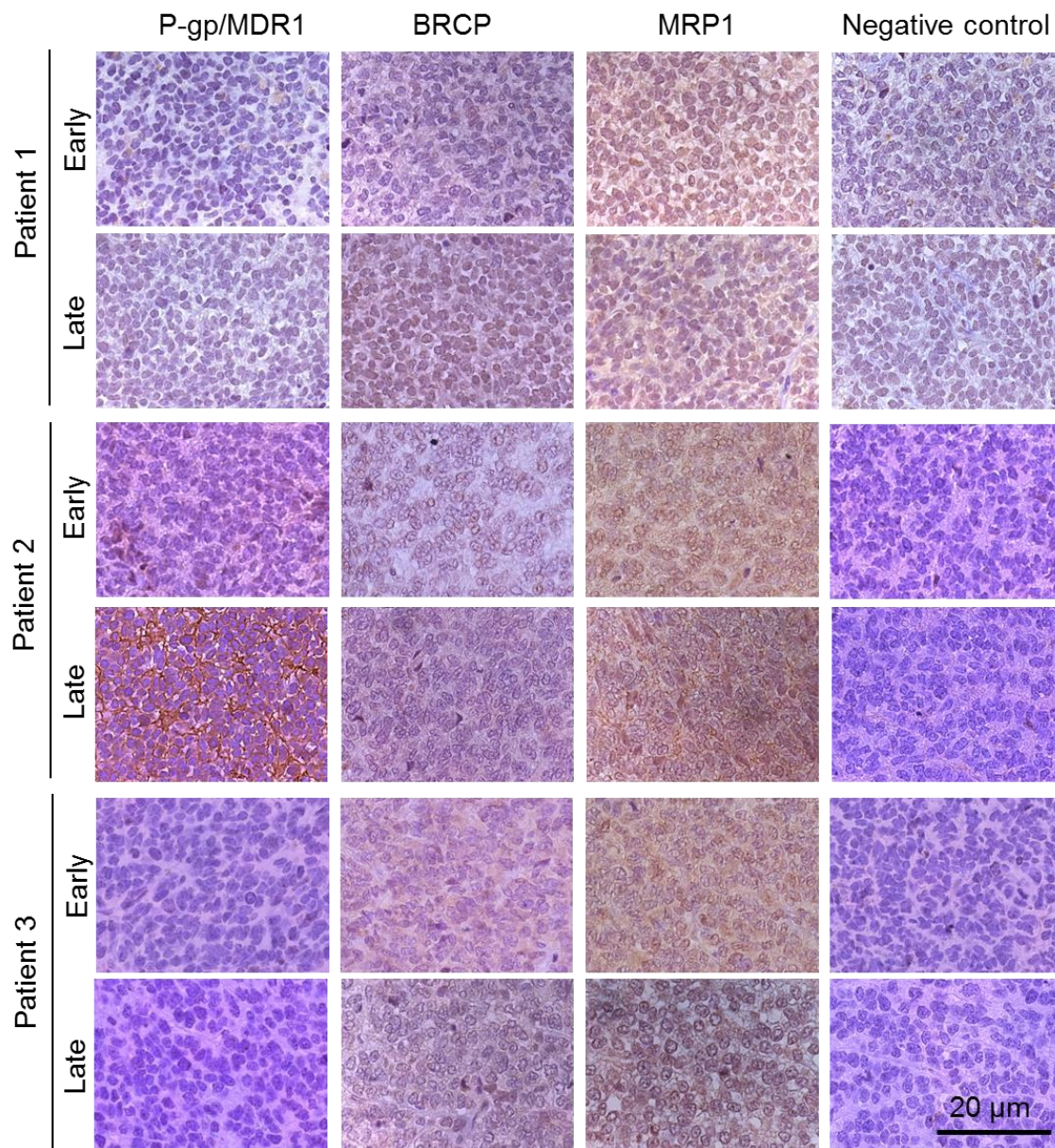


**Figure S3.** Immunostaining of PDX samples for P-gp/MDR1, BCRP and MRP1 transporters. P-gp/MDR1-stained sample of patient 2 (late sample; also shown in Fig. 3B) is shown as reference for positive membrane staining.

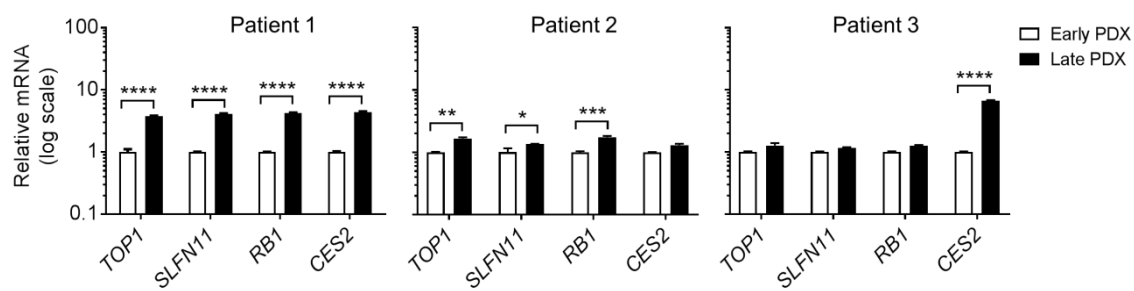


**Figure S4.** Expression of genes involved in irinotecan activity in early and late PDX tissue samples from patients 1-3. Values are relative to gene expression in the early PDX sample. \* $P = 0.0352$ ; \*\* $P = 0.0009$ ; \*\*\* $P = 0.0003$ ; \*\*\*\* $P < 0.0001$  (ANOVA test with Sidak correction for multiple comparisons).





# SUMMARY OF RESULTS

---



**1. Successful establishment and characterization of PDX models established from biopsies and necropsies of pediatric patients.**

We established 30 pediatric sarcoma PDX models from patients newly diagnosed and relapsed with Ewing sarcoma, osteosarcoma and rhabdomyosarcoma, from November 2010 to November 2019. We collected 68 biopsy samples from 51 patients obtaining a 44% of successful engraftment in immunodeficient mice.

We analyzed 12 PDX models and their corresponding patient biopsy sample by immunohistochemistry. The histopathology of the tumors, by hematoxylin and eosin staining, and the expression of tumor-related proteins, CD99 (Ewing sarcoma), SPARC (osteosarcoma) and MyoD1 (rhabdomyosarcoma), did not change significantly upon successive mouse-to-mouse passaging. We also compared the marker of cell proliferation Ki67 in patient tumor biopsies at early and late successive passages in PDX tumors. We observed that the percentage of Ki67-positive nuclei was lower in the PDX at F0, compared to the patient biopsy sample. PDX at generations higher than F0 showed an increasing number of Ki67-positive cells. Although the difference in Ki67 staining were not statistically significant, tumors at F5 filial generation achieved endpoint significantly faster than those at the earlier stage F2 ( $P = 0.0042$ ). We also compared the CNA profiles of two tumor biopsies and PDX tissues at early and late filial generations using the Cytoscan technology. We selected one Ewing sarcoma tumor with a stable genome and one rhabdomyosarcoma with highly aberrant chromosomic profiles for CNA analysis. We observed that karyotype alterations present in the biopsy sample were shared in both PDX models, at F2 and F5 generations.

We evaluated the activity of irinotecan in 20 subcutaneous PDX models and we observed that all of them had a measurable response after one treatment cycle. We found that 45% of the models achieved complete response to treatment and all achieved at least stable disease. In three of the PDXs, we evaluated the response to irinotecan at different filial generations and found that both tumors at passage  $F \leq 2$  and  $F \geq 6$  showed similar response. Upon treatment cessation, PDX tumors at both passages grew similarly and achieved similar median survivals until endpoint (established at a tumor volume of  $1500 \text{ mm}^3$ ). We also compared response to treatment of patient and PDX of four newly diagnosed rhabdomyosarcomas. We found that the three patients treated with irinotecan in combination with carboplatin achieved the same response to treatment as their corresponding PDX treated with irinotecan.

In summary, we demonstrated that PDX models stably represent patient disease from the morphology, genetics and functional perspectives.

## **2. Identification of factors favoring PDX engraftment and association between PDX engraftment and prognosis in pediatric patients.**

We collected data from patients and PDX models in order to identify factors favoring successful engraftment in mice. Patient clinical information included gender, age, date of diagnosis, risk stratification, presence of metastasis, relapse, date of death or last follow up, treatment and clinical response. We also collected information about primary tumor tissue of origin, timing of surgery, molecular tissue analysis and sample collection method. We observed that age older than 12 years and relapse were factors associated with increased engraftment rate when pooling all diseases together (Ewing sarcoma, osteosarcoma and rhabdomyosarcoma). We analyzed the Ewing sarcoma patient cohort separately and found that age older than 12 years was not determinant, while relapse and presence of metastasis at diagnosis was significantly associated with engraftment. We also studied if the engraftment of a first biopsy from one patient predicted the engraftment of successive biopsies obtained from the same patient during disease progression. We found that 9 out of 11 second biopsies engrafted after a first positive PDX engraftment. However, the association was not statistically significant.

We used the collected information to address whether successful engraftment in mice of tumor biopsies of newly diagnosed and relapsed sarcoma patients had a prognostic effect on the overall survival (OS) and event-free survival (EFS) of these patients. Median EFS and OS for patients with positive engraftment was significantly shorter than those of patients with negative engraftment, 7.56 vs 22.4 months ( $P = 0.00021$ ) and 19.9 vs 42.5 months ( $P = 0.0069$ ), respectively. In the diagnostic cohort, positive engraftment resulted in shorter median EFS (20.6 months) compared to negative-engraftment (median EFS not reached) ( $P = 0.040$ ). In this cohort, patients with positive engraftment also had shorter median OS (34.2 months), although not statistically significant compared to patients with negative engraftment (median OS not reached) ( $P = 0.19$ ). In the relapse cohort, we did not find a significant association of positive and negative engraftment with median EFS (4.56 vs 12.2 months, respectively) ( $P = 0.17$ ) and OS (16.7 vs 25.7 months, respectively) ( $P = 0.30$ ). We also studied 18 newly diagnosed Ewing sarcoma patients and showed that positive engraftment predicted relapse of patients classified as standard risk ( $P = 0.0357$ ).

In summary, we showed that positive engraftment of tumor biopsies in mice is a prognostic factor related to poorer EFS of newly diagnosed pediatric patients with the most frequent bone and soft tissue sarcomas.

### **3. Changes in anticancer drug activity and intratumoral drug distribution during the evolution of Ewing sarcoma.**

We established three pairs of Ewing sarcoma PDX models from biopsies obtained at diagnosis (early) and relapse/refractory (late) stage from three patients. We analyzed the CNA profiles of early and late PDX pairs. We observed that in patients 1 and 2, who achieved complete remission after treatment but relapsed more than one year later, most of the CNAs of the early PDX were conserved in the paired late tumor. In contrast, patient 3, who did not achieve remission and was refractory to treatment, showed substantially different CNA profiles in both PDX models. These findings suggest that late tumors likely evolved clonally from the early tumor cells in patient 1 and 2, while tumors from patient 3 are of different clonal origin.

PDX-derived primary cells from patients 1 and 2 were five to ten-fold more resistant to the anticancer drug SN-38, compared to their early counterparts ( $P < 0.0001$ ). In both PDX pairs, irinotecan treatment led to inferior tumor control in mice bearing the late PDX, which relapsed more rapidly upon treatment cessation (patient 1) or had a poorer response during treatment (patient 2). In contrast, for patient 3, there was no increased resistance to SN-38 of primary tumor cells derived from the late stage and the late PDX engrafted in mice was actually more sensitive to irinotecan. Analysis of intratumoral microdialysis samples and tumor homogenates revealed that at earlier stage during treatment, in patient 1 and 2, a greater proportion of SN-38 was intracellular rather than unbound in the tumor extracellular fluid ( $P = 0.0128$  and  $P < 0.0001$ , respectively). For patient 3, however, a higher amount of intracellular SN-38 was found in the late PDX model ( $P = 0.0010$ ).

In patient 2, we observed a remarkable 9500-fold overexpression of the ABCB1 gene ( $P = 0.0001$ ) in the late PDX by PCR. The protein encoded by such gene, MDR1/P-gp, was also overexpressed in the late PDX upon immunohistochemistry analysis. This result could explain the shift in SN-38 distribution towards the extracellular compartment. *In vitro* assays and live cell imaging studies showed that intracellular irinotecan accumulation was diminished in the late PDX-derived cells (up to 53% lower at one minute,  $P = 0.0226$ ) and that drug uptake was faster in early PDX-derived cells. We were able to reverse the increased resistance to SN-38 of the late PDX primary tumor cells using a P-gp inhibitor, elacridar.

In summary, we evidenced that anticancer agents are displaced from the intracellular compartment during tumor evolution under treatment pressure. The unique set of clinically relevant paired PDXs established at early and late tumor stages strengthened our experimental conclusions.



# DISCUSSION

---





The scientific contributions of this thesis include the establishment and characterization of a preclinical platform of mouse PDX to study pediatric sarcomas, such as Ewing sarcoma, osteosarcoma and rhabdomyosarcoma. These PDXs and the clinical information collected from patients and their biopsies led us to identify factors favoring PDX engraftment and study its association with prognosis. Using PDX pairs established from single patients, we studied the treatment-driven evolution of Ewing sarcoma tumors during disease progression. These multidisciplinary projects were possible due to key contributions from key experts working in the field of molecular biology, preclinical pharmacology, pediatric oncology, pathology, surgery and animal welfare.

Upon the selection of pediatric sarcomas as the unmet medical need to address, we identified that preclinical models resembling molecular genomics and histology of these diseases were scarce or not available in the scientific community. Thus, one of the main goals of my PhD work was to develop and characterize a preclinical tool to improve pediatric sarcoma research. We selected PDX models because they likely provide better translational relevance than xenograft models established from cell lines immortalized in culture. Cell cultures are clonally more homogenous, have greater invasive capabilities due to the adaptation to *in vitro* growing conditions and are considered less representative of tumor patients, compared to PDX models [10, 11]. Several of the preclinical therapies developed using tumor cell lines failed or did not achieve the expected clinical translation [9, 24].

To select the approach to engraft PDX at SJD, we considered the orthotopic *versus* subcutaneous location in the immunodeficient mice. Orthotopic engraftment is especially relevant to reproduce the complex microenvironment of the original tumor [15]. However, we decided to select the subcutaneous site because it offers the advantage of a simple surgical procedure, easier follow-up by palpation and it does not require imaging systems to visualize tumor engraftment [245].

As highlighted by Hidalgo *et al.*, a thorough characterization of the PDXs helps ensure that they correspond and represent the main characteristics of patient tumors [9]. Following this guide, we demonstrated that our established subcutaneous PDX models expressed specific tumor-related proteins and recapitulated chromosomic alterations of the original primary tumor. Upon comparison of the CNAs in the PDX and the original biopsy, we confirmed that patient alterations were conserved in the tumor xenograft. These results are consistent with previous data from DeRose *et al.*, who reported a bank of breast cancer grafts that maintained the key features of the patient tumors, including histopathology, clinical markers, gene expression profiles and copy number variations [20]. One observation of our study was surprising: cells in tumor patients showed higher rates of Ki67 positivity (marker of proliferation) compared to the first generation in mice (passage F0), that increased in the successive passages. Even though these differences were not significant, we observed that F2 PDXs grew

significantly slower than F5 ones. This supports that there might be a clonal selection during xenograft establishment that could facilitate and accelerate the growth of tumor samples in mice. Indeed, DeRose *et al.* showed in a breast cancer cohort that some clonal clusters were dominant in the PDX but not in the original tumor patient [20].

This PhD thesis describes one of the largest preclinical platforms of pediatric sarcoma xenografts reported to date. The engraftment rates of 42% for Ewing sarcoma, 42% for osteosarcoma and 53% for rhabdomyosarcoma biopsy samples are comparable to the study from Nanni *et al.* that obtained 36% and 24% successful engraftment rates for osteosarcoma and Ewing sarcoma, respectively [246].

The purpose of our studies of irinotecan activity in PDX models was to confirm the stability of the preclinical response at different filial generations and the ability to replicate clinical response to treatment in patients. Our results support that PDXs predict drug efficacy in personalized therapy studies. We selected the irinotecan protracted administration schedule because it showed clinical efficacy against pediatric sarcomas. Wagner reviewed the objective response to the protracted irinotecan treatment observed in patients with relapsed rhabdomyosarcoma and Ewing sarcoma in key phase II and III studies [230, 241]. In the clinical practice, irinotecan is administered to patients in combination with other chemotherapeutic drugs such as vincristine, carboplatin, temozolamide, docetaxel or ifosfamide, for treatment of intermediate and high-risk pediatric sarcomas [235, 236, 239, 241]. For example, Raciborska *et al.* reported a response rate of 68% in patients with relapsed Ewing sarcoma after treatment combining irinotecan, temozolamide and vincristine [238].

Aparicio, Hidalgo and Kung highlighted the difficulties of using PDX models in the day-to-day clinical decisions as a real-time predictive tool due to the slowness to develop the PDX models and to obtain preclinical study results [10]. They suggested that PDXs could be more useful to identify future patients in novel precision medicine strategies [9, 10]. Even though the factor “time” is the main limiting factor of personalized medicine, we calculated that 50% of our patients with an associated stable PDX model could have potentially benefited from our platform, i.e., experimentation in their models could have provided timely data to select their treatments.

The hypothesis that successful PDX engraftment could be associated with patient outcome emerged from our initial observations during more than 5 years of work. We observed that some patients with Ewing sarcoma, whose tumors engrafted at the initial diagnosis of the disease, relapsed unexpectedly. We also detected in the literature that successful PDX engraftment and worse prognosis had been associated in EGFR-mutant lung adenocarcinoma [29], uveal melanoma [50] and

pediatric liver cancers [54]. For instance, Pergolini *et al.* demonstrated that pancreatic ductal adenocarcinoma engraftment in mice was associated with worse recurrence-free survival and worse OS [247]. Another example is provided by DeRose *et al.*, who showed that the ability of breast cancer biopsies to grow in mice might reflect a more aggressive phenotype that was independent of clinical markers such as estrogen receptor (ER), progesterone receptor (PR) or human epidermal growth factor receptor 2 (HER2) [20]. They observed that positive engraftment of tumor samples correlated with shorter survival across all subjects included, indicating that the PDX established represented the most aggressive disease. In newly diagnosed patients with no detectable metastasis at the time of surgery, they observed that the ability of a tumor to generate stable orthotopic tumor grafts significantly correlated with reduced survival. They concluded that PDX engraftment provided retrospective prognostic information about the course of the disease and has potential to be used as a surrogate indicator of risk for disease progression [20]. Consequently, we performed a formal retrospective analysis of this phenomenon in our hands, once we had enough number of samples. We showed that positive engraftment was also associated with shorter median EFS and OS in patients with the most frequent pediatric sarcomas. However, the most relevant information was that, as observed by DeRose *et al.*, PDX engraftment at the time of diagnosis could help us identify aggressive pediatric sarcoma tumors with worse EFS, predicting relapse and disease progression. A consequence of this observation is that PDXs do not completely represent the heterogeneity of the whole disease because only the most aggressive tumors are able to engraft in mice.

Because our cohort of PDXs had a predominant representation of Ewing sarcomas, we explored deeper the clinical meaning of our findings in these patients. Clinical protocols such as GEIS21 classify Ewing sarcoma patients as standard risk or high risk, depending on the primary tumor localization, presence of metastasis at diagnosis or bone marrow micrometastasis [176]. Patients classified as high risk receive more intensive treatment than the standard risk ones [176]. Our observation that all patients with a stable PDX and classified as standard risk at diagnosis relapsed and died during the course of this study suggests that the factor “stable PDX” could be used in the future to classify such patients as high-risk. Prospective clinical trials should address this specific question.

Our findings that patients factors “age older than 12 years old” and “relapsed disease” correlated highly with engraftment are in agreement with the observations of Stewart *et al.*, who reported in lung adenocarcinoma that age was also a key factor in the tumor biopsy engraftment [29] and Nicolle *et al.*, who showed higher engraftment rates in recurrent hepatoblastoma tumors [54]. One limitation of our study was that the three tumor types were not equally represented, as we analyzed 31 patients with Ewing sarcoma, 10 with osteosarcoma and 10 with rhabdomyosarcoma. When we analyzed the Ewing sarcoma cohort, we found that

the factors favoring engraftment were relapse and the presence of metastasis at diagnosis. Chen *et al.* also showed in non-small cell lung cancer that advanced patients with metastasis had greater engraftment rates [248]. Interestingly, we did not observe in the Ewing sarcoma cohort that patients older than 12 years old had better engraftment, even though patients with Ewing sarcoma older than 14 years old had significantly worse prognosis [171].

During the project, we realized that collecting complete clinical data associated to preclinical models is challenging and very important to build optimal and powerful preclinical tools. Thus, we implemented the guide proposed by Meehan *et al.*, also known as PDX Minimal Information (PDX-MI) [75]. The PDX-MI guide helps preclinical institutions build robust and standardized databases to accurately report PDX models. Tables built using these guides include information regarding the methods to obtain the biopsy, tissue histology, tumor grade and classification, presence of specific markers and molecular analysis, previous treatment received in the patient, mouse strain, sample conservation, site of tumor implantation, use of Matrigel, time necessary to achieve a PDX of one specific volume, treatment tested and responses obtained in the different PDX models.

Our finding that both freshly excised and cryopreserved samples had similar rates of engraftment has relevant practical implications. One of the limiting factors when establishing PDX is the time between the sampling and the implantation, which according to Abel *et al.*, should not be longer than 48 h [249]. Our results do not rule out that the viability of cryopreserved samples is tumor type-dependent, but at least one study, by Hernandez *et al.*, showed that cryopreserved samples from pancreatic ductal adenocarcinoma engraft well in immunodeficient mice [250]. Another relevant conclusion of our work was that even small samples obtained by less invasive methods, such as the Tru-Cut, allowed to establish PDXs. The small sample size obtained by Tru-Cut might be less representative of the original tumor. However, as demonstrated by Sitt *et al.*, the ultrasound-guided Tru-cut synovial biopsy had a 99% accuracy for diagnosing synovial tumors and the 96% of biopsies obtained in their study had sufficient synovial tissue for histological analysis [28]. In agreement with these results, we consider that the Tru-cut biopsy is a safe and reliable surgery technique with a high diagnostic accuracy, sensitivity and specificity, which is useful to study disease progression when obtaining multiple biopsies over time from the same patient.

Our study on the functional evolution of Ewing sarcoma during disease progression took advantage of the successful engraftment at our laboratory of “early” and “late” biopsy samples from three patients. This resource of PDX pairs was an important novelty, because most PDX models represent disease stages related to “recurrence” or “progression”, in contrast to the stage “primary diagnosis”, which is rare [27]. Stewart *et al.* proposed that the acquisition of multiple samples from the same patient help study tumor evolution upon disease progression and the main

mechanisms involved in tumor chemoresistance [29]. Our conclusions upon the analysis of CNA profiles from the three pairs of PDX models were consistent with the study of Bhang *et al.* who showed that there are pre-existing subpopulations of resistant cells in tumors that are able to escape under treatment, suggesting that resistant clones are present before treatment [39]. We determined that if both early and late tumors have similar CNA profiles, it is likely that late tumors will develop chemoresistance to previous treatment probably due to the restriction of drug uptake to the intracellular compartment. In contrast, if the CNA are substantially different, the late tumor could maintain the clinical response to the therapies used in the early stages of disease. However, these suitable explanations should be taken cautiously as the main limitation of our work is the small number of cases analyzed.

Our choice of irinotecan/SN-38 as model drugs for *in vitro* and *in vivo* work was justified by the high sensitivity of our analytical technique to quantify SN-38, which we developed previously in-house [99]. Having a sensitive analytical technique was key, because the volume of microdialysis and biological samples was minimal in our experiments. We also selected other drugs included in the standard of care protocol of Ewing sarcoma such as doxorubicin and etoposide, both substrates of P-gp protein transporter. Our study identified the overexpression of P-gp as the likely cause for the shift of the SN-38 compartment distribution from the intracellular space, in the early PDX model of patient 2, to the tumor extracellular space, in the late PDX of the same patient. P-gp was discovered in 1970 by Biedler *et al.* who observed that this protein conferred a 2500-fold increase in drug resistance to actinomycin D in mammalian cell lines [251]. In agreement with the overexpression of P-gp in patient 2, Juliano *et al.* identified that P-gp was the cause of the reduced cellular drug exposure and the degree of drug resistance was related with the relative amount of surface P-gp [252]. The physiological impact of P-gp was elucidated by Schinkel *et al.* who reported in 1994 an increment of 100-fold in the penetration of ivermectin, an antiparasitic medication, into the brain of mice lacking de gene *ABCB1* [253]. Since then, several authors have described that the up-regulation of drug efflux by MRPs is one of the principal causes of drug resistance in tumor cells as these group of proteins are able to mediate the outflow of a wide range of chemotherapeutic drugs [130-132].

Our finding in the samples of patient 2 is consistent with the results observed by Hijazi *et al.* that showed that 50% of Ewing sarcoma tumors become positive to immunohistochemical P-gp analysis after treatment [254]. However, this pathology study contained only 15 cases with matched tumors before and after treatment, which is likely an insufficient number of samples to obtain general conclusions. We observed in our studies that the modulation of P-gp protein activity has influence in the active extrusion of SN-38/irinotecan from the intracellular compartment to the extracellular space. Follit *et al.* and Nanayakkara *et al.* identified *in silico* three compounds that inhibit P-gp directly blocking the pumping action, and showed successful reversion of paclitaxel resistance in prostate cancer cell line with high

expression of P-gp [255, 256]. In this regard, the use of inhibitors of P-gp such as elacridar, the one we used in our study, could help to explain in part the reason of acquired chemoresistance in tumor cells. However, the translation of targeting P-gp in the clinical practice is still unclear and several clinical trials failed due to the toxicity observed in patients. Despite these results, the modulation of other MDR proteins such as MRP1 by the small molecular inhibitor ibrutinib has been approved by the US FDA for the treatment of chronic lymphocytic leukemia. Further trials could identify and develop promising candidates targeting P-gp to treat tumors that are multidrug resistant due to P-gp overexpression.

Taken together, the results of my PhD thesis provide potential clinical impact in pediatric sarcoma research. The novel set of Ewing sarcoma, osteosarcoma and rhabdomyosarcoma preclinical models will be useful for future preclinical studies and for the design of clinical trials. The identification of PDX engraftment as a bad prognosis factor of Ewing sarcoma patients could be introduced in the design of future clinical studies. The paired-PDX samples from early and late stages of patient disease are novel and original resources for the scientific community. Our approach to study intratumoral drug pharmacokinetics to understand resistance to treatment will remain limited to the handful of laboratories that perform microdialysis, but we will continue refining this method to improve our understanding of the relationship between intratumoral drug distribution and drug response.







# CONCLUSIONS

---



## CONCLUSIONS

In this thesis we developed a novel preclinical PDX platform of the most frequent pediatric sarcomas, including Ewing sarcoma, osteosarcoma and rhabdomyosarcoma. We used this new resource to identify factors related with successful PDX engraftment, to study the association between engraftment and patient prognosis, and to measure changes in drug distribution and activity during the evolution of Ewing sarcoma disease.

The main conclusions related with the development of the preclinical models of pediatric sarcoma patients are:

1. Using fresh and cryopreserved tumor specimens from 31 newly diagnosed and 37 relapsed patients with Ewing sarcoma, osteosarcoma and rhabdomyosarcoma, we robustly established 30 PDX models from the 68 samples obtained, which represents a 44% of successful engraftment rate.
2. We analyzed representative cases of the PDX platform and determined that the PDX models resembled the histology (12 cases) and genetics (2 cases) of the original human tumors and that these characteristics remained stable over successive passages in mice.
3. The anticancer activity of irinotecan in 20 PDXs was significant, with 45% of the models achieving complete response to this drug. Three patients treated with irinotecan in combination with carboplatin achieved the same response to treatment as their corresponding PDXs. Our data support that PDX predict clinical efficacy of personalized medicine while keeping a stable tumor architecture and heterogeneity.

Next, we focused on the identification of factors related with successful engraftment and its association as a prognostic indicator in pediatric sarcoma patients. The main conclusions of this section are:

1. The factors related to higher engraftment rates in our pediatric sarcoma cohort (51 patients in total) were age older than 12 years old and relapse. In the Ewing sarcoma cohort (31 patients) the factors were advanced disease and presence of metastasis at diagnosis, but not age older than 12 years.
2. Positive PDX engraftment was associated with shorter median EFS and OS. Positive PDX engraftment at the time of patient diagnosis identified aggressive pediatric sarcoma tumors with poorer prognosis, predicting disease progression.
3. PDX engraftment might help re-classify patients newly diagnosed with standard risk Ewing sarcoma. In 18 newly diagnosed Ewing sarcoma patients, positive engraftment predicted relapse of patients classified as

standard risk. We propose that such patients should be classified as high-risk, upon confirmation of this finding in prospective clinical trials.

Finally, we characterized the pharmacokinetics and pharmacodynamics of irinotecan during the evolution of Ewing sarcoma. The main conclusions of this section are:

1. We established three pairs of Ewing sarcoma PDXs from the same patients at primary diagnosis and at later disease stages.
2. We demonstrated the development of chemoresistance was related to decreased intracellular drug concentration *in vitro* and *in vivo* in two PDX pairs, corresponding to two patients that achieved complete response to therapy but relapsed in the long-term. In these two patients, copy number alteration profiles were similar in both paired xenografts obtained at diagnosis and at long-term relapse, suggesting a common clonal origin of tumors at both disease stages.
3. We identified the overexpression of P-glycoprotein as the likely cause of treatment-induced chemoresistance and limited drug distribution in tumor cells in one of the tumor pairs.





# REFERENCES

---





## REFERENCES

1. Rygaard, J. and C.O. Povlsen, *Heterotransplantation of a human malignant tumour to "Nude" mice*. Acta Pathol Microbiol Scand, 1969. **77**(4): p. 758-60.
2. Cobb, L.M., *The behaviour of carcinoma of the large bowel in man following transplantation into immune deprived mice*. Br J Cancer, 1973. **28**(5): p. 400-11.
3. Pickard, R.G., L.M. Cobb, and G.G. Steel, *The growth kinetics of xenografts of human colorectal tumours in immune deprived mice*. Br J Cancer, 1975. **31**(1): p. 36-45.
4. Selby, P.J., et al., *A human testicular teratoma serially transplanted in immune-deprived mice*. Br J Cancer, 1979. **39**(5): p. 578-83.
5. Fiebig, H.H., et al., *Comparison of tumor response in nude mice and in the patients*. Behring Inst Mitt, 1984(74): p. 343-52.
6. Osieka, R., *Human malignant melanoma: preclinical and clinical drug evaluation*. Behring Inst Mitt, 1984(74): p. 353-67.
7. Gao, H., et al., *High-throughput screening using patient-derived tumor xenografts to predict clinical trial drug response*. Nat Med, 2015. **21**(11): p. 1318-25.
8. Byrne, A.T., et al., *Interrogating open issues in cancer precision medicine with patient-derived xenografts*. Nat Rev Cancer, 2017. **17**(4): p. 254-268.
9. Hidalgo, M., et al., *Patient-derived xenograft models: an emerging platform for translational cancer research*. Cancer Discov, 2014. **4**(9): p. 998-1013.
10. Aparicio, S., M. Hidalgo, and A.L. Kung, *Examining the utility of patient-derived xenograft mouse models*. Nat Rev Cancer, 2015. **15**(5): p. 311-6.
11. Kung, A.L., *Practices and Pitfalls of Mouse Cancer Models in Drug Discovery*. 2006. **96**: p. 191-212.
12. Johnson, B.E., et al., *Mutational analysis reveals the origin and therapy-driven evolution of recurrent glioma*. Science, 2014. **343**(6167): p. 189-193.
13. Hidalgo, M., et al., *A pilot clinical study of treatment guided by personalized tumorgrafts in patients with advanced cancer*. Mol Cancer Ther, 2011. **10**(8): p. 1311-6.
14. Morelli, M.P., et al., *Prioritizing phase I treatment options through preclinical testing on personalized tumorgraft*. J Clin Oncol, 2012. **30**(4): p. e45-8.
15. Siolas, D. and G.J. Hannon, *Patient-derived tumor xenografts: transforming clinical samples into mouse models*. Cancer Res, 2013. **73**(17): p. 5315-9.
16. Tentler, J.J., et al., *Patient-derived tumour xenografts as models for oncology drug development*. Nat Rev Clin Oncol, 2012. **9**(6): p. 338-50.
17. Morton, C.L. and P.J. Houghton, *Establishment of human tumor xenografts in immunodeficient mice*. Nature Protocols, 2007. **2**(2): p. 247-250.
18. Hughes, C.S., L.M. Postovit, and G.A. Lajoie, *Matrigel: a complex protein mixture required for optimal growth of cell culture*. Proteomics, 2010. **10**(9): p. 1886-90.
19. Benton, G., et al., *In vitro microtumors provide a physiologically predictive tool for breast cancer therapeutic screening*. PLoS One, 2015. **10**(4): p. e0123312.
20. DeRose, Y.S., et al., *Tumor grafts derived from women with breast cancer authentically reflect tumor pathology, growth, metastasis and disease outcomes*. Nat Med, 2011. **17**(11): p. 1514-20.
21. Braekveldt, N., et al., *Neuroblastoma patient-derived orthotopic xenografts retain metastatic patterns and geno- and phenotypes of patient tumours*. International Journal of Cancer, 2015. **136**(5): p. E252-E261.
22. Julien, S., et al., *Characterization of a large panel of patient-derived tumor xenografts representing the clinical heterogeneity of human colorectal cancer*. Clin Cancer Res, 2012. **18**(19): p. 5314-28.
23. Johnson, J.I., et al., *Relationships between drug activity in NCI preclinical in vitro and in vivo models and early clinical trials*. Br J Cancer, 2001. **84**(10): p. 1424-31.
24. Dong, X., et al., *Patient-derived first generation xenografts of non-small cell lung cancers: promising tools for predicting drug responses for personalized chemotherapy*. Clin Cancer Res, 2010. **16**(5): p. 1442-51.

25. Daniel, V.C., et al., *A primary xenograft model of small-cell lung cancer reveals irreversible changes in gene expression imposed by culture in vitro*. *Cancer Res*, 2009. **69**(8): p. 3364-73.
26. Okano, M., et al., *Orthotopic Implantation Achieves Better Engraftment and Faster Growth Than Subcutaneous Implantation in Breast Cancer Patient-Derived Xenografts*. *J Mammary Gland Biol Neoplasia*, 2020. **25**(1): p. 27-36.
27. Stewart, E., et al., *Orthotopic patient-derived xenografts of paediatric solid tumours*. *Nature*, 2017. **549**(7670): p. 96-100.
28. Sitt, J.C., et al., *Ultrasound-guided synovial Tru-cut biopsy: indications, technique, and outcome in 111 cases*. *Eur Radiol*, 2017. **27**(5): p. 2002-2010.
29. Stewart, E.L., et al., *Clinical Utility of Patient-Derived Xenografts to Determine Biomarkers of Prognosis and Map Resistance Pathways in EGFR-Mutant Lung Adenocarcinoma*. *J Clin Oncol*, 2015. **33**(22): p. 2472-80.
30. Castillo-Ecija, H., et al., *Prognostic value of patient-derived xenograft engraftment in pediatric sarcomas*. *J Pathol Clin Res*, 2021. **7**(4): p. 338-349.
31. Hanahan, D. and R.A. Weinberg, *Hallmarks of cancer: the next generation*. *Cell*, 2011. **144**(5): p. 646-74.
32. Anderson, N.M. and M.C. Simon, *The tumor microenvironment*. *Curr Biol*, 2020. **30**(16): p. R921-R925.
33. Fiedler, E.C. and M.T. Hemann, *Aiding and Abetting: How the Tumor Microenvironment Protects Cancer from Chemotherapy*. *Annual Review of Cancer Biology*, 2019. **3**(1): p. 409-428.
34. Ribeiro Franco, P.I., et al., *Tumor microenvironment components: Allies of cancer progression*. *Pathol Res Pract*, 2020. **216**(1): p. 152729.
35. Jin, M.Z. and W.L. Jin, *The updated landscape of tumor microenvironment and drug repurposing*. *Signal Transduct Target Ther*, 2020. **5**(1): p. 166.
36. Zhang, X., et al., *A renewable tissue resource of phenotypically stable, biologically and ethnically diverse, patient-derived human breast cancer xenograft models*. *Cancer Res*, 2013. **73**(15): p. 4885-97.
37. Reyat, F., et al., *Molecular profiling of patient-derived breast cancer xenografts*. *Breast Cancer Res*, 2012. **14**(1): p. R11.
38. Diaz, L.A., Jr., et al., *The molecular evolution of acquired resistance to targeted EGFR blockade in colorectal cancers*. *Nature*, 2012. **486**(7404): p. 537-40.
39. Bhang, H.E., et al., *Studying clonal dynamics in response to cancer therapy using high-complexity barcoding*. *Nat Med*, 2015. **21**(5): p. 440-8.
40. Bruna, A., et al., *A Biobank of Breast Cancer Explants with Preserved Intra-tumor Heterogeneity to Screen Anticancer Compounds*. *Cell*, 2016. **167**(1): p. 260-274 e22.
41. Tabassum, D.P. and K. Polyak, *Tumorigenesis: it takes a village*. *Nat Rev Cancer*, 2015. **15**(8): p. 473-83.
42. Cassidy, J.W., C. Caldas, and A. Bruna, *Maintaining Tumor Heterogeneity in Patient-Derived Tumor Xenografts*. *Cancer Res*, 2015. **75**(15): p. 2963-8.
43. El-Sayes, N., A. Vito, and K. Mossman, *Tumor Heterogeneity: A Great Barrier in the Age of Cancer Immunotherapy*. *Cancers (Basel)*, 2021. **13**(4).
44. Schueler, J., et al., *Induction of Acquired Resistance towards EGFR Inhibitor Gefitinib in a Patient-Derived Xenograft Model of Non-Small Cell Lung Cancer and Subsequent Molecular Characterization*. *Cells*, 2019. **8**(7).
45. Das Thakur, M., et al., *Modelling vemurafenib resistance in melanoma reveals a strategy to forestall drug resistance*. *Nature*, 2013. **494**(7436): p. 251-5.
46. Monsma, D.J., et al., *Using a rhabdomyosarcoma patient-derived xenograft to examine precision medicine approaches and model acquired resistance*. *Pediatr Blood Cancer*, 2014. **61**(9): p. 1570-7.
47. Monsma, D.J., et al., *Melanoma patient derived xenografts acquire distinct Vemurafenib resistance mechanisms*. *Am J Cancer Res*, 2015. **5**(4): p. 1507-18.

## REFERENCES

48. Cottu, P., et al., *Acquired resistance to endocrine treatments is associated with tumor-specific molecular changes in patient-derived luminal breast cancer xenografts*. Clin Cancer Res, 2014. **20**(16): p. 4314-25.
49. Oh, B.Y., et al., *Correlation between tumor engraftment in patient-derived xenograft models and clinical outcomes in colorectal cancer patients*. Oncotarget, 2015. **6**(18): p. 16059-68.
50. Nemati, F., et al., *Establishment and characterization of a panel of human uveal melanoma xenografts derived from primary and/or metastatic tumors*. Clin Cancer Res, 2010. **16**(8): p. 2352-62.
51. Stebbing, J., et al., *Patient-derived xenografts for individualized care in advanced sarcoma*. Cancer, 2014. **120**(13): p. 2006-15.
52. John, T., et al., *The ability to form primary tumor xenografts is predictive of increased risk of disease recurrence in early-stage non-small cell lung cancer*. Clin Cancer Res, 2011. **17**(1): p. 134-41.
53. Garrido-Laguna, I., et al., *Tumor Engraftment in Nude Mice and Enrichment in Stroma-Related Gene Pathways Predict Poor Survival and Resistance to Gemcitabine in Patients with Pancreatic Cancer*. Clinical Cancer Research, 2011. **17**(17): p. 5793-5800.
54. Nicolle, D., et al., *Patient-Derived Mouse Xenografts From Pediatric Liver Cancer Predict Tumor Recurrence and Advise Clinical Management*. Hepatology, 2016. **VOL. 64, NO. 4.**
55. Gould, S.E., M.R. Junntila, and F.J. de Sauvage, *Translational value of mouse models in oncology drug development*. Nat Med, 2015. **21**(5): p. 431-9.
56. Poh, A., *Novartis Compiles Mouse Avatar "Encyclopedia"*. Cancer Discov, 2016. **6**(1): p. 5-6.
57. Ledford, H., *US cancer institute to overhaul tumour cell lines*. Nature, 2016. **530**(7591): p. 391.
58. Malaney, P., S.V. Nicosia, and V. Dave, *One mouse, one patient paradigm: New avatars of personalized cancer therapy*. Cancer Lett, 2014. **344**(1): p. 1-12.
59. Koga, Y. and A. Ochiai, *Systematic Review of Patient-Derived Xenograft Models for Preclinical Studies of Anti-Cancer Drugs in Solid Tumors*. Cells, 2019. **8**(5).
60. Houghton, P.J., et al., *The pediatric preclinical testing program: description of models and early testing results*. Pediatr Blood Cancer, 2007. **49**(7): p. 928-40.
61. Kim, K.J., et al., *Inhibition of vascular endothelial growth factor-induced angiogenesis suppresses tumour growth in vivo*. Nature, 1993. **362**(6423): p. 841-4.
62. Yang, J.C., et al., *A randomized trial of bevacizumab, an anti-vascular endothelial growth factor antibody, for metastatic renal cancer*. N Engl J Med, 2003. **349**(5): p. 427-34.
63. Hurwitz, H., et al., *Bevacizumab plus irinotecan, fluorouracil, and leucovorin for metastatic colorectal cancer*. N Engl J Med, 2004. **350**(23): p. 2335-42.
64. Olive, K.P., et al., *Inhibition of Hedgehog signaling enhances delivery of chemotherapy in a mouse model of pancreatic cancer*. Science, 2009. **324**(5933): p. 1457-61.
65. Von Hoff, D.D., et al., *Gemcitabine plus nab-paclitaxel is an active regimen in patients with advanced pancreatic cancer: a phase I/II trial*. J Clin Oncol, 2011. **29**(34): p. 4548-54.
66. Fichtner, I., et al., *Anticancer drug response and expression of molecular markers in early-passage xenotransplanted colon carcinomas*. Eur J Cancer, 2004. **40**(2): p. 298-307.
67. Pompili, L., et al., *Patient-derived xenografts: a relevant preclinical model for drug development*. J Exp Clin Cancer Res, 2016. **35**(1): p. 189.
68. Marangoni, E., et al., *A new model of patient tumor-derived breast cancer xenografts for preclinical assays*. Clin Cancer Res, 2007. **13**(13): p. 3989-98.
69. Bertotti, A., et al., *A molecularly annotated platform of patient-derived xenografts ("xenopatients") identifies HER2 as an effective therapeutic target in cetuximab-resistant colorectal cancer*. Cancer Discov, 2011. **1**(6): p. 508-23.
70. Ricci, F., et al., *Patient-derived ovarian tumor xenografts recapitulate human clinicopathology and genetic alterations*. Cancer Res, 2014. **74**(23): p. 6980-90.

71. Topp, M.D., et al., *Molecular correlates of platinum response in human high-grade serous ovarian cancer patient-derived xenografts*. *Mol Oncol*, 2014. **8**(3): p. 656-68.
72. Anderson, W.C., et al., *Initiation and characterization of small cell lung cancer patient-derived xenografts from ultrasound-guided transbronchial needle aspirates*. *PLoS One*, 2015. **10**(5): p. e0125255.
73. Nunes, M., et al., *Evaluating patient-derived colorectal cancer xenografts as preclinical models by comparison with patient clinical data*. *Cancer Res*, 2015. **75**(8): p. 1560-6.
74. Zhang, X.C., et al., *Establishment of patient-derived non-small cell lung cancer xenograft models with genetic aberrations within EGFR, KRAS and FGFR1: useful tools for preclinical studies of targeted therapies*. *J Transl Med*, 2013. **11**: p. 168.
75. Meehan, T.F., et al., *PDX-MI: Minimal Information for Patient-Derived Tumor Xenograft Models*. *Cancer Res*, 2017. **77**(21): p. e62-e66.
76. Izumchenko, E., et al., *Patient-derived xenografts effectively capture responses to oncology therapy in a heterogeneous cohort of patients with solid tumors*. *Annals of Oncology*, 2017. **28**(10): p. 2595-2605.
77. Sharma, P. and J.P. Allison, *The future of immune checkpoint therapy*. *Science*, 2015. **348**(6230): p. 56-61.
78. Greaves, M. and C.C. Maley, *Clonal evolution in cancer*. *Nature*, 2012. **481**(7381): p. 306-313.
79. Bedard, P.L., et al., *Tumour heterogeneity in the clinic*. *Nature*, 2013. **501**(7467): p. 355-64.
80. Collins, A.T. and S.H. Lang, *A systematic review of the validity of patient derived xenograft (PDX) models: the implications for translational research and personalised medicine*. *PeerJ*, 2018. **6**: p. e5981.
81. Lin, D., et al., *High fidelity patient-derived xenografts for accelerating prostate cancer discovery and drug development*. *Cancer Res*, 2014. **74**(4): p. 1272-83.
82. Pan, C.X., et al., *Development and Characterization of Bladder Cancer Patient-Derived Xenografts for Molecularly Guided Targeted Therapy*. *PLoS One*, 2015. **10**(8): p. e0134346.
83. Tsimberidou, A.M., et al., *Personalized medicine for patients with advanced cancer in the phase I program at MD Anderson: validation and landmark analyses*. *Clin Cancer Res*, 2014. **20**(18): p. 4827-36.
84. Berger, M.F., et al., *The genomic complexity of primary human prostate cancer*. *Nature*, 2011. **470**(7333): p. 214-20.
85. Cancer Genome Atlas Research, N., *Integrated genomic analyses of ovarian carcinoma*. *Nature*, 2011. **474**(7353): p. 609-15.
86. Peterson, J.K. and P.J. Houghton, *Integrating pharmacology and in vivo cancer models in preclinical and clinical drug development*. *Eur J Cancer*, 2004. **40**(6): p. 837-44.
87. Hammer, S., et al., *Comparative profiling of the novel epothilone, sagopilone, in xenografts derived from primary non-small cell lung cancer*. *Clin Cancer Res*, 2010. **16**(5): p. 1452-65.
88. Crystal, A.S., et al., *Patient-derived models of acquired resistance can identify effective drug combinations for cancer*. *Science*, 2014. **346**(6216): p. 1480-6.
89. Vassal, G., et al., *Access to essential anticancer medicines for children and adolescents in Europe*. *Ann Oncol*, 2021. **32**(4): p. 560-568.
90. Abrahamsson, P. and O. Winso, *An assessment of calibration and performance of the microdialysis system*. *J Pharm Biomed Anal*, 2005. **39**(3-4): p. 730-4.
91. Blakeley, J. and J. Portnow, *Microdialysis for assessing intratumoral drug disposition in brain cancers: a tool for rational drug development*. *Expert Opin Drug Metab Toxicol*, 2010. **6**(12): p. 1477-91.
92. Hammarlund-Udenaes, M., *Microdialysis as an Important Technique in Systems Pharmacology-a Historical and Methodological Review*. *AAPS J*, 2017. **19**(5): p. 1294-1303.
93. Araujo, B.V., et al., *Microdialysis as a tool to determine free kidney levels of voriconazole in rodents: a model to study the technique feasibility for a moderately lipophilic drug*. *J Pharm Biomed Anal*, 2008. **47**(4-5): p. 876-81.

94. Plock, N. and C. Kloft, *Microdialysis--theoretical background and recent implementation in applied life-sciences*. Eur J Pharm Sci, 2005. **25**(1): p. 1-24.
95. Pigatto, M.C., et al., *Population Pharmacokinetic Modeling of Etoposide Free Concentrations in Solid Tumor*. Pharm Res, 2016. **33**(7): p. 1657-70.
96. Brunner, M. and O. Langer, *Microdialysis versus other techniques for the clinical assessment of in vivo tissue drug distribution*. AAPS J, 2006. **8**(2): p. E263-71.
97. Chaurasia, C.S., et al., *AAPS-FDA Workshop White Paper: microdialysis principles, application, and regulatory perspectives*. J Clin Pharmacol, 2007. **47**(5): p. 589-603.
98. Zhou, Q. and J.M. Gallo, *In vivo microdialysis for PK and PD studies of anticancer drugs*. AAPS J, 2005. **7**(3): p. E659-67.
99. Monterrubio, C., et al., *Combined Microdialysis-Tumor Homogenate Method for the Study of the Steady State Compartmental Distribution of a Hydrophobic Anticancer Drug in Patient-Derived Xenografts*. Pharm Res, 2015. **32**(9): p. 2889-900.
100. Kho, C.M., et al., *A Review on Microdialysis Calibration Methods: the Theory and Current Related Efforts*. Mol Neurobiol, 2017. **54**(5): p. 3506-3527.
101. Zapata, A., V.I. Chefer, and T.S. Shippenberg, *Microdialysis in rodents*. Curr Protoc Neurosci, 2009. **Chapter 7**: p. Unit7 2.
102. Tabatabaei, P., et al., *Intratumoral retrograde microdialysis treatment of high-grade glioma with cisplatin*. Acta Neurochirurgica, 2020. **162**(12): p. 3043-3053.
103. Simmel, F., et al., *Pilot investigation on long-term subcutaneous microdialysis: proof of principle in humans*. AAPS J, 2013. **15**(1): p. 95-103.
104. Zhou, T. and A. Kalanuria, *Cerebral Microdialysis in Neurocritical Care*. Curr Neurol Neurosci Rep, 2018. **18**(12): p. 101.
105. Muller, M., *Microdialysis in clinical drug delivery studies*. Adv Drug Deliv Rev, 2000. **45**(2-3): p. 255-69.
106. Rea, H. and B. Kirby, *A Review of Cutaneous Microdialysis of Inflammatory Dermatoses*. Acta Derm Venereol, 2019. **99**(11): p. 945-952.
107. Ettinger, S.N., et al., *Urea as a recovery marker for quantitative assessment of tumor interstitial solutes with microdialysis*. Cancer Res, 2001. **61**(21): p. 7964-70.
108. Menacherry, S., W. Hubert, and J.B. Justice, Jr., *In vivo calibration of microdialysis probes for exogenous compounds*. Anal Chem, 1992. **64**(6): p. 577-83.
109. Chefer, V.I., et al., *Overview of brain microdialysis*. Curr Protoc Neurosci, 2009. **Chapter 7**: p. Unit7 1.
110. Loos, W.J., et al., *Pitfalls of the application of microdialysis in clinical oncology: controversial findings with docetaxel*. J Pharm Biomed Anal, 2007. **45**(2): p. 288-94.
111. Whitaker, G. and C.E. Lunte, *Investigation of microdialysis sampling calibration approaches for lipophilic analytes: doxorubicin*. J Pharm Biomed Anal, 2010. **53**(3): p. 490-6.
112. Lindberger, M., T. Tomson, and S. Lars, *Microdialysis sampling of carbamazepine, phenytoin and phenobarbital in subcutaneous extracellular fluid and subdural cerebrospinal fluid in humans: an in vitro and in vivo study of adsorption to the sampling device*. Pharmacol Toxicol, 2002. **91**(4): p. 158-65.
113. Traunmuller, F., et al., *Development of a high-performance liquid chromatography method for the determination of caspofungin with amperometric detection and its application to in vitro microdialysis experiments*. J Chromatogr B Analyt Technol Biomed Life Sci, 2006. **843**(2): p. 142-6.
114. Nirogi, R., et al., *Approach to reduce the non-specific binding in microdialysis*. J Neurosci Methods, 2012. **209**(2): p. 379-87.
115. Rosenbloom, A.J., D.M. Sipe, and V.W. Weedn, *Microdialysis of proteins: performance of the CMA/20 probe*. J Neurosci Methods, 2005. **148**(2): p. 147-53.
116. May, M., et al., *Enhanced human tissue microdialysis using hydroxypropyl- $\beta$ -cyclodextrin as molecular carrier*. PLoS One, 2013. **8**(4): p. e60628.

117. Blochl-Daum, B., et al., *Measurement of extracellular fluid carboplatin kinetics in melanoma metastases with microdialysis*. Br J Cancer, 1996. **73**(7): p. 920-4.
118. Sani, S.N., et al., *The effects of drug transporter inhibitors on the pharmacokinetics and tissue distribution of methotrexate in normal and tumor-bearing mice: a microdialysis study*. Cancer Chemother Pharmacol, 2010. **66**(1): p. 159-69.
119. Zamboni, W.C., et al., *Inter- and intratumoral disposition of platinum in solid tumors after administration of cisplatin*. Clin Cancer Res, 2002. **8**(9): p. 2992-9.
120. Zamboni, W.C., et al., *Relationship between tumor extracellular fluid exposure to topotecan and tumor response in human neuroblastoma xenograft and cell lines*. Cancer Chemother Pharmacol, 1999. **43**(4): p. 269-76.
121. Zamboni, W.C., et al., *Studies of the efficacy and pharmacology of irinotecan against human colon tumor xenograft models*. Clin Cancer Res, 1998. **4**(3): p. 743-53.
122. Smith, J.A., et al., *Equivalency challenge: Evaluation of Lipodox(R) as the generic equivalent for Doxil(R) in a human ovarian cancer orthotopic mouse model*. Gynecol Oncol, 2016. **141**(2): p. 357-363.
123. Monterrubio, C., et al., *SN-38-loaded nanofiber matrices for local control of pediatric solid tumors after subtotal resection surgery*. Biomaterials, 2016. **79**: p. 69-78.
124. Monterrubio, C., et al., *Targeted drug distribution in tumor extracellular fluid of GD2-expressing neuroblastoma patient-derived xenografts using SN-38-loaded nanoparticles conjugated to the monoclonal antibody 3F8*. J Control Release, 2017. **255**: p. 108-119.
125. Buerger, C., et al., *Development of a liquid chromatography method for the determination of linezolid and its application to in vitro and human microdialysis samples*. J Chromatogr B Analyt Technol Biomed Life Sci, 2003. **796**(1): p. 155-64.
126. Carcaboso, A.M., et al., *Tyrosine kinase inhibitor gefitinib enhances topotecan penetration of gliomas*. Cancer Res, 2010. **70**(11): p. 4499-508.
127. Groothuis, D.R., et al., *Changes in blood-brain barrier permeability associated with insertion of brain cannulas and microdialysis probes*. Brain Res, 1998. **803**(1-2): p. 218-30.
128. Zhuang, Y., et al., *Topotecan central nervous system penetration is altered by a tyrosine kinase inhibitor*. Cancer Res, 2006. **66**(23): p. 11305-13.
129. Shen, J., et al., *Compartment-specific roles of ATP-binding cassette transporters define differential topotecan distribution in brain parenchyma and cerebrospinal fluid*. Cancer Res, 2009. **69**(14): p. 5885-92.
130. Adamska, A., et al., *Molecular and cellular mechanisms of chemoresistance in pancreatic cancer*. Adv Biol Regul, 2018. **68**: p. 77-87.
131. Zhang, Y.K., et al., *Multidrug Resistance Proteins (MRPs) and Cancer Therapy*. AAPS J, 2015. **17**(4): p. 802-12.
132. Nedeljkovic, M. and A. Damjanovic, *Mechanisms of Chemotherapy Resistance in Triple-Negative Breast Cancer-How We Can Rise to the Challenge*. Cells, 2019. **8**(9).
133. Ricci, J.W., et al., *Novel ABCG2 Antagonists Reverse Topotecan-Mediated Chemotherapeutic Resistance in Ovarian Carcinoma Xenografts*. Mol Cancer Ther, 2016. **15**(12): p. 2853-2862.
134. Norouzi-Barough, L., et al., *Molecular mechanisms of drug resistance in ovarian cancer*. J Cell Physiol, 2018. **233**(6): p. 4546-4562.
135. Norris, M.D., *Expression of the multidrug-resistance-associated protein NB*. NEJM, 1996.
136. Oda, Y., et al., *Reverse transcriptase-polymerase chain reaction amplification of MDR1 gene expression in adult soft tissue sarcomas*. Diagn Mol Pathol, 1996. **5**(2): p. 98-106.
137. Nakanishi, H., et al., *P-glycoprotein expression in soft-tissue sarcomas*. J Cancer Res Clin Oncol, 1997. **123**(6): p. 352-6.
138. Zhang, H., et al., *In vitro, in vivo and ex vivo characterization of ibrutinib: a potent inhibitor of the efflux function of the transporter MRP1*. Br J Pharmacol, 2014. **171**(24): p. 5845-57.
139. Tamaki, A., et al., *The controversial role of ABC transporters in clinical oncology*. Essays Biochem, 2011. **50**(1): p. 209-32.



## REFERENCES

140. Gottesman, M.M., T. Fojo, and S.E. Bates, *Multidrug resistance in cancer: role of ATP-dependent transporters*. Nat Rev Cancer, 2002. **2**(1): p. 48-58.
141. Abraham, J., et al., *A phase I study of the P-glycoprotein antagonist tariquidar in combination with vinorelbine*. Clin Cancer Res, 2009. **15**(10): p. 3574-82.
142. Nobili, S., et al., *Pharmacological strategies for overcoming multidrug resistance*. Curr Drug Targets, 2006. **7**(7): p. 861-79.
143. Lu, W. and Y. Kang, *Epithelial-Mesenchymal Plasticity in Cancer Progression and Metastasis*. Dev Cell, 2019. **49**(3): p. 361-374.
144. Lamouille, S., J. Xu, and R. Derynck, *Molecular mechanisms of epithelial-mesenchymal transition*. Nat Rev Mol Cell Biol, 2014. **15**(3): p. 178-96.
145. Mani, S.A., et al., *The epithelial-mesenchymal transition generates cells with properties of stem cells*. Cell, 2008. **133**(4): p. 704-15.
146. Lawson, D.A., et al., *Single-cell analysis reveals a stem-cell program in human metastatic breast cancer cells*. Nature, 2015. **526**(7571): p. 131-5.
147. Rhim, A.D., et al., *EMT and dissemination precede pancreatic tumor formation*. Cell, 2012. **148**(1-2): p. 349-61.
148. Fischer, K.R., et al., *Epithelial-to-mesenchymal transition is not required for lung metastasis but contributes to chemoresistance*. Nature, 2015. **527**(7579): p. 472-6.
149. Zheng, X., et al., *Epithelial-to-mesenchymal transition is dispensable for metastasis but induces chemoresistance in pancreatic cancer*. Nature, 2015. **527**(7579): p. 525-530.
150. Liu, X., et al., *Oncogenes associated with drug resistance in ovarian cancer*. J Cancer Res Clin Oncol, 2015. **141**(3): p. 381-95.
151. Cooley, M., et al., *Molecular determinants of chemotherapy resistance in ovarian cancer*. Pharmacogenomics, 2015. **16**(16): p. 1763-7.
152. Ricci, M.S. and W.X. Zong, *Chemotherapeutic approaches for targeting cell death pathways*. Oncologist, 2006. **11**(4): p. 342-57.
153. Campbell, K.J., et al., *MCL-1 is a prognostic indicator and drug target in breast cancer*. Cell Death Dis, 2018. **9**(2): p. 19.
154. Inao, T., et al., *Bcl-2 inhibition sensitizes triple-negative human breast cancer cells to doxorubicin*. Oncotarget, 2018. **9**(39): p. 25545-25556.
155. Kale, J., E.J. Osterlund, and D.W. Andrews, *BCL-2 family proteins: changing partners in the dance towards death*. Cell Death Differ, 2018. **25**(1): p. 65-80.
156. Hassan, M., et al., *Apoptosis and molecular targeting therapy in cancer*. Biomed Res Int, 2014. **2014**: p. 150845.
157. Fraser, M., et al., *Chemoresistance in human ovarian cancer: the role of apoptotic regulators*. Reprod Biol Endocrinol, 2003. **1**: p. 66.
158. Bhakta, N., et al., *Childhood cancer burden: a review of global estimates*. The Lancet Oncology, 2019. **20**(1): p. e42-e53.
159. Lupo, P.J. and L.G. Spector, *Cancer Progress and Priorities: Childhood Cancer*. Cancer Epidemiol Biomarkers Prev, 2020. **29**(6): p. 1081-1094.
160. Filbin, M. and M. Monje, *Developmental origins and emerging therapeutic opportunities for childhood cancer*. Nat Med, 2019. **25**(3): p. 367-376.
161. Erdmann, F., et al., *Childhood cancer: Survival, treatment modalities, late effects and improvements over time*. Cancer Epidemiol, 2021. **71**(Pt B): p. 101733.
162. Kattner, P., et al., *Compare and contrast: pediatric cancer versus adult malignancies*. Cancer and Metastasis Reviews, 2019. **38**(4): p. 673-682.
163. Gatta, G., et al., *Childhood cancer survival in Europe 1999–2007: results of EUROCare-5—a population-based study*. The Lancet Oncology, 2014. **15**(1): p. 35-47.
164. Force, L.M., et al., *The global burden of childhood and adolescent cancer in 2017: an analysis of the Global Burden of Disease Study 2017*. The Lancet Oncology, 2019. **20**(9): p. 1211-1225.



165. Pritchard-Jones, K., et al., *Sustaining innovation and improvement in the treatment of childhood cancer: lessons from high-income countries*. The Lancet Oncology, 2013. **14**(3): p. e95-e103.
166. Jones, D.T.W., et al., *Molecular characteristics and therapeutic vulnerabilities across paediatric solid tumours*. Nat Rev Cancer, 2019. **19**(8): p. 420-438.
167. Grobner, S.N., et al., *The landscape of genomic alterations across childhood cancers*. Nature, 2018. **555**(7696): p. 321-327.
168. Sweet-Cordero, E.A. and J.A. Biegel, *The genomic landscape of pediatric cancers: Implications for diagnosis and treatment*. Science, 2019. **363**(6432): p. 1170-1175.
169. Grunewald, T.G., et al., *Sarcoma treatment in the era of molecular medicine*. EMBO Mol Med, 2020. **12**(11): p. e11131.
170. Stewart, E., et al., *The Childhood Solid Tumor Network: A new resource for the developmental biology and oncology research communities*. Dev Biol, 2016. **411**(2): p. 287-293.
171. Grunewald, T.G.P., et al., *Ewing sarcoma*. Nat Rev Dis Primers, 2018. **4**(1): p. 5.
172. Riggi, N., M.L. Suva, and I. Stamenkovic, *Ewing's Sarcoma*. N Engl J Med, 2021. **384**(2): p. 154-164.
173. Gaspar, N., et al., *Ewing Sarcoma: Current Management and Future Approaches Through Collaboration*. J Clin Oncol, 2015. **33**(27): p. 3036-46.
174. Pappo, A.S. and U. Dirksen, *Rhabdomyosarcoma, Ewing Sarcoma, and Other Round Cell Sarcomas*. J Clin Oncol, 2018. **36**(2): p. 168-179.
175. Juergens, C., et al., *Safety assessment of intensive induction with vincristine, ifosfamide, doxorubicin, and etoposide (VIDE) in the treatment of Ewing tumors in the EURO-E.W.I.N.G. 99 clinical trial*. Pediatr Blood Cancer, 2006. **47**(1): p. 22-9.
176. Mora, J., et al., *GEIS-21: a multicentric phase II study of intensive chemotherapy including gemcitabine and docetaxel for the treatment of Ewing sarcoma of children and adults: a report from the Spanish sarcoma group (GEIS)*. Br J Cancer, 2017. **117**(6): p. 767-774.
177. Stahl, M., et al., *Risk of recurrence and survival after relapse in patients with Ewing sarcoma*. Pediatr Blood Cancer, 2011. **57**(4): p. 549-53.
178. Delattre, O., et al., *Gene fusion with an ETS DNA-binding domain caused by chromosome translocation in human tumours*. Nature, 1992. **359**(6391): p. 162-5.
179. Lessnick, S.L. and M. Ladanyi, *Molecular pathogenesis of Ewing sarcoma: new therapeutic and transcriptional targets*. Annu Rev Pathol, 2012. **7**: p. 145-59.
180. Crompton, B.D., et al., *The Genomic Landscape of Pediatric Ewing Sarcoma*. Cancer Discovery, 2014. **4**(11): p. 1326-1341.
181. Tirode, F., et al., *Genomic landscape of Ewing sarcoma defines an aggressive subtype with co-association of STAG2 and TP53 mutations*. Cancer Discov, 2014. **4**(11): p. 1342-53.
182. Rocchi, A., et al., *CD99 inhibits neural differentiation of human Ewing sarcoma cells and thereby contributes to oncogenesis*. J Clin Invest, 2010. **120**(3): p. 668-80.
183. Pasello, M., M.C. Manara, and K. Scotlandi, *CD99 at the crossroads of physiology and pathology*. J Cell Commun Signal, 2018. **12**(1): p. 55-68.
184. Machado, I., et al., *Molecular diagnosis of Ewing sarcoma family of tumors: a comparative analysis of 560 cases with FISH and RT-PCR*. Diagn Mol Pathol, 2009. **18**(4): p. 189-99.
185. Prudowsky, Z.D. and J.T. Yustein, *Recent Insights into Therapy Resistance in Osteosarcoma*. Cancers (Basel), 2020. **13**(1).
186. Mirabello, L., R.J. Troisi, and S.A. Savage, *International osteosarcoma incidence patterns in children and adolescents, middle ages and elderly persons*. Int J Cancer, 2009. **125**(1): p. 229-34.
187. Anninga, J.K., et al., *Chemotherapeutic adjuvant treatment for osteosarcoma: where do we stand?* Eur J Cancer, 2011. **47**(16): p. 2431-45.
188. Kager, L., G. Tamamyan, and S. Bielack, *Novel insights and therapeutic interventions for pediatric osteosarcoma*. Future Oncol, 2017. **13**(4): p. 357-368.

## REFERENCES

189. Link, M.P., et al., *The effect of adjuvant chemotherapy on relapse-free survival in patients with osteosarcoma of the extremity*. N Engl J Med, 1986. **314**(25): p. 1600-6.
190. Sayles, L.C., et al., *Genome-Informed Targeted Therapy for Osteosarcoma*. Cancer Discov, 2019. **9**(1): p. 46-63.
191. Ferrari, S., et al., *Neoadjuvant chemotherapy with high-dose Ifosfamide, high-dose methotrexate, cisplatin, and doxorubicin for patients with localized osteosarcoma of the extremity: a joint study by the Italian and Scandinavian Sarcoma Groups*. J Clin Oncol, 2005. **23**(34): p. 8845-52.
192. Martin, J.W., J.A. Squire, and M. Zielenska, *The genetics of osteosarcoma*. Sarcoma, 2012. **2012**: p. 627254.
193. Meyers, P.A., et al., *Osteogenic sarcoma with clinically detectable metastasis at initial presentation*. J Clin Oncol, 1993. **11**(3): p. 449-53.
194. Kager, L., et al., *Primary metastatic osteosarcoma: presentation and outcome of patients treated on neoadjuvant Cooperative Osteosarcoma Study Group protocols*. J Clin Oncol, 2003. **21**(10): p. 2011-8.
195. Roberts, R.D., et al., *Provocative questions in osteosarcoma basic and translational biology: A report from the Children's Oncology Group*. Cancer, 2019. **125**(20): p. 3514-3525.
196. Zhang, X. and Z. Guan, *PET/CT in the diagnosis and prognosis of osteosarcoma*. Front Biosci (Landmark Ed), 2018. **23**: p. 2157-2165.
197. Ritter, J. and S.S. Bielack, *Osteosarcoma*. Ann Oncol, 2010. **21 Suppl 7**: p. vii320-5.
198. Sun, Y., et al., *Analysis of imaging characteristics of primary malignant bone tumors in children*. Oncol Lett, 2017. **14**(5): p. 5801-5810.
199. Ognjanovic, S., et al., *Trends in childhood rhabdomyosarcoma incidence and survival in the United States, 1975-2005*. Cancer, 2009. **115**(18): p. 4218-26.
200. Dasgupta, R., J. Fuchs, and D. Rodeberg, *Rhabdomyosarcoma*. Semin Pediatr Surg, 2016. **25**(5): p. 276-283.
201. Martin-Giacalone, B.A., et al., *Pediatric Rhabdomyosarcoma: Epidemiology and Genetic Susceptibility*. J Clin Med, 2021. **10**(9).
202. Oberlin, O., et al., *Prognostic factors in metastatic rhabdomyosarcomas: results of a pooled analysis from United States and European cooperative groups*. J Clin Oncol, 2008. **26**(14): p. 2384-9.
203. Skapek, S.X., et al., *Rhabdomyosarcoma*. Nat Rev Dis Primers, 2019. **5**(1): p. 1.
204. Crist, W.M., et al., *Intergroup rhabdomyosarcoma study-IV: results for patients with nonmetastatic disease*. J Clin Oncol, 2001. **19**(12): p. 3091-102.
205. Arndt, C.A., et al., *Vincristine, actinomycin, and cyclophosphamide compared with vincristine, actinomycin, and cyclophosphamide alternating with vincristine, topotecan, and cyclophosphamide for intermediate-risk rhabdomyosarcoma: children's oncology group study D9803*. J Clin Oncol, 2009. **27**(31): p. 5182-8.
206. Stevens, M.C., et al., *Treatment of nonmetastatic rhabdomyosarcoma in childhood and adolescence: third study of the International Society of Paediatric Oncology--SIOP Malignant Mesenchymal Tumor 89*. J Clin Oncol, 2005. **23**(12): p. 2618-28.
207. Bisogno, G., et al., *Sequential high-dose chemotherapy for children with metastatic rhabdomyosarcoma*. Eur J Cancer, 2009. **45**(17): p. 3035-41.
208. Qualman, S.J., et al., *Intergroup Rhabdomyosarcoma Study: update for pathologists*. Pediatr Dev Pathol, 1998. **1**(6): p. 550-61.
209. Dziuba, I., et al., *Rhabdomyosarcoma in children - current pathologic and molecular classification*. Pol J Pathol, 2018. **69**(1): p. 20-32.
210. Arnold, M.A. and F.G. Barr, *Molecular diagnostics in the management of rhabdomyosarcoma*. Expert Rev Mol Diagn, 2017. **17**(2): p. 189-194.
211. Nishio, J., et al., *Use of a novel FISH assay on paraffin-embedded tissues as an adjunct to diagnosis of alveolar rhabdomyosarcoma*. Lab Invest, 2006. **86**(6): p. 547-56.

212. Galili, N., et al., *Fusion of a fork head domain gene to PAX3 in the solid tumour alveolar rhabdomyosarcoma*. Nat Genet, 1993. **5**(3): p. 230-5.
213. Shapiro, D.N., et al., *Fusion of PAX3 to a member of the forkhead family of transcription factors in human alveolar rhabdomyosarcoma*. Cancer Res, 1993. **53**(21): p. 5108-12.
214. Cao, L., et al., *Genome-wide identification of PAX3-FKHR binding sites in rhabdomyosarcoma reveals candidate target genes important for development and cancer*. Cancer Res, 2010. **70**(16): p. 6497-508.
215. Shern, J.F., et al., *Comprehensive genomic analysis of rhabdomyosarcoma reveals a landscape of alterations affecting a common genetic axis in fusion-positive and fusion-negative tumors*. Cancer Discov, 2014. **4**(2): p. 216-31.
216. Chen, X., et al., *Targeting oxidative stress in embryonal rhabdomyosarcoma*. Cancer Cell, 2013. **24**(6): p. 710-24.
217. Martino, E., et al., *The long story of camptothecin: From traditional medicine to drugs*. Bioorg Med Chem Lett, 2017. **27**(4): p. 701-707.
218. Kciuk, M., B. Marciniak, and R. Kontek, *Irinotecan-Still an Important Player in Cancer Chemotherapy: A Comprehensive Overview*. Int J Mol Sci, 2020. **21**(14).
219. Pizzolato, J.F. and L.B. Saltz, *The camptothecins*. The Lancet, 2003. **361**(9376): p. 2235-2242.
220. Bomgaars, L., S.L. Berg, and S.M. Blaney, *The development of camptothecin analogs in childhood cancers*. Oncologist, 2001. **6**(6): p. 506-16.
221. Li, W., et al., *Overcoming ABC transporter-mediated multidrug resistance: Molecular mechanisms and novel therapeutic drug strategies*. Drug Resist Updat, 2016. **27**: p. 14-29.
222. Han, J.Y., et al., *Associations of ABCB1, ABCC2, and ABCG2 polymorphisms with irinotecan-pharmacokinetics and clinical outcome in patients with advanced non-small cell lung cancer*. Cancer, 2007. **110**(1): p. 138-47.
223. Sawada, S., et al., *Synthesis and antitumor activity of 20(S)-camptothecin derivatives: A-ring modified and 7,10-disubstituted camptothecins*. Chem Pharm Bull (Tokyo), 1991. **39**(12): p. 3183-8.
224. Li, Q.Y., et al., *Review camptothecin: current perspectives*. Curr Med Chem, 2006. **13**(17): p. 2021-39.
225. de Man, F.M., et al., *Individualization of Irinotecan Treatment: A Review of Pharmacokinetics, Pharmacodynamics, and Pharmacogenetics*. Clin Pharmacokinet, 2018. **57**(10): p. 1229-1254.
226. Guemei, A.A., et al., *Human plasma carboxylesterase and butyrylcholinesterase enzyme activity: correlations with SN-38 pharmacokinetics during a prolonged infusion of irinotecan*. Cancer Chemother Pharmacol, 2001. **47**(4): p. 283-90.
227. Di Paolo, A., et al., *Pharmacokinetic and pharmacogenetic predictive markers of irinotecan activity and toxicity*. Curr Drug Metab, 2011. **12**(10): p. 932-43.
228. Rivory, L.P., et al., *Kinetics of the in vivo interconversion of the carboxylate and lactone form of irinotecan (CPT-11) and of its metabolite SN38 in patients*. Cancer Res., 1994. **15**(54): p. 6330-6333.
229. Stein, A., W. Voigt, and K. Jordan, *Chemotherapy-induced diarrhea: pathophysiology, frequency and guideline-based management*. Ther Adv Med Oncol, 2010. **2**(1): p. 51-63.
230. Wagner, L.M., *Fifteen years of irinotecan therapy for pediatric sarcoma: where to next?* Clin Sarcoma Res, 2015. **5**: p. 20.
231. Furman, W.L., et al., *Direct translation of a protracted irinotecan schedule from a xenograft model to a phase I trial in children*. J Clin Oncol, 1999. **17**(6): p. 1815-24.
232. Houghton, P.J., et al., *Efficacy of topoisomerase I inhibitors, topotecan and irinotecan, administered at low dose levels in protracted schedules to mice bearing xenografts of human tumors*. Cancer Chemother Pharmacol, 1995. **36**(5): p. 393-403.
233. Bomgaars, L.R., et al., *Phase II trial of irinotecan in children with refractory solid tumors: a Children's Oncology Group Study*. J Clin Oncol, 2007. **25**(29): p. 4622-7.

## REFERENCES

234. Hawkins, D.S., et al., *Addition of Vincristine and Irinotecan to Vincristine, Dactinomycin, and Cyclophosphamide Does Not Improve Outcome for Intermediate-Risk Rhabdomyosarcoma: A Report From the Children's Oncology Group*. J Clin Oncol, 2018. **36**(27): p. 2770-2777.
235. Pappo, A.S., et al., *Two consecutive phase II window trials of irinotecan alone or in combination with vincristine for the treatment of metastatic rhabdomyosarcoma: the Children's Oncology Group*. J Clin Oncol, 2007. **25**(4): p. 362-9.
236. Mascarenhas, L., et al., *Randomized phase II window trial of two schedules of irinotecan with vincristine in patients with first relapse or progression of rhabdomyosarcoma: a report from the Children's Oncology Group*. J Clin Oncol, 2010. **28**(30): p. 4658-63.
237. Mixon, B.A., et al., *Vincristine, irinotecan, and temozolomide for treatment of relapsed alveolar rhabdomyosarcoma*. J Pediatr Hematol Oncol, 2013. **35**(4): p. e163-6.
238. Raciborska, A., et al., *Vincristine, irinotecan, and temozolomide in patients with relapsed and refractory Ewing sarcoma*. Pediatr Blood Cancer, 2013. **60**(10): p. 1621-5.
239. Dharmarajan, K.V., L.H. Wexler, and S.L. Wolden, *Concurrent radiation with irinotecan and carboplatin in intermediate- and high-risk rhabdomyosarcoma: a report on toxicity and efficacy from a prospective pilot phase II study*. Pediatr Blood Cancer, 2013. **60**(2): p. 242-7.
240. Kurucu, N., N. Sari, and I.E. Ilhan, *Irinotecan and temozolamide treatment for relapsed Ewing sarcoma: a single-center experience and review of the literature*. Pediatr Hematol Oncol, 2015. **32**(1): p. 50-9.
241. Wagner, L.M., et al., *Temozolomide and intravenous irinotecan for treatment of advanced Ewing sarcoma*. Pediatr Blood Cancer, 2007. **48**(2): p. 132-9.
242. Casey, D.A., et al., *Irinotecan and temozolomide for Ewing sarcoma: the Memorial Sloan-Kettering experience*. Pediatr Blood Cancer, 2009. **53**(6): p. 1029-34.
243. Yoon, J.H., et al., *A study of docetaxel and irinotecan in children and young adults with recurrent or refractory Ewing sarcoma family of tumors*. BMC Cancer, 2014. **14**: p. 622.
244. Crews, K.R., et al., *Effect of fractionated ifosfamide on the pharmacokinetics of irinotecan in pediatric patients with osteosarcoma*. J Pediatr Hematol Oncol, 2004. **26**(11): p. 764-7.
245. Byrne, A.T., et al., *Interrogating open issues in cancer precision medicine with patient-derived xenografts*. Nature Reviews Cancer, 2017. **17**(4): p. 254-268.
246. Nanni, P., et al., *Bone sarcoma patient-derived xenografts are faithful and stable preclinical models for molecular and therapeutic investigations*. Sci Rep, 2019. **9**(1): p. 12174.
247. Pergolini, I., et al., *Tumor engraftment in patient-derived xenografts of pancreatic ductal adenocarcinoma is associated with adverse clinicopathological features and poor survival*. PLoS One, 2017. **12**(8): p. e0182855.
248. Chen, Y., et al., *Tumor characteristics associated with engraftment of patient-derived non-small cell lung cancer xenografts in immunocompromised mice*. Cancer, 2019. **125**(21): p. 3738-3748.
249. Abel, L., et al., *Impact of immediate cryopreservation on the establishment of patient derived xenografts from head and neck cancer patients*. J Transl Med, 2021. **19**(1): p. 180.
250. Hernandez, M.C., et al., *Successful Secondary Engraftment of Pancreatic Ductal Adenocarcinoma and Cholangiocarcinoma Patient-Derived Xenografts After Previous Failed Primary Engraftment*. Transl Oncol, 2019. **12**(1): p. 69-75.
251. Biedler, J.L. and H. Riehm, *Cellular resistance to actinomycin D in Chinese hamster cells in vitro: cross-resistance, radioautographic, and cytogenetic studies*. Cancer Res, 1970. **30**(4): p. 1174-84.
252. Juliano, R.L. and V. Ling, *A surface glycoprotein modulating drug permeability in Chinese hamster ovary cell mutants*. Biochim Biophys Acta, 1976. **455**(1): p. 152-62.
253. Schinkel, A.H., et al., *Disruption of the mouse mdr1a P-glycoprotein gene leads to a deficiency in the blood-brain barrier and to increased sensitivity to drugs*. Cell, 1994. **77**(4): p. 491-502.

254. Hijazi, Y.M., et al., *Immunohistochemical detection of P-glycoprotein in Ewing's sarcoma and peripheral primitive neuroectodermal tumors before and after chemotherapy*. Am J Clin Pathol, 1994. **102**(1): p. 61-7.
255. Follit, C.A., et al., *In silico identified targeted inhibitors of P-glycoprotein overcome multidrug resistance in human cancer cells in culture*. Pharmacol Res Perspect, 2015. **3**(5): p. e00170.
256. Nanayakkara, A.K., et al., *Targeted inhibitors of P-glycoprotein increase chemotherapeutic-induced mortality of multidrug resistant tumor cells*. Sci Rep, 2018. **8**(1): p. 967.



